OSCILLATING BODIES IN SUPERSONIC FLOW

Rodger Besley Carter

Library
Naval Postgraduate School
Monterey, California 93940

NAVAL POSTGRADUATE SCHOOL
Monterey, California

THESIS

OSCILLATING BODIES IN

SUPERSONIC FLOW

by

Rodger Besley Carter

Thesis Advisor: G.J. Hokenson

December 1972

T12...45

Approved for public release; distribution unlimited.

Oscillating Bodies in Supersonic Flow

by

Rodger Besley Carter
Lieutenant, United States Navy
B.S., United States Naval Academy, 1966

Submitted in partial fulfillment of the
requirements for the degree of

MASTER OF SCIENCE IN AERONAUTICAL ENGINEERING

from the

NAVAL POSTGRADUATE SCHOOL
December 1972

Naval Postgraduate School
Monterey, California 93940

ABSTRACT

Three shapes - a cone, a wedge, and a flat plate - were oscillated at various frequencies up to 16 cycles per second in a Mach 2.8 flow to determine the extent of the validity of the quasi-steady flow assumption. Instantaneous static pressure measurements and schlieren high speed movies were made and analyzed.

It was found that at approximately 6 cycles per second the measured pressures started a linear deviation from quasi-steady flow. The absolute pressure being measured, the amplitude, and the transverse velocity of the static pressure port were additional variables. The schlieren photography did not show any measurable change in the inviscid shock structure from quasi-steady flow.

TABLE OF CONTENTS

LIST OF FIGURES

FIGURE

TABLE OF SYMBOLS

LATIN SYMBOLS

a	speed of sound
AOA	angle of attack
c/s	cycles per second
cm/s	centimeters per second
f	frequency
f_n	natural frequency
fps	frames per second
h	damping ratio
Hg	Mercury
ID	inside diameter
L	length
M	Mach number
P	pressure
P_o	True Pressure
psi	pounds per square inch
r	tubing radius
T	period (1/f)
t	time
V	volume

GREEK SYMBOLS

ϕ	cone azimuth angle
Φ	phase shift angle

θ_c	cone half angle
θ_w	wedge half angle
ρ	density
μ	viscosity

SUBSCRIPTS

c	cone
∞	value at infinity
n	natural
o	true value
w	wedge

ACKNOWLEDGEMENTS

The author wishes to express his gratitude to Dr. G. J. Hokenson for his guidance and support as thesis advisor during the included work.

The author also wishes to express appreciation to Model Maker Glen Middleton and Machinist John Moulton for their expert construction of the wind tunnel models, to Aerospace Engineering Technicians Norm Leckenby and Pat Hickey for their valuable advice and assistance in setting up the apparatus and maintaining the wind tunnel, to Electronics Technician Cecil Gordon for his advice and assistance with instrumentation, to Model Maker Gordon Gulbranson for construction of model cases, and finally to Laboratory Supervisors Ted Dunton and Bob Besel for their overall assistance and advice.

The author also expresses appreciation to the photo Lab for their assistance in compiling the movie.

And most importantly, the author wishes to thank his wife for her typing assistance and moral support.

I. INTRODUCTION

Since the Bell X-1 first exceeded Mach one on October 14, 1947, mankind has gone faster than ever dreamed possible. Contributing to this advance in speed, many supersonic wind tunnel models have been designed and tested; most of these tests have been done with stationary models. But aircraft or aerospace vehicles move about in a dynamic situation, often with unsteady effects predominating in the vehicle aerodynamics. How good are steady state predictions when applied to vehicles in non-steady motion? How fast does the vehicle have to turn before a fast rate of angular movement causes the flow field to differ from a slow rate of angular movement? In other words, at supersonic speeds what are the limits of a quasi-steady assumption?

The inviscid flow theory of supersonic 2-dimensional wedge flow is well understood and closely agrees with experimental steady flow results; likewise for the inviscid conical flow about a cone at zero incidence. However, for a cone at an angle of attack, the non-linear ordinary differential equation two point boundary value problem becomes a set of elliptic non-linear partial differential equations in two independent variables. The flow is still assumed conical in that the flow has constant properties along any one-dimensional ray from the cone vertex. The shock has the shape of a skewed cone and, as the angle of

attack is increased, the flow field equations, which are normally elliptic in a cross section plane, become hyperbolic in some region of that plane, and the conical assumption is no longer valid. This occurs when the cone angle of attack is such that the upper-most ray of the cone is approximately parallel to the flow. At this point the entropy singularity initially situated at the leeward generator of the body moves off the body into the flow field, causing the hyperbolic equation region. In other words, the flow streamlines on the body, which follow conical rays at zero angle of attack, shift toward the leeward-most cone ray as the angle of attack is increased and their convergence at high angles of attack leads to the entropy singularity in the non-viscous theory. A head on view following similar streamlines as they cross the shock (outer ring) and converge on the cone body which is at an angle of attack (difference of two vertex dots) follows:

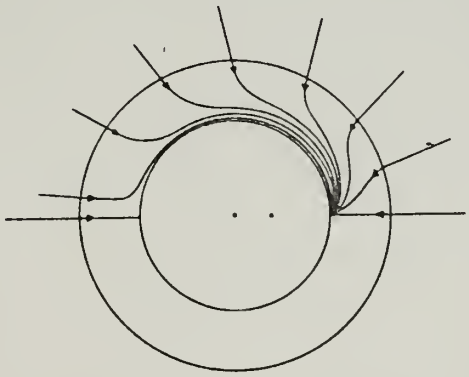

The numerical solution of the cone at angles of attack is presented in Reference 1.

The present study makes instantaneous measurements of the wall static pressures on a cone, a wedge, and a flat plate model at both constant angles of attack and with the model oscillating at various amplitudes and frequencies. The quasi-steady assumption is that the data at a specific angle of attack would correspond to measurements taken if the model were moving through that angle of attack. How fast a body can sinusoidally oscillate before steady state pressure measurements no longer correlate is answered in this report for the conditions investigated. In addition to the pressure measurements, high speed schlieren movies of the oscillating models were made and analyzed.

II. EQUIPMENT AND PROCEDURES

A. WIND TUNNEL

The study was conducted in the supersonic blowdown wind tunnel located in the Department of Aeronautics Laboratories of the Naval Postgraduate School. The tunnel, as schematically shown in Figure 1, is supplied by a Sullivan compressor which pumps up a large storage tank to 300 psi. The tank is then vented into a smaller plenum chamber through a regulator which maintains the plenum chamber pressure at the value desired. The compressor is capable of pumping up the storage tank in about forty minutes, allowing about five to seven minutes of useful running time. To obtain the desired Mach number, various Mach number blocks can be inserted in the test section.

For this investigation Mach 2.8 blocks were selected because these produced a "clean" supersonic flow, and because this is the range of current high performance manned supersonic aircraft. The resulting usable test section was four by five inches cross section and one foot long. Nine-inch diameter interferometer quality glass windows located on either side of the test section permitted visual study of the flow. The test section and accompanying equipment are shown in Figures 2 and 3.

B. MODELS

The stainless steel cone model, shown in Figure 4, was 1.2 inches long and had a total included angle of 40°,

hence a half angle (θ_c) of 20°. There were six in-line static pressure ports evenly distributed on opposite sides of the cone, and the cone itself could be rotated on its base so that the ports would be at any angle relative to the flow and vertical axis plane. That is, when viewed from the front, the ports could be positioned on top and bottom, on each side, or any angle in between.

The stainless steel wedge model, shown in Figures 5 and 6, was 1.24 inches square in planform, and had a total included angle of 30° hence a half angle (θ_w) of 15°. There was one pressure port each on the centerline of the upper and lower surfaces located so as to be forward of Mach lines from the leading edge tips for a Mach number as low as 1.5.

The stainless steel flat plate model, shown in Figure 7, had a planform of 1.98 by 4.95 inches, and had three wall static pressure ports, all distributed forward of Mach number 1.5 Mach lines from both the tips and the other pressure ports. For each of the models, the stainless steel and tygon pressure tubing was led out of the hollow mounting axle so as not to create a disturbance in the flow. To avoid a sharp bend the tubing had to be partially brought out of the bottom of the flat plate model as shown in Figure 8.

C. TEST SECTION SET UP

The model mounting axle protruded through reamed holes in the test section windows, both equipped with nylon

bushings. On one side of the tunnel the pressure tap tubing came out the hollow axle (see Figure 2) and on the other side (see Figure 3) the driving mechanism and angular position gearing were connected to the model axle. The angular gearing was of the anti-backlash type, and transferred the shaft rotation to a potentiometer. The driving mechanism, shown in Figure 9, consisted of a four- or eleven-inch lever arm connected to a long four-foot rod which in turn was connected to a flywheel-eccentric. The flywheel was driven by an electric motor (see Figure 10) through a variable speed hydraulic transmission. Thus by varying the connection point on the flywheel-eccentric and the lever arm length, the model could be made to oscillate at any desired amplitude; and by varying the flywheel rotation speed, the frequency of oscillation could be selected. The powered system was capable of frequencies as low as 0.5 cycles per second, and lower frequencies could be obtained by hand turning. The maximum frequency depended on the amplitude desired because of the forces involved. Higher amplitudes put higher forces on the system, as made visible by the bending of the four-foot rod. At frequencies above 10 cycles per second a damper was used to damp out the rod vibrations. Qualitatively, it appeared that the system was structurally limited to 16 cycles per second; therefore this was the highest frequency measured.

D. PRESSURE TRANSDUCER

Pressure transducers which could be embedded on the model surface or placed inside the model were unavailable. To optimize frequency response, short pressure lead and small volume transducers were located just outside the tunnel. Statham Instruments PS258TC-15-350 Transducers were mounted on the outside of the tunnel window and the installation incorporated a maximum tubing length of 8.2 inches between the pressure taps and the transducers (see Figure 11).

E. INSTRUMENTATION

The instrumentation layout is shown in Figure 12. A detailed list of equipment follows:

1. Pressure Transducer - Statham Instruments PA258TC-15-350 , 0-15 psia range, maximum allowable 150% of rated range, non-linearity and hysteresis specification - less than 1.5%, natural frequency 4200 cycles per second [2].
2. Bridge Balance - network with 50k potentiometer across input and 5k resistor on one leg of output.
3. 12 Volt DC power Supply - Powermate Model BP-34C.
4. Dc Digital Millivolt Meter - Digitec Model 251-3.
5. XY Plotter - Hewlett-Packard Model 7035 B.
6. Oscilloscope - Tekronix 551 Dual Beam.
7. Potentiometer - Fairchild Controls Number 751-2053A.
8. 11.5 Volt DC Power Supply - Systems Research Model 3566.

9. DC Digital Voltmeter - Digitec Model 251-1.

10. Frequency Counter - Dynasiences Digital Readout Electronic Counter AN/USM-245A.

The Equipment Setup is shown in Figures 13, 14, and 15.

F. CALIBRATION

1. Zero Angle of Attack and Amplitude Calibration

The model position for zero angle of attack was found by making the pressure difference between an upper pressure port and lower pressure port zero. For this the second pressure transducer and associated balance and power supply were used. The crosshairs of a transit, as shown in Figure 16, were then put on the tip of the model and the angular potentiometer was adjusted to zero volts reading.

The amplitude was set by using the angular relationship:

$$\text{desired max AOA} = \tan^{-1}\left(\frac{\text{flywheel attachment point radius}}{\text{model axle lever arm length}}\right)$$

These distances are shown in Figure 9.

2. Pressure Transducer Calibration - Static

The pressure transducer was connected to a U-tube mercury column manometer and vacuum pump for calibration. By adjusting the power supply voltage, the transducer bridge could be balanced so that the voltmeter read out directly in inches of mercury in exact correspondence with the mercury column over the range of pressures encountered. The static pressure calibration curve is shown in Figure 17.

3. Pressure Transducer Calibration - Dynamic

The fundamental question of whether the pressure transducer system was capable of responding to the oscillating pressures on the model without any phase lag or amplitude distortion was determined by measuring the system's natural frequency in response to a step input. This experiment is described in Appendix A, and the results indicated a system natural frequency (f_n) of 2410 cycles per second and a damping ratio (h) of 0.7. The transient response of the pressure transducer system depended on the response of the pressure transducer itself and the response of the pressure-transmitting fluid and connecting tubing. This leads to the formula:

$$f_n = \sqrt{\frac{3 \pi r^2 a^2}{4 LV}}$$

given by Holman [3]. In this equation the pressure transducer volume (V) was determined by liquid displacement to be 5.257×10^{-4} cubic inches. The tube length (L) was 8.2 inches, the inside radius (r) was 0.0225 inches, and the speed of sound (a) was computed at 70°F. These numbers resulted in a computed natural frequency of 7140 cycles per second. If the volume is doubled, as an uncertainty factor, the natural frequency reduces to 5050.

The damping ratio

$$h = \frac{2\mu}{\rho a r^3} \sqrt{\frac{3LV}{\pi}}$$

also from Holman, was computed to be 0.019.

Holman also gives formulas for the pressure amplitude ratio, (ratio of measured to impressed pressure):

$$\frac{P}{P_o} = \frac{1}{\{[1-(\frac{f}{f_n})^2]^2 + 4h^2(\frac{f}{f_n})^2\}^{1/2}}$$

and for the phase angle lag:

$$\Phi = \tan^{-1} \frac{-2h(\frac{f}{f_n})}{1-(\frac{f}{f_n})^2}$$

These were computed for each of the values of natural frequency and damping ratio:

f	f_n	h	p/P_o	Φ
16	2410	.7	1.00000088	-.53257
16	2000*	.5*	1.00003199	-.4584
16	7140	.019	1.000005018	-.00487
16	5050	.019	1.000010232	-.00696

* from Appendix A.

From these results it was determined that the pressure transducer system was quite capable of giving essentially zero phase lag and amplitude distortion measurements for the conditions of the experiment.

G. DATA MEASUREMENT PROCEDURES

The non-oscillatory pressure versus angle of attack curves (see Appendices B, C, and D) were recorded on the XY plotter while turning the flywheel slowly by hand. A double trace was recorded, starting at the low pressure and returning to it with the model making one full cycle.

The oscillatory wall static pressure and the angle of attack were recorded on the oscilloscope at 1,2,4,6,8,10, 12,14, and 16 cycles per second. The motor transmission was adjusted (see Figure 18) so that the desired period was read on the frequency counter which had been checked with a sine wave generator. This was an extremely convenient setup permitting any desired frequency of oscillation to be exactly set in only a few minutes. The wind tunnel was then turned on and the plenum chamber pressure set. Polaroid time exposure pictures were taken of the previously calibrated dual beam oscilloscope using the internal time base. The upper trace was from the angle of attack potentiometer and the lower trace was from the pressure transducer. Approximately two runs per high pressure storage tank were possible, with two or three pressure taps recorded during each run. By switching the pressure port tubing, only one transducer was used, and the extra transducer was frequently used for comparison. It was found that running the Sullivan compressor during data acquisition did not affect the instrumentation.

H. SCHLIEREN PHOTOGRAPHY

A Hycam Model K2004E 16mm high speed movie camera (see Figure 19) was used in conjunction with the wind tunnel schlieren system as shown in Figure 1. Both the cone and the wedge were photographed at 2,4,8, and 16 cycles per second at 200, 400, 800 and 1600 pictures or frames per second. Thus 100 frames per cycle were taken, so that all speeds would look the same when projected. To adjust for the correct light exposure of ASA 200 film, it was found that numbers 1, 7, and 5 Dupont Varigam Filters were necessary for 200 and 400 fps speeds, a number 1 and 7 filter were needed for 800 fps, and a number 1 filter was used at 1600 fps. A pulse timer was used to put a blip at 100 or 1000 pulses per second on the film edge every few frames, depending on the film speed selected, thereby giving an additional check of the film speed and the model speed.

The resulting films were then edited with appropriate title shots to make a six-minute film. The attaching and detaching of the shock in starting and stopping the tunnel was also recorded.

In addition, a string of five frames of the film were blown up at four model positions:

1. Model at top of cycle
2. Model going down through zero AOA
3. Model at bottom of cycle
4. Model going up through zero AOA

Frames with the body at the exact same position relative to the tunnel were selected from the five frames and are in Appendix E.

III. RESULTS AND DISCUSSION

The basis for all pressure data taken in the experiment was the Statham pressure transducer whose calibration curve, shown in Figure 16, verifies that the pressure transducer was linear throughout the range of interest. Setting the voltage so as to read in inches of mercury directly was very convenient, and facilitated the continuous monitoring of the transducer calibration.

The dynamic calibration measurement of the pressure transducer system, presented in Appendix A, showed that the system had excellent response characteristics, and therefore negligible time delay in the data could be attributed to the pressure measuring system itself. The disagreement between the measured and theoretical natural frequency and damping ratio was large; however, both natural frequencies were of the same order and indicated that the system would respond to 16 cycles per second with negligible phase shift and amplitude distortion.

The measured cone static data agreed very well with Jones' data [4]. The theoretical and experimental quasi-steady measurements are plotted in Figure 20 for the cone at pressure tap angle $\phi = 0°$ and $180°$. In this plot, the theoretical curve was generated using the measured non-oscillatory zero angle of attack static pressure as a reference. Similar curves can be generated for the other

ϕ angles, and for the wedge or the flat plate; but since the essence of this investigation was to compare non-oscillatory data with oscillatory data, not experiment with theory, these additional curves were not reproduced here. When stationary at zero angle of attack, the measured shock angles and static pressures agree with those calculated by compressible flow theory within 1% for both the cone and the wedge [5]. The measured and computed shock angle for the cone was 30.5°, and similarly for the wedge was 34°. The computed theoretical cone pressure was 10.7 inches Hg; for the wedge it was 10.6 inches Hg, which agreed with the measured pressure within 3% experimental error.

The data presented in Appendices B, C, and D is quite extensive, and deserves considerable examination. At the beginning of each Appendix is a diagram labeling the various pressure ports. In the case of the cone the ϕ angle relationship is also shown. All the data were taken at Mach 2.8 with the plenum chamber pressure within 2% of 52.7 psi; these quantities are repeated at the beginning of each section, along with the grid scaling and other specific variables pertaining to the pressure traces which follow thereafter. The upper trace was always the angular potentiometer voltage, calibrated for maximum scaling, and the lower trace was always the pressure transducer voltage, also calibrated for maximum scale use. One unfortunate

characteristic of the 551 Dual Beam Oscilloscope is that the upper or lower trace is so limited in range on the grid that it is impossible to superimpose the two traces except in the small center one third of the grid.

Section B gives a trace of each of the six cone pressure taps for comparison. As can be seen, there is very little difference among them and therefore subsequent measurements were made using only two pressure taps, one extra for comparison. The pressure traces which did not cross were thought easiest to interpret and the forward-most and aft-most pressure taps on that side were chosen. This would have been pressure taps two and six in all cases; but when the cone was rotated to the ϕ angles 225° and 45°, the pressure taps one and five were put in that position.

The next Section, C, contains the data of primary interest. At this ϕ angle, 0° and 180°, the pressure taps were at the top and bottom of the cone, where they should encounter the greatest oscillatory effects. The first part is with the angle of attack varying ± 20°, and little difference in the traces is apparent until frequencies of at least six cycles per second are reached. On this trace the low pressure part of the pressure trace can be seen beginning to shift to the right. This trend continues, and is very noticeable at 16 cycles per second. The high pressure part of the pressure trace does not appear to shift until 8 cycles per second, and also becomes very noticeable at 16 cycles per second. There is a similar shift in the

center part of the pressure trace curve, causing the non-oscillatory zero angle of attack pressure to occur at higher or lower angle of attack than expected from the quasi-steady assumption, depending on which direction the cone is moving. These same trends are found in all of the categories of pressure trace data to varying degrees. These shifts will hereafter be referred to as high, low, or middle pressure shifts, or just pressure shifts.

In the second part of this section the angle of attack was increased to ±24°, and the same pressure shift trends were seen. At this angle of attack the uppermost ray (considering the positive angle of attack case) of the cone has gone past the horizontal, and is itself at an angle of attack of 4° relative to the flow; thus, the flow must expand to follow the cone surface, which is the limit of the numerical solution presented by D.J. Jones in Reference 1. Because of the higher pressures encountered, the pressure scaling was very coarse.

The non-oscillatory data in the next part, are exactly as originally recorded on the XY plotter in red and blue ink. Additional plots are given for all the pressure taps. The repeatability and lack of hysteresis was very good; however, the wind tunnel had small fluctuations in its "steady" flow, which is shown by the small perturbations in the XY plots. These same perturbations can be seen on the oscillating pressure traces which were previously discussed, although these perturbations are less noticeable at the higher frequencies.

The next Section, D, is for the pressure taps 45° between the horizontal and vertical planes of the flow. Again the same pressure shifts are noticed to begin at 6 cycles per second.

The last Section of the cone data, E, is for the pressure taps on the sides of the cone, which gave an unusual pressure trace. The non-oscillatory XY plots show that the static pressure on the sides of the cone decreases with increasing angle of attack and was sensitive to the particular pressure tap characteristics as well as location. By characteristics it is meant the minor disparities of the holes. Because of the expanded scaling of the pressure trace, the tunnel fluctuations are very apparent. The last two traces, for 8 and 10 cycles per second, are deceptive in that the scope calibration was slightly shifted, bringing the entire pressure trace upward and giving the effect of more pressure shift than there actually was.

The wedge data in Appendix C have pressure shifts which can be seen to be as low as 4 cycles per second. There is also noted a seemingly characteristic bump in the high pressure part of the trace, which is on both sides of the curve at low frequency and only on the right side at high frequency. The wedge, at 20 degrees angle of attack, is deflecting the flow 34° on the high pressure side. At Mach 2.8 the theoretical detachment angle is 32.6°, which is equivalent to a wedge angle of attack of 16.4°; hence the bump is apparently related to the shock attaching and

detaching, as is confirmed by the photography data. The detachment causes a decrease in pressure to the transducer and, with the pressure tap moving away from the locally detaching shock, the slight decrease in pressure is absorbed by the pressure tap when the wedge is oscillating fast enough. On the other hand, when the wedge is moving into the attaching shock, its local pressure is decreasing and the shock attachment is amplified giving the noticeable bump on the pressure trace.

The final pressure trace data, included in Appendix D, were obtained from the flat plate model oscillating at ±5°. This model was generally unsatisfactory, in that it blocked the tunnel much earlier than anticipated, thereby leading to construction of the wedge model. However, because the data show very little pressure shift, the amplitude of the oscillation must be considered as an important variable.

Due to time limitations, only four important aspects of this large quantity of data have been analyzed in this report. First, the shift in the angle of attack, at which the maximum, minimum, and non-oscillatory zero angle of attack pressure occurred, was plotted versus frequency of oscillation in cycles per second, as shown in Figures 21 thru 24. The zero angle of attack pressure shift was going from high to low pressure, that is, on the windward side proceeding into the flow. Second, the pressure change, from the non-oscillatory pressure, versus frequency of oscillation, was plotted for high, low, and zero angles of attack, as

shown in Figures 25 thru 28. Again, the zero angle of attack data were taken as the pressure was going from high to low pressure. Third, the time lag between the pressure trace peaks and the angle of attack trace peaks, and the non-oscillatory zero angle of attack pressure and position, was computed (centimeters measured times the time scale, s/cm) and plotted versus frequency, as shown in Figures 29 thru 32. Fourth, the phase angle shift was computed (time lag times frequency) and plotted versus frequency, as shown in Figures 33 thru 36. In all these curves, once the value went to zero it was no longer plotted.

From these four sets of data, the following significant trends were noted:

1. The departure of the oscillatory pressure data, from the non-oscillatory pressure data, occurred at approximately six cycles per second for all models; therefore, the quasi-steady approximation is good up to this frequency.

2. The greatest departure of the data occurred when the transverse velocity of the model was a maximum, that is when passing through zero angle of attack.

3. The curves show greater departure of data points taken at low pressures than data points taken at high pressures; hence, the higher the pressure measured, the less it was affected by the frequency of oscillation. In other words the high pressure peaks on the traces shifted less than did the zero angle of attack or the low pressure peaks.

4. The greater oscillation amplitudes exhibited greater deviation from non-oscillatory conditions because of the proportionately greater transverse velocity through zero angle of attack, and the greater pressure extremes being measured.

5. All the curves appear to be linear, and the phase lag curves appear to originate from zero.

As the plots show, the data have a good amount of experimental data spread, and some curves do not follow these trends completely or as well as others.

The results indicate that the variables which most strongly control the departure of oscillatory data from the non-oscillatory data appear to be: the frequency, the magnitude of the pressure being measured, the amplitude of oscillation, and the resultant transverse velocity of the static pressure port.

The high speed schlieren photographs, presented in Appendix E, show the models at the top and bottom of their cycles, and at zero angle of attack going in both directions. The frames were selected by carefully matching the angle relative to the vertical bar of the wind tunnel, and identical angles are presented for each frequency. The shock angles of the flow were compared, high frequency to low frequency, within each category for each model. The differences in the shock angles were of the order of 1/2 degree, which was of the same order as the accuracy of the measurements. Therefore, it is observed that the high speed

schlieren photography data do not show any significant difference in the shock wave angles at high and low oscillation speeds. This inability to measure the small changes that may exist is most probably because of the short resident time of the inviscid flow past the body. (The flow is in the vicinity of the body approximately 3.8 microseconds). Since the inviscid flow is the dominant feature of the shock structure, it was not too surprisong that oscillatory effects did not show up. On the other hand, the residence time of the flow in the viscous shock layer of the body is many orders of magnitude greater, and the oscillation effects were perceivable in the pressure measurements.

The photographs do show quite well the action of the flow going around the bodies. For the cone, the curved shock in the vicinity of the cone afterbody and the flow disturbance generated at the base on the leeward side are clearly seen. For the wedge, the curved shock caused by excessive turning angle and the almost imperceivable standoff distance at the leading edge are shown. On some of the photos the static pressure tubing was not completely sealed, and the air bleeding back into the tunnel can be seen. Small perturbations in the upstream flow are also present in the photographs.

IV. CONCLUSIONS

The present data show that at approximately six cycles per second the quasi-steady assumption begins to be invalid for the models studied. However, other variables, namely the magnitude of the pressure being measured, the amplitude of oscillation, the transverse velocity of the static pressure port, as well as the flow velocity appear to play an important part. Attempts to combine these variables into a meaningful non-dimensional parameter were begun; however, due to time considerations this work was left for later more complete analysis.

The experimentally measured shock angles, on the other hand, were relatively unaffected by the model oscillations and followed the quasi-steady assumption up to the highest oscillation frequency measured.

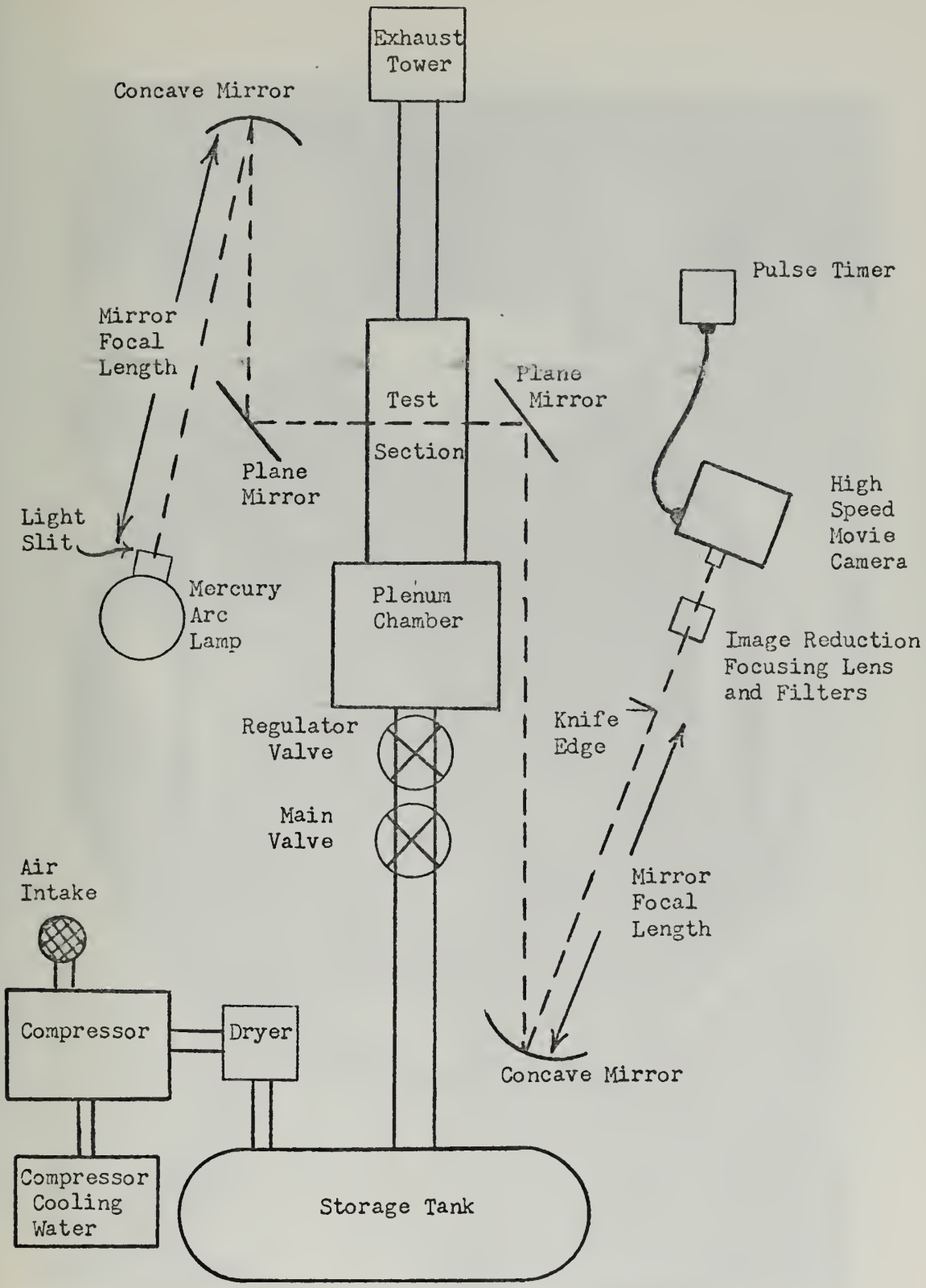

FIGURE 1 WIND TUNNEL AND SCHLIEREN LAYOUT

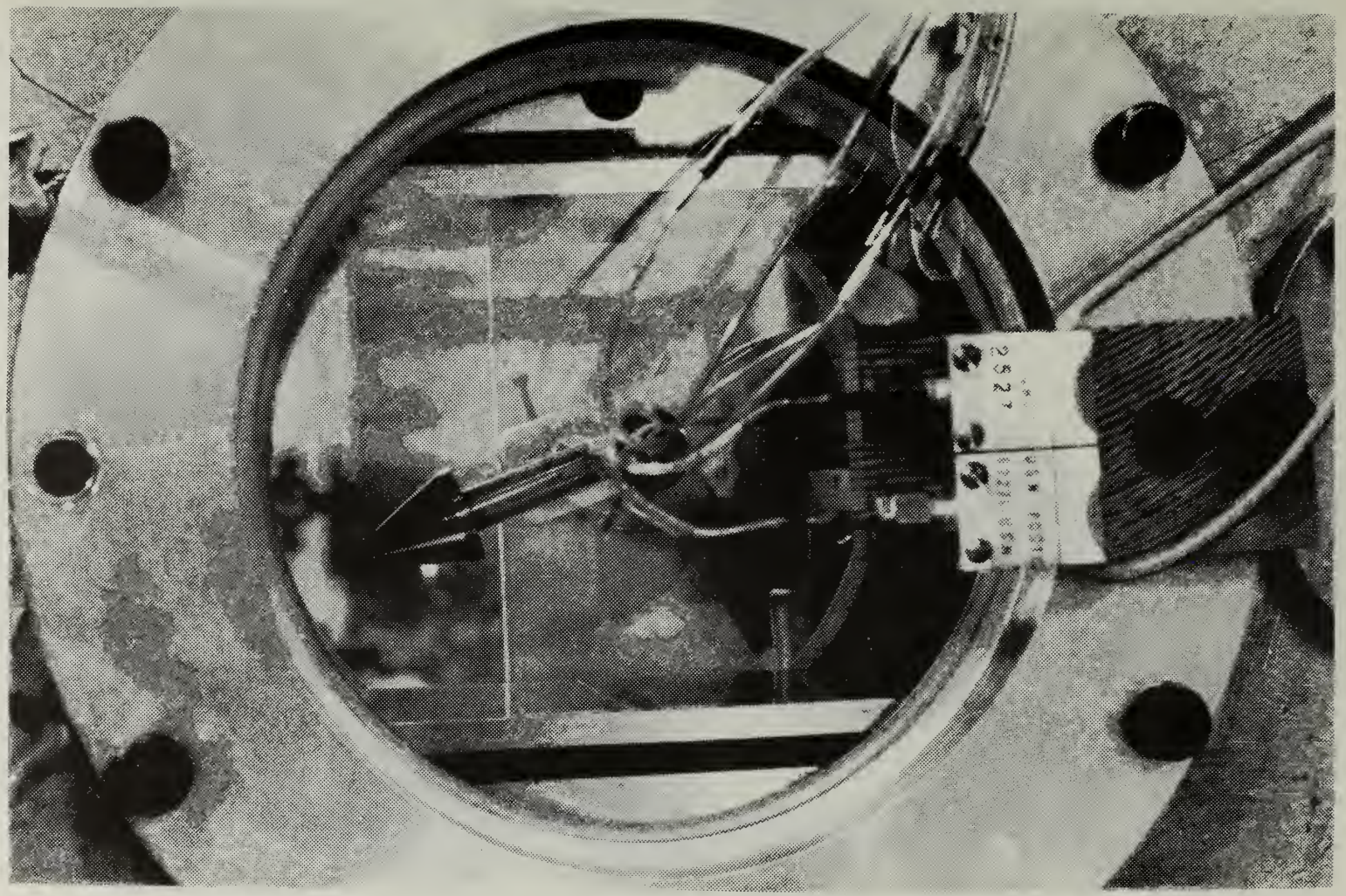

FIGURE 2 TEST SECTION, PRESSURE TRANSDUCER SIDE

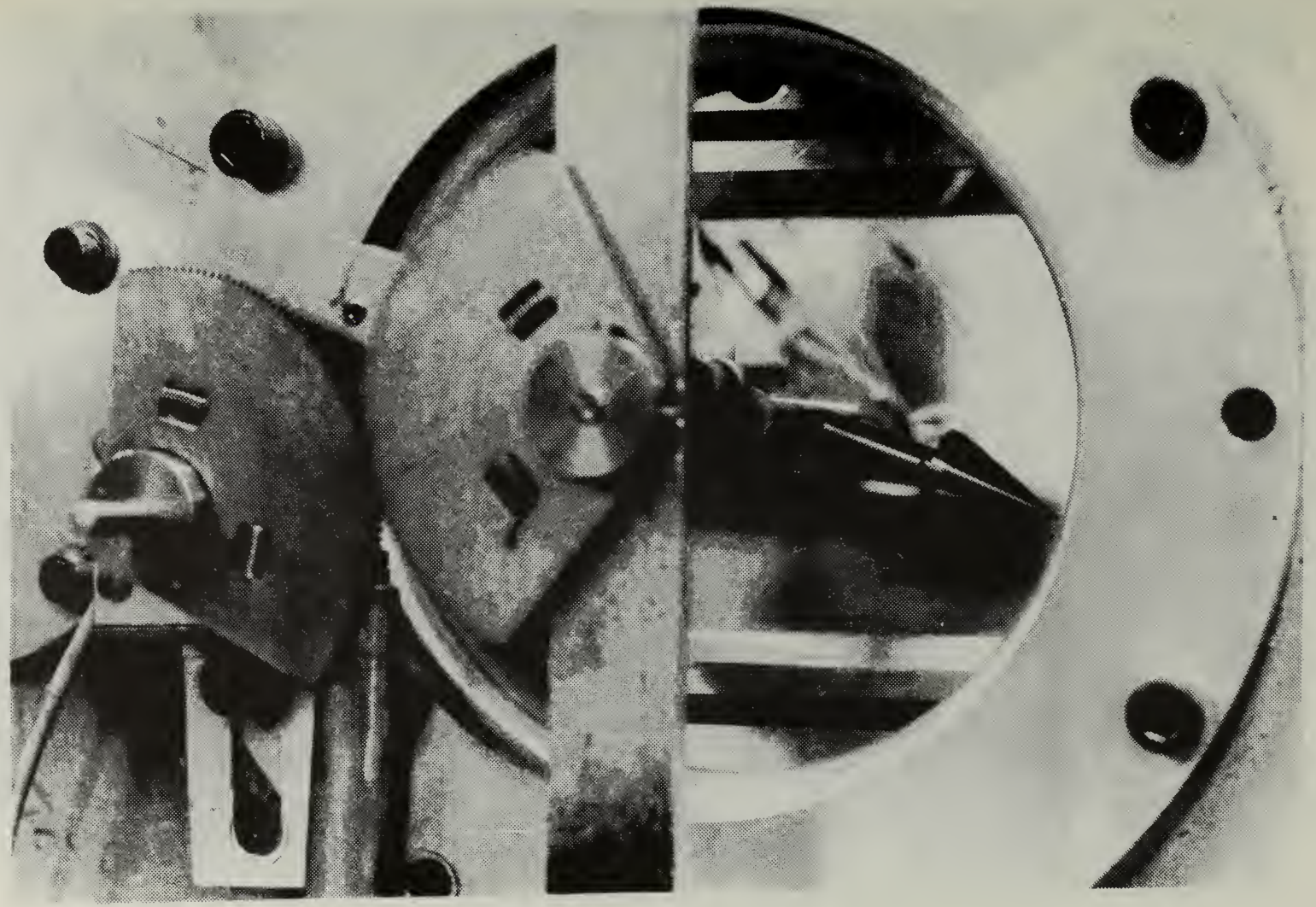

FIGURE 3 TEST SECTION, ANGULAR GEARING SIDE

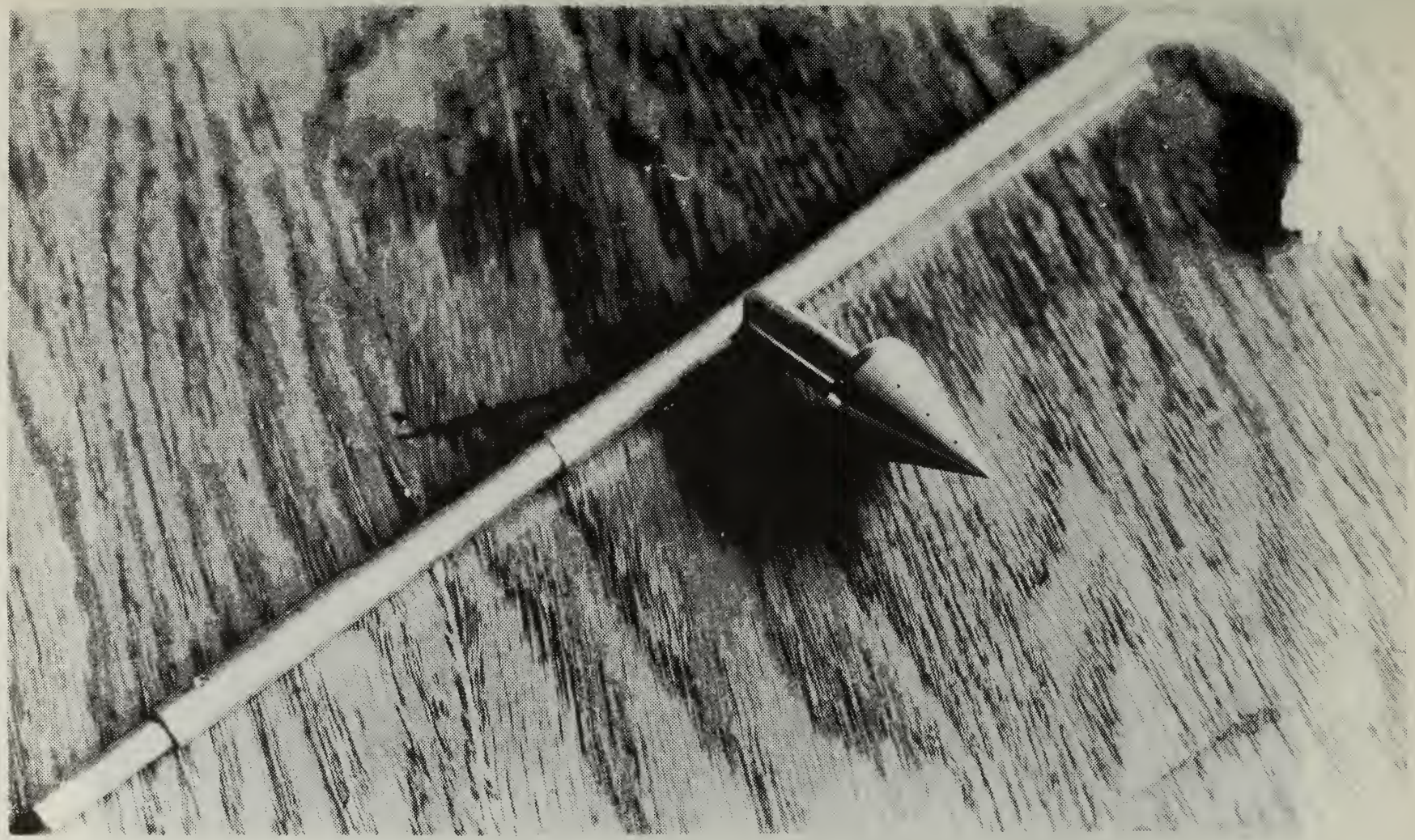

FIGURE 4 CONE MODEL

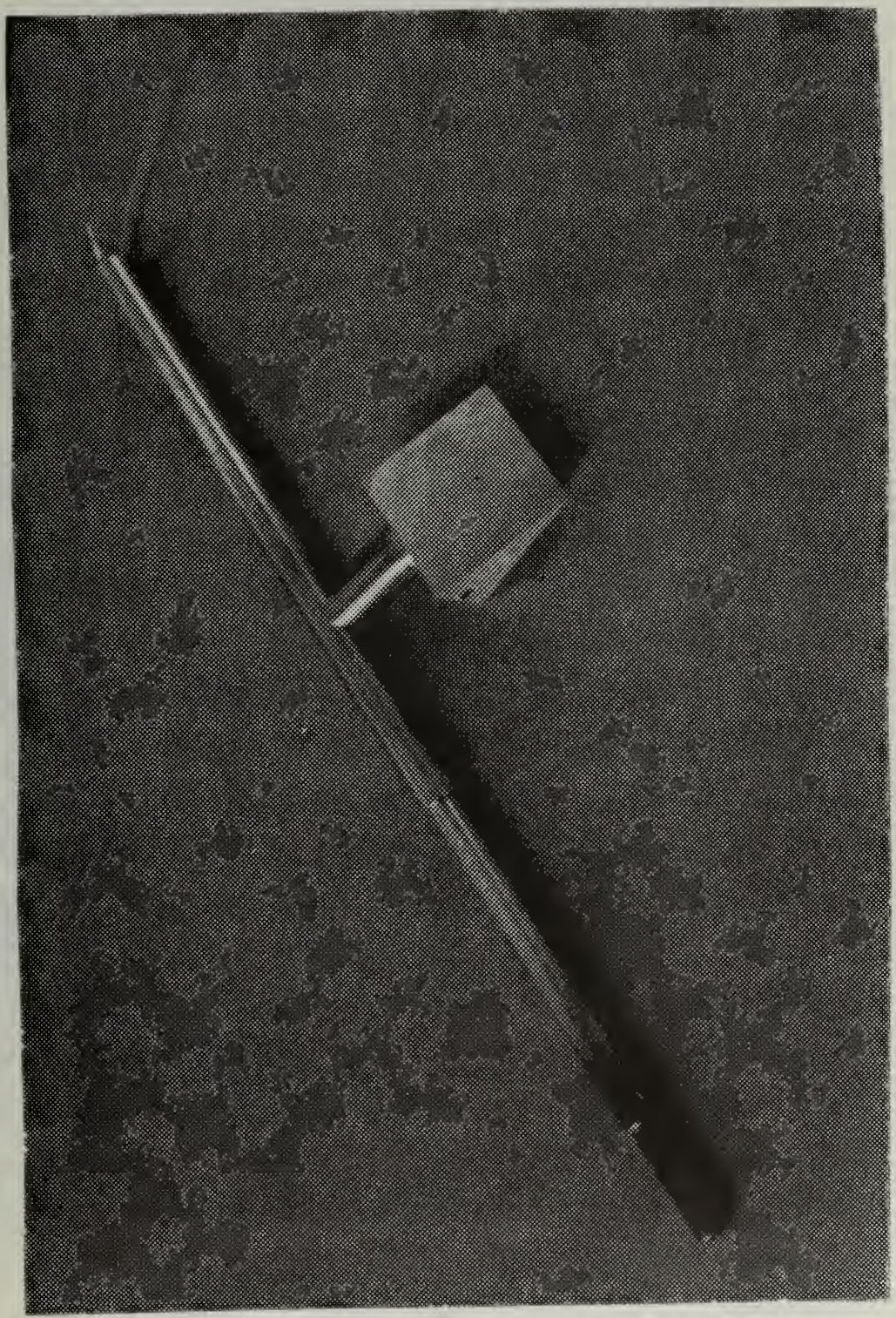

FIGURE 5 WEDGE MODEL

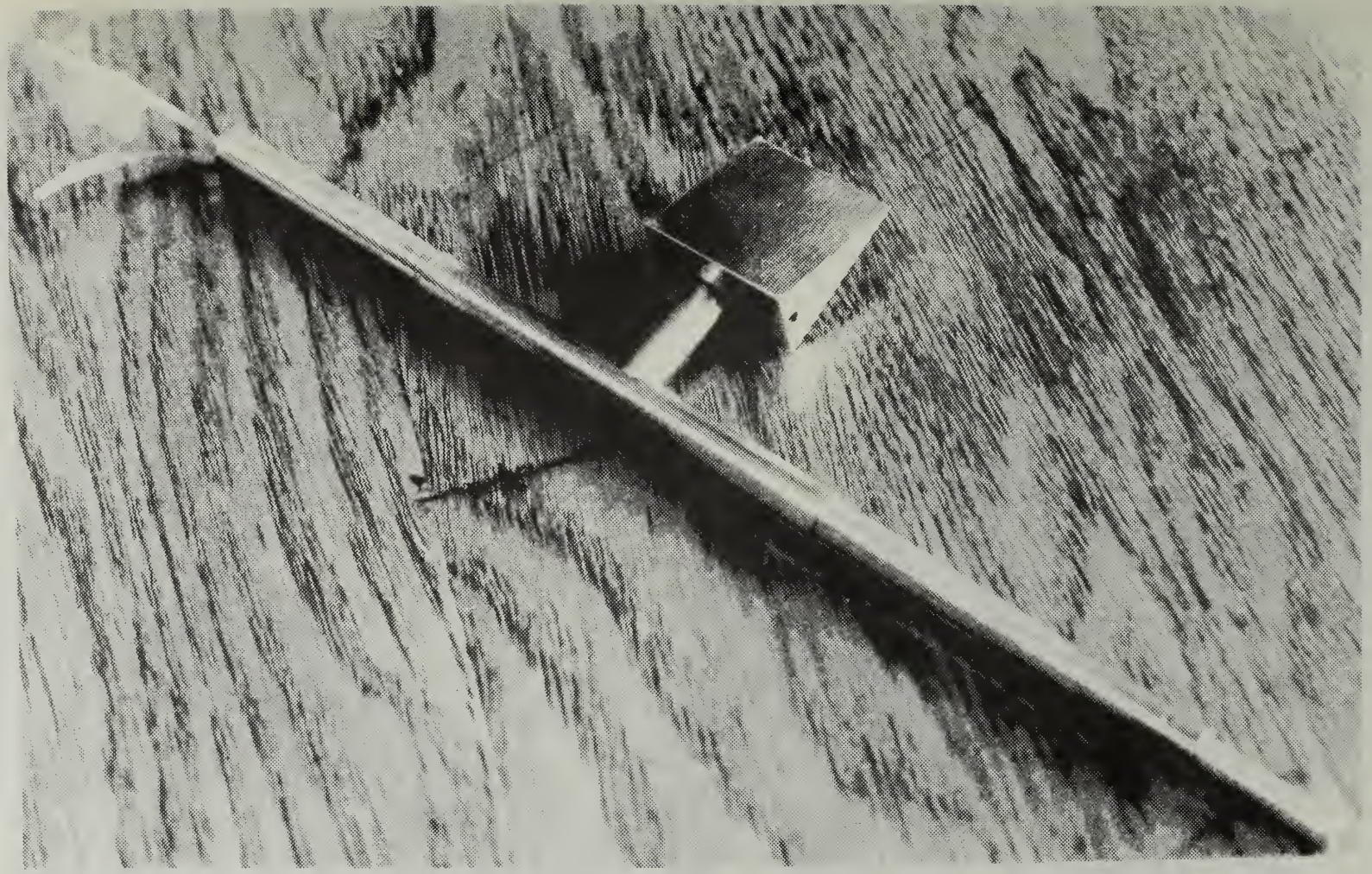

FIGURE 6 WEDGE MODEL

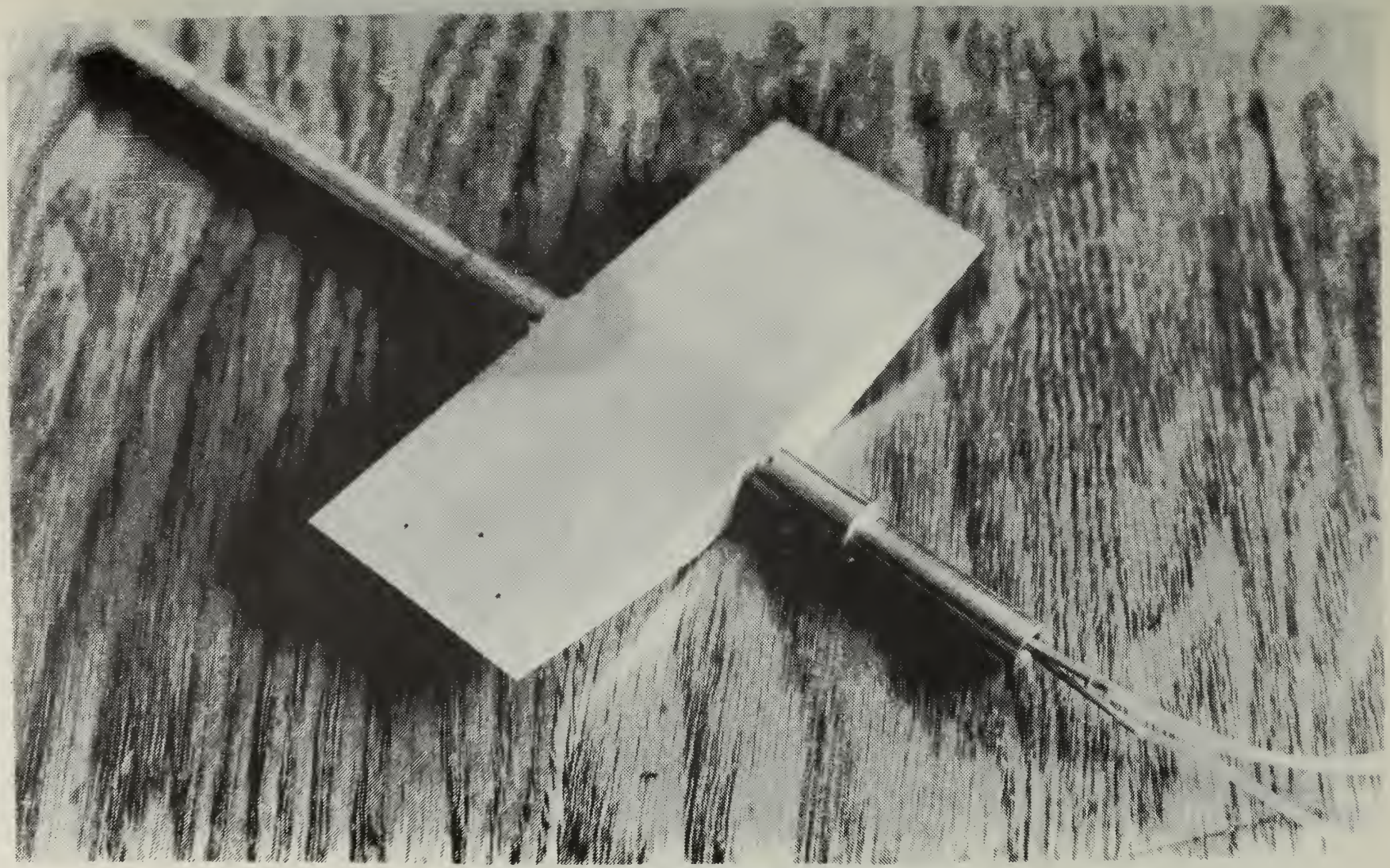

FIGURE 7 FLAT PLATE MODEL

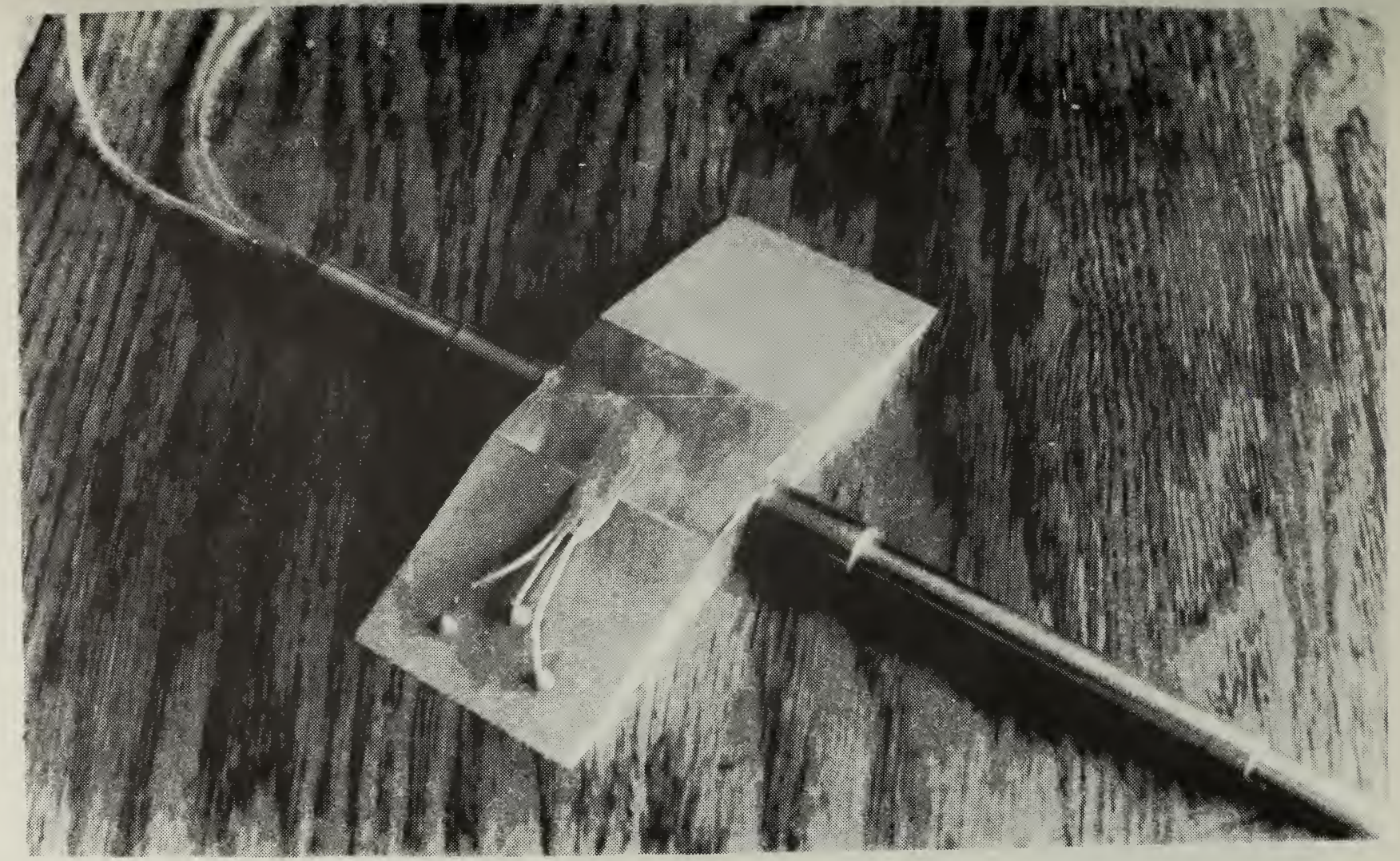

FIGURE 8 FLAT PLAT MODEL, BOTTEM VIEW

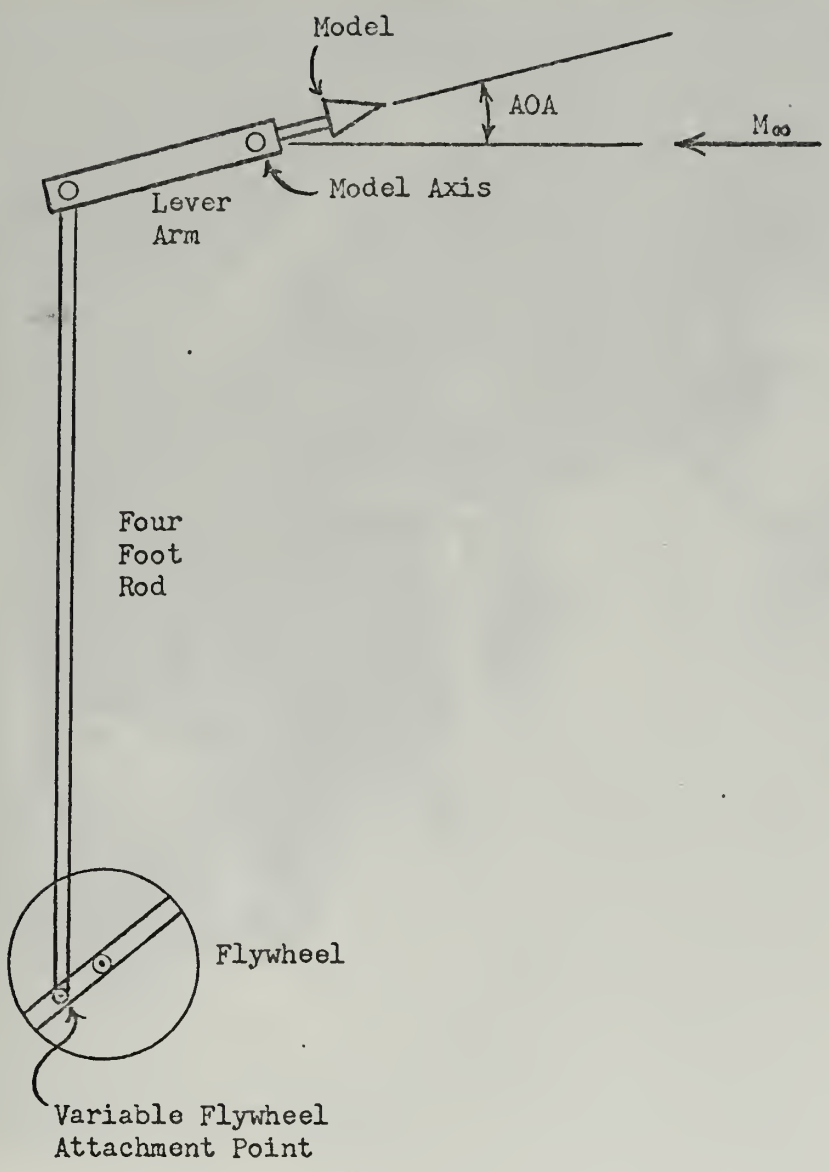

FIGURE 9

WIND TUNNEL MODEL DRIVING MECHANISM

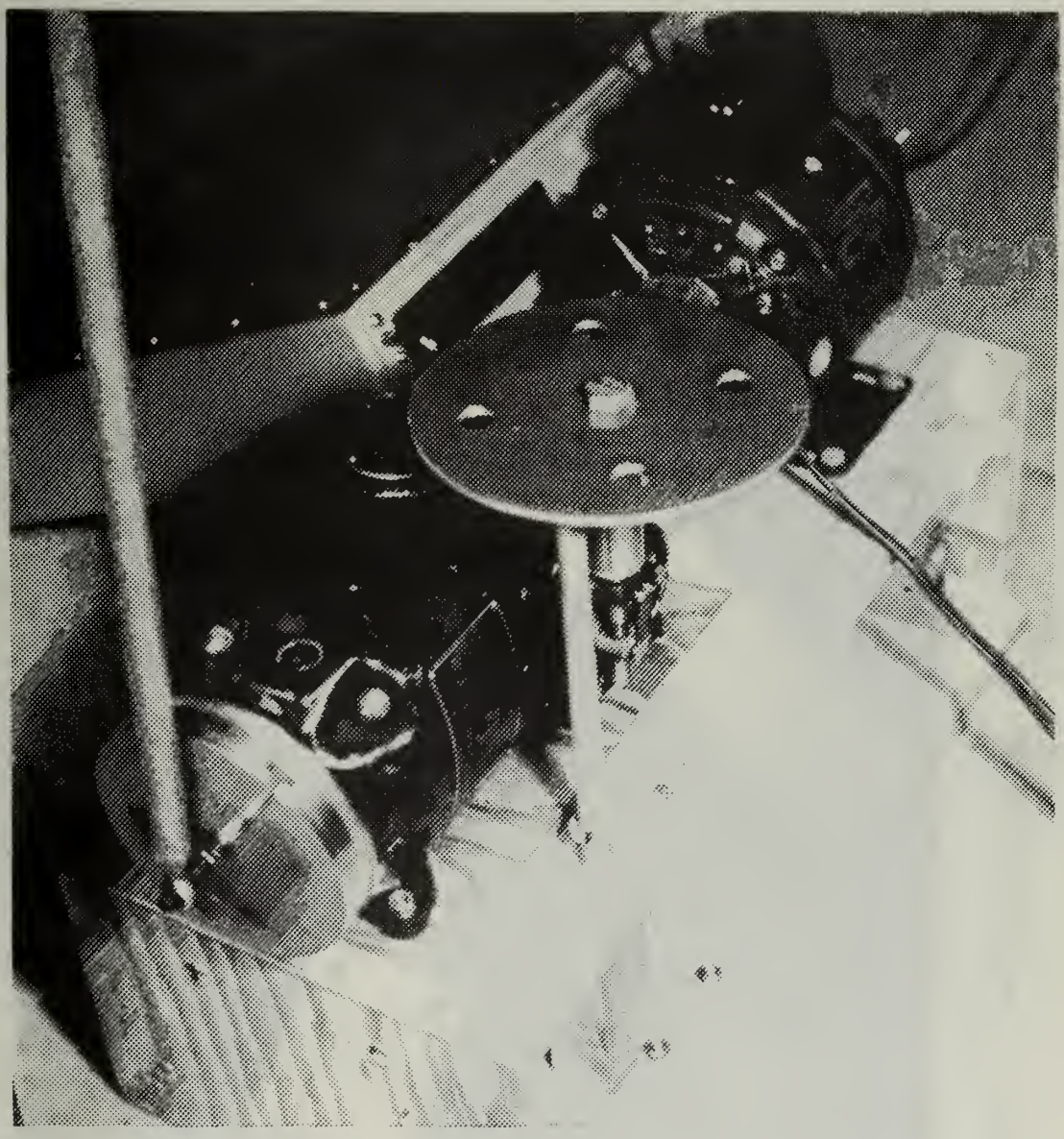

FIGURE 10

TRANSMISSION, MOTOR, FLYWHEEL, AND FREQUENCY COUNTER

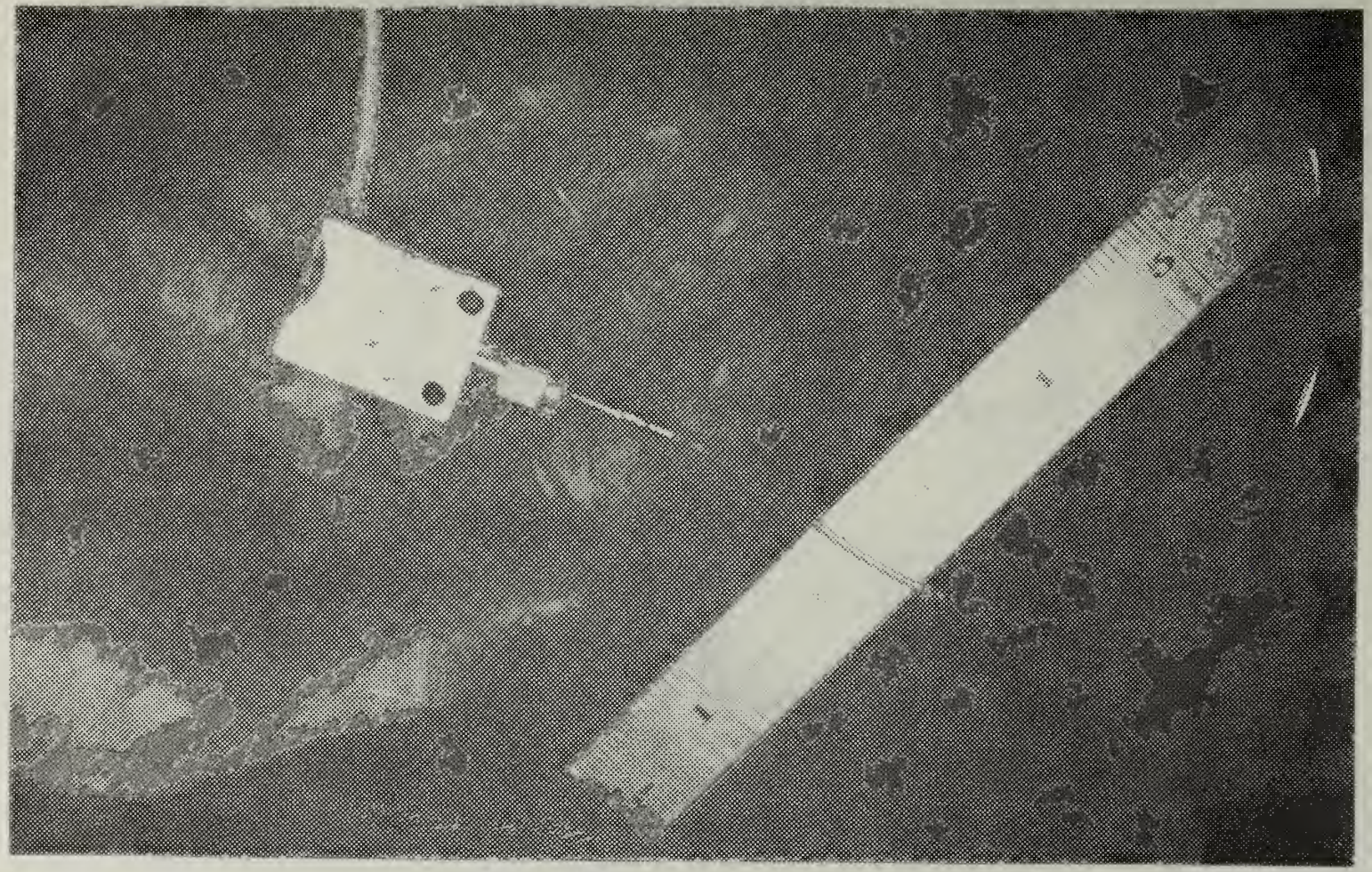

FIGURE 11 PRESSURE TRANSDUCER AND 8.2 INCHES OF TUBING

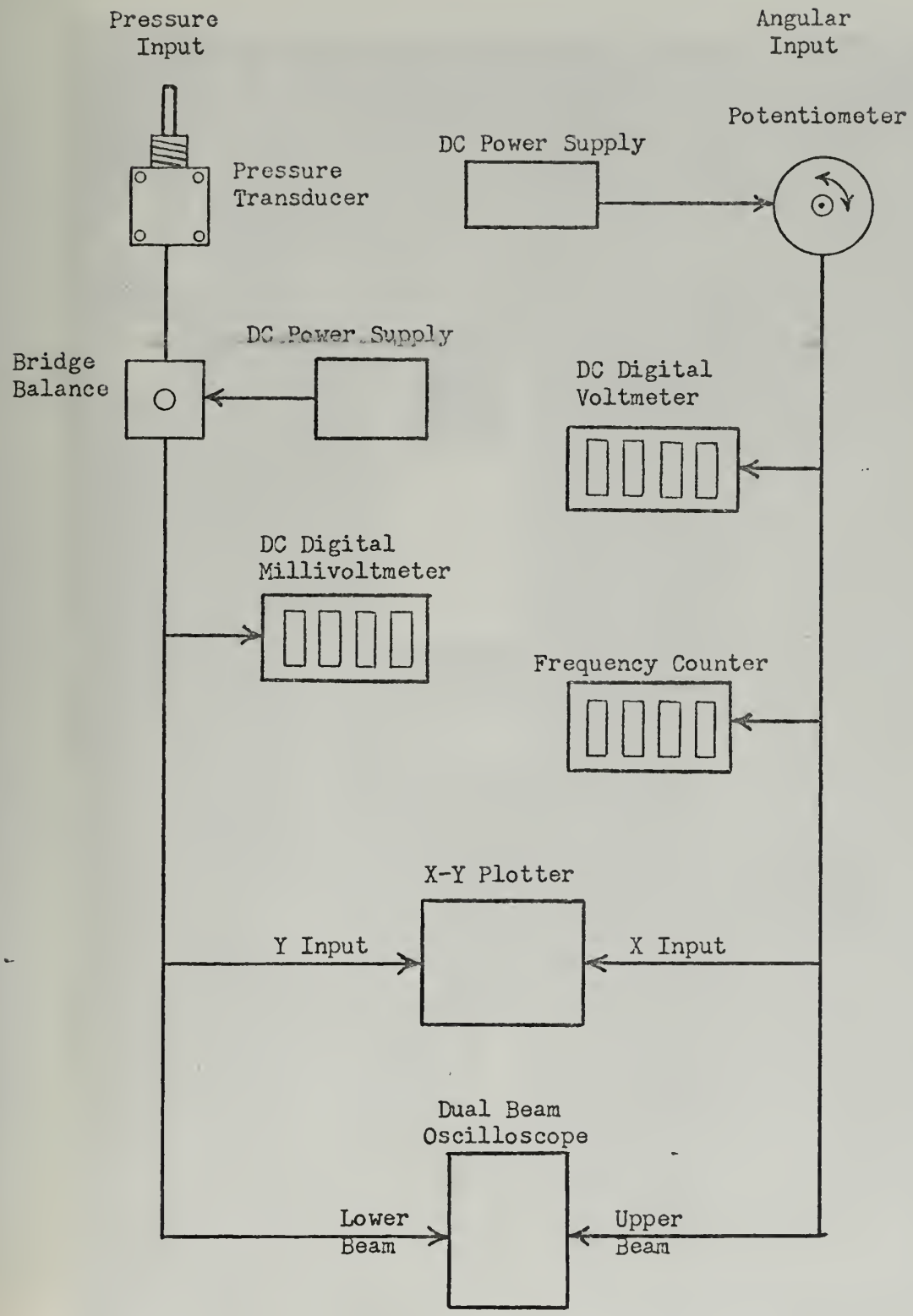

FIGURE 12 INSTRUMENTATION LAYOUT

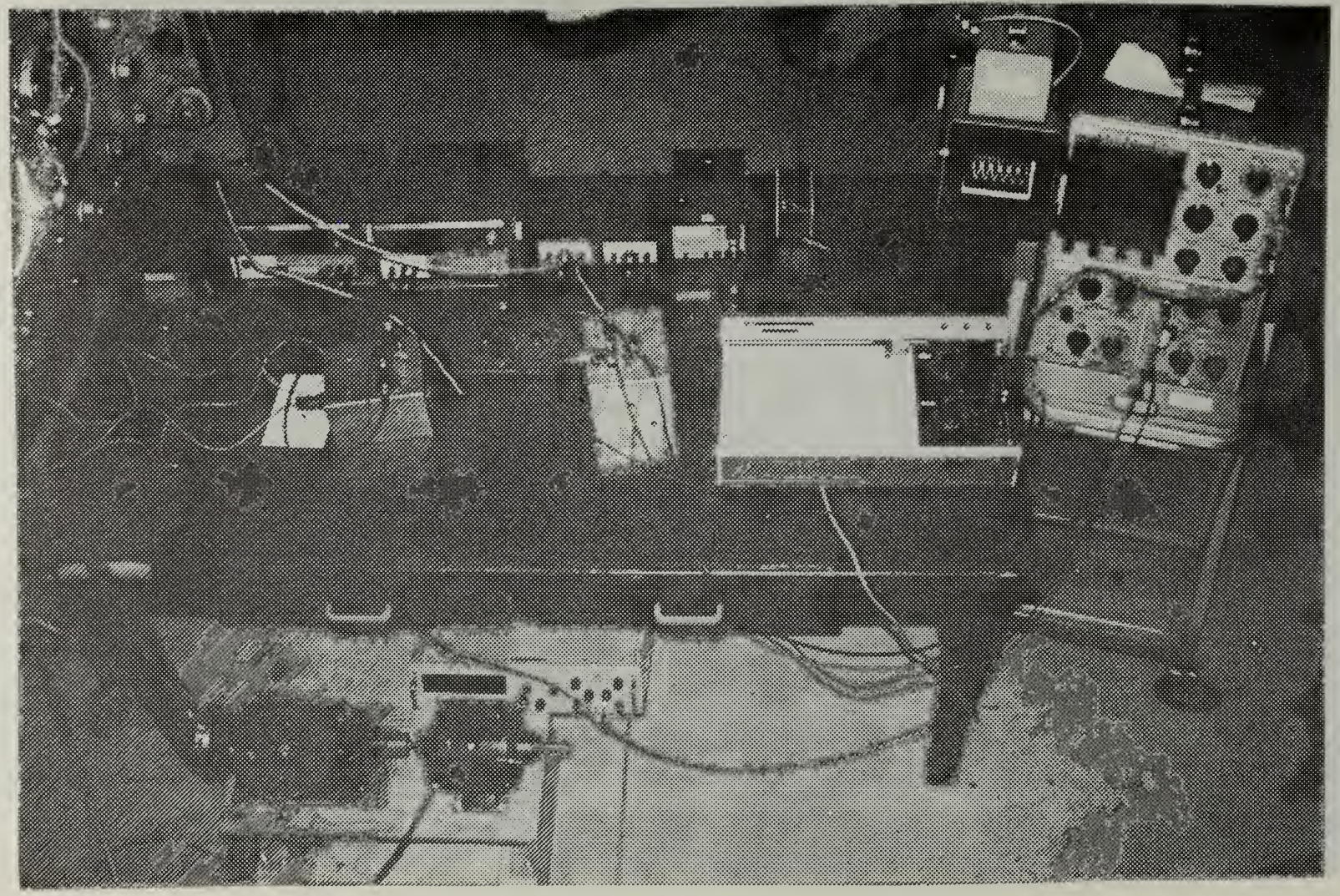

FIGURE 13 EQUIPMENT LAYOUT

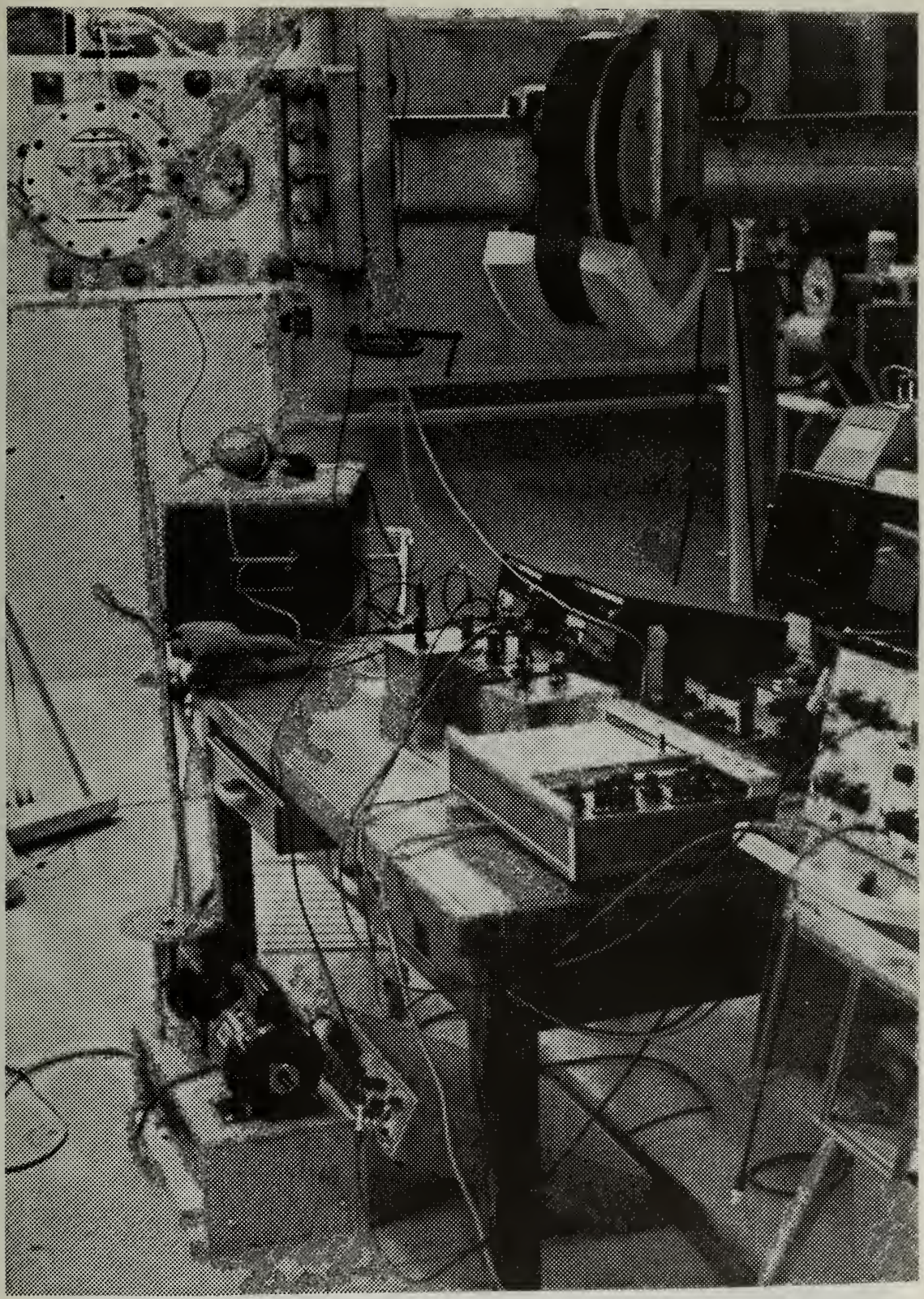

FIGURE 14 EQUIPMENT SETUP

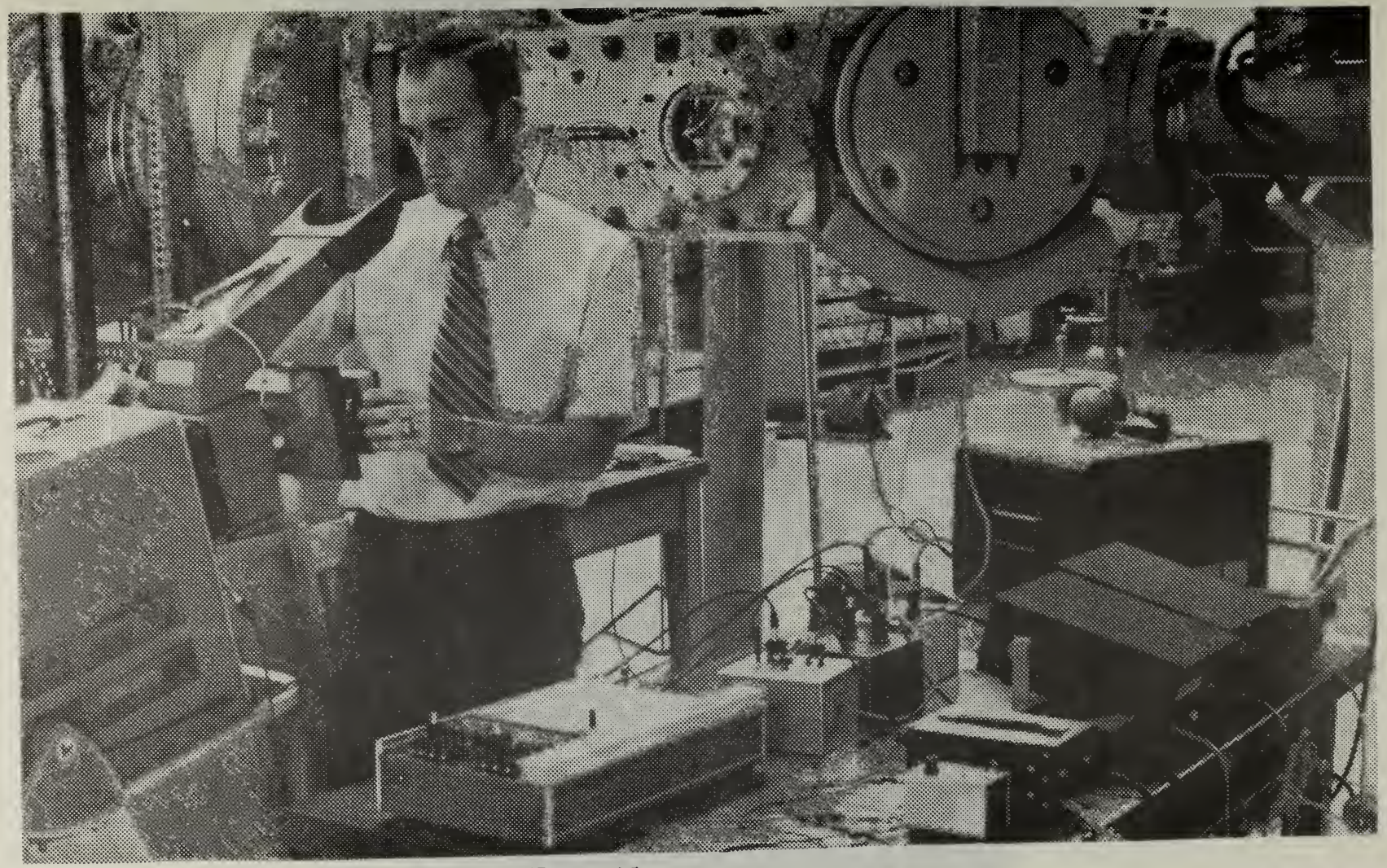

FIGURE 15 EQUIPMENT SETUP

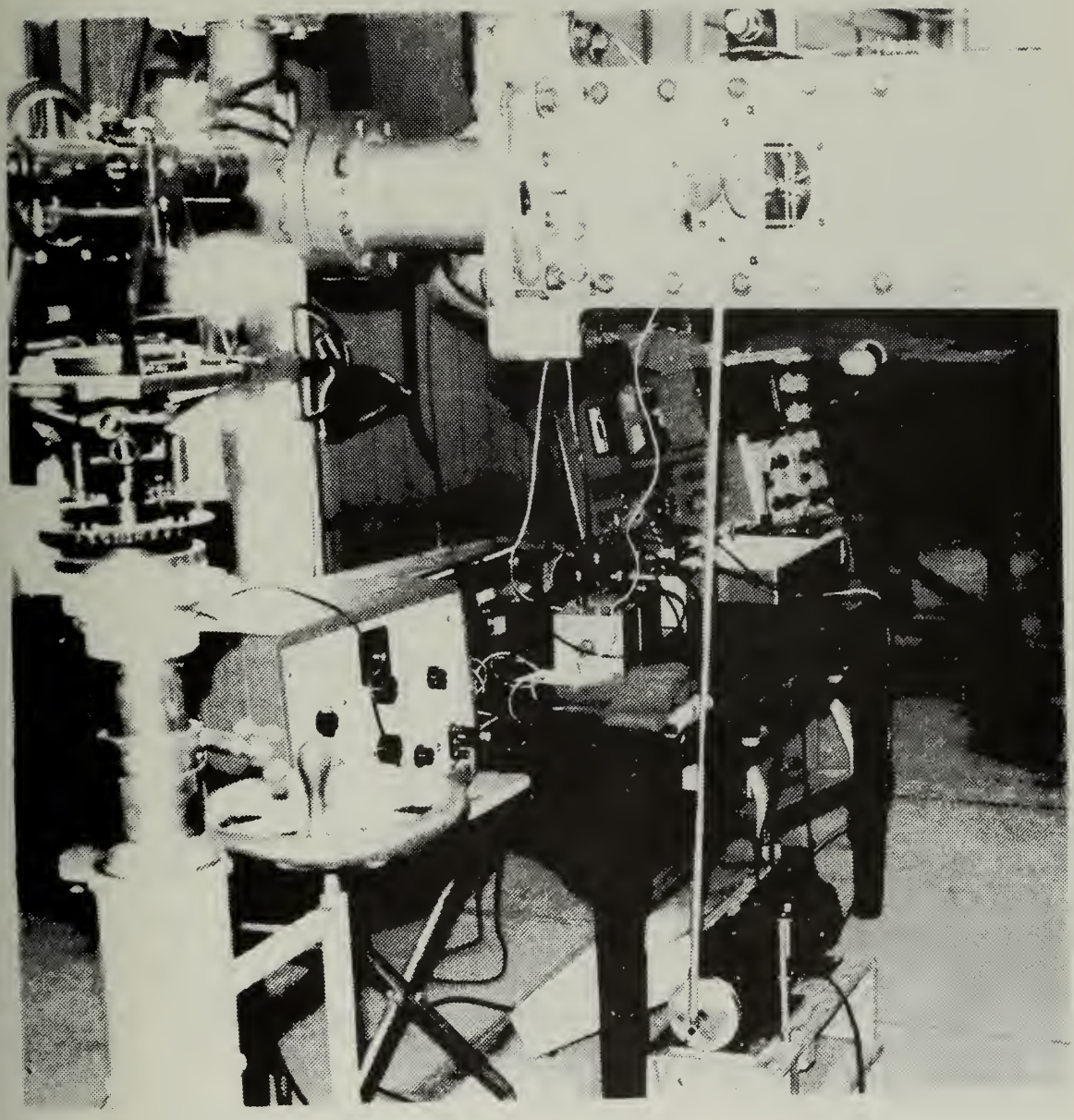

FIGURE 16

TRANSIT SETUP

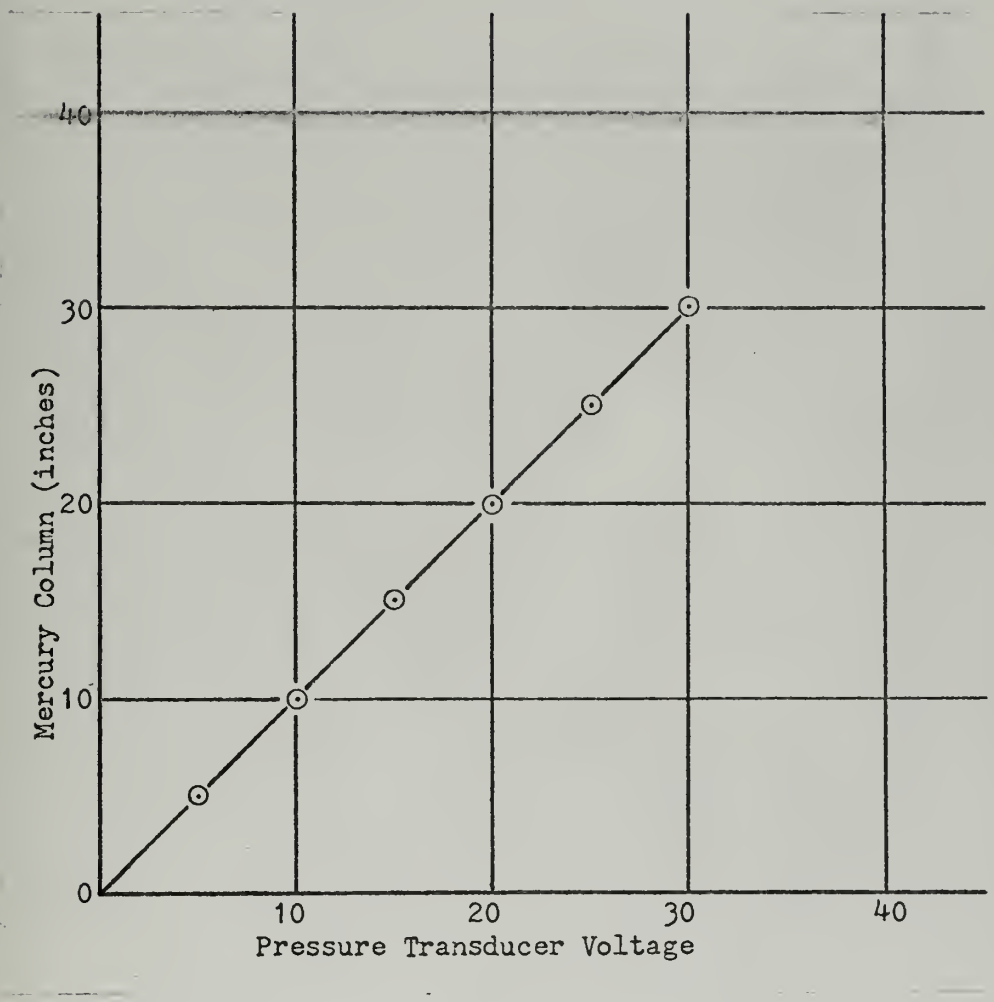

FIGURE 17

PRESSURE TRANSDUCER STATIC CALIBRATION CURVE

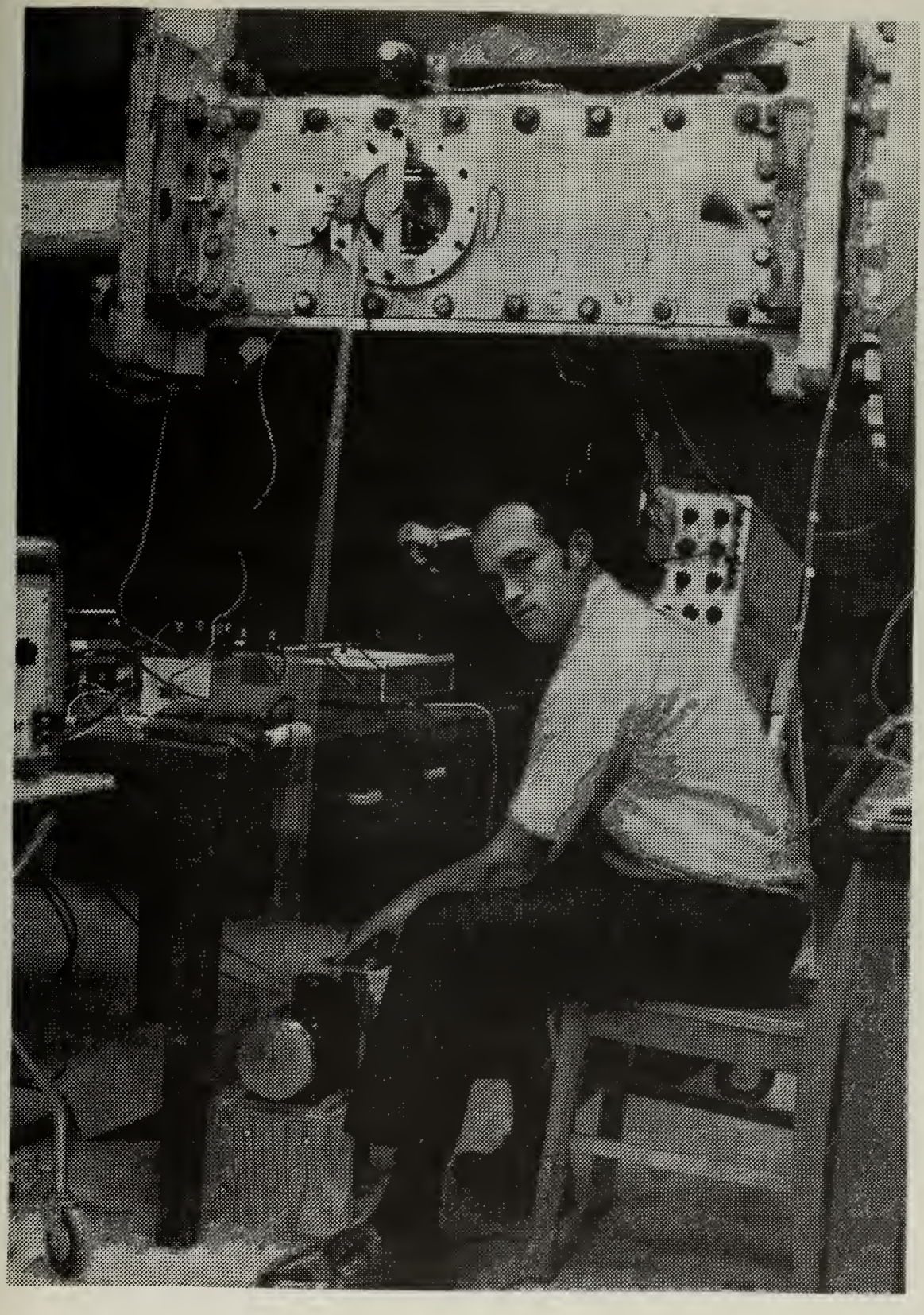

FIGURE 18 FREQUENCY ADJUSTMENT

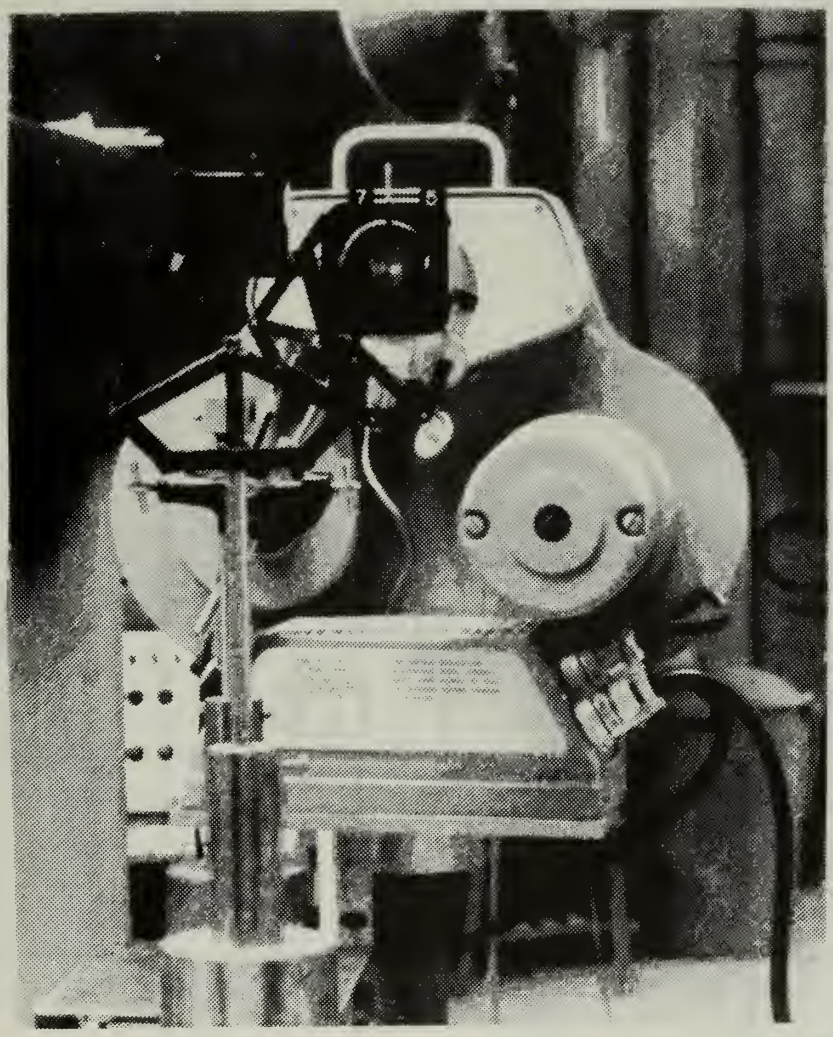

FIGURE 19

HIGH SPEED MOVIE CAMERA, FOCUSING LENS,

FILTERS, AND KNIFE EDGE

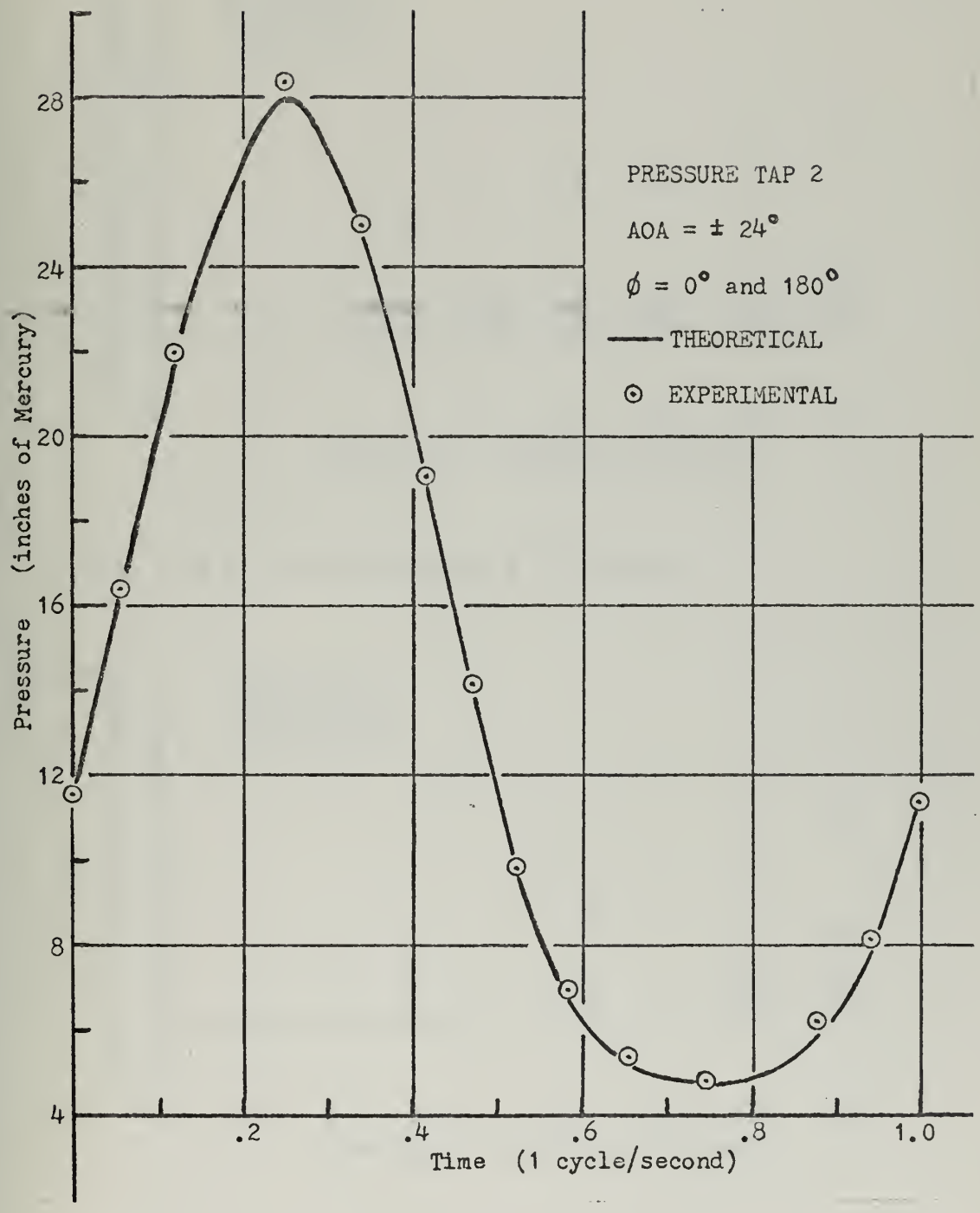

FIGURE 20

CONE PRESSURE COMPARISON PLOT

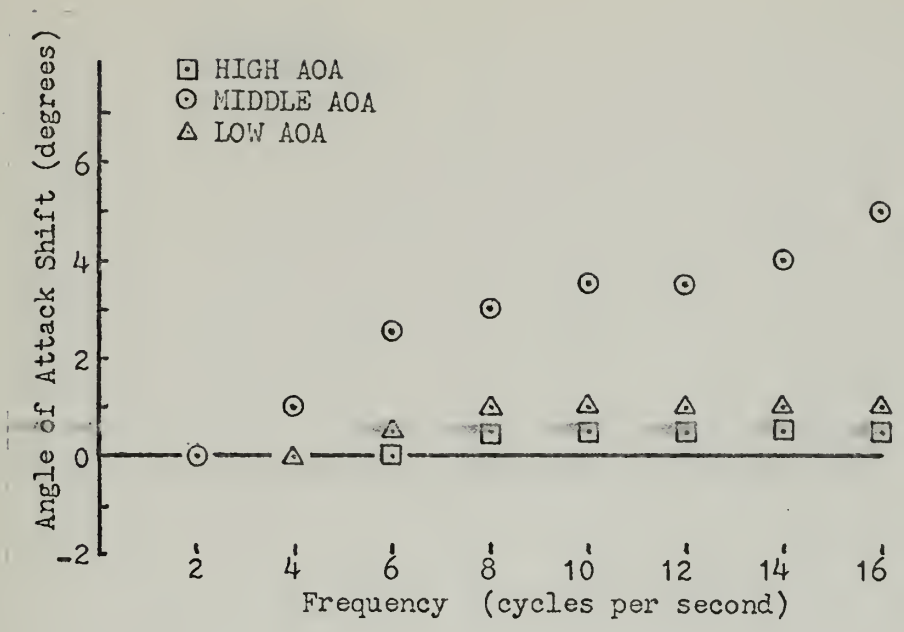

CONE -- ϕ = 0° and 180°, AOA = ± 20°, Tap 6.

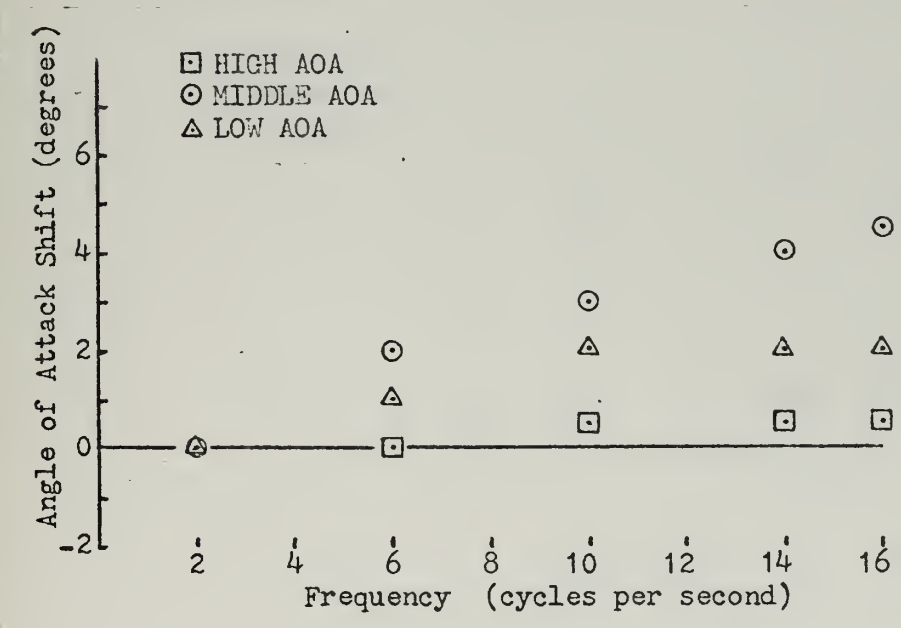

CONE -- ϕ = 0° and 180°, AOA = ± 24°, Tap 6.

FIGURE 21 ANGLE OF ATTACK SHIFT CURVES

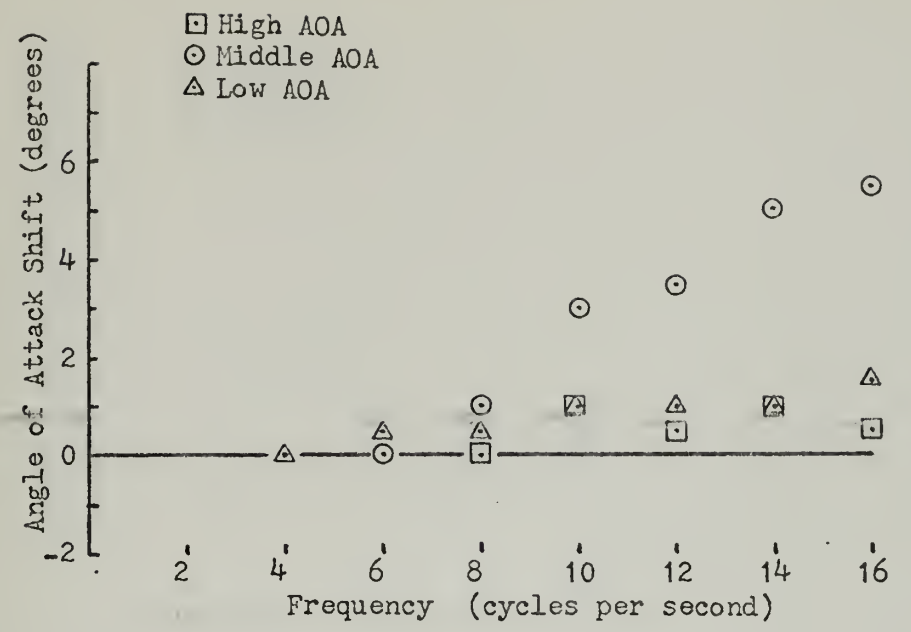

CONE -- ϕ = 225° and 45°, AOA = ± 20°, Tap 5.

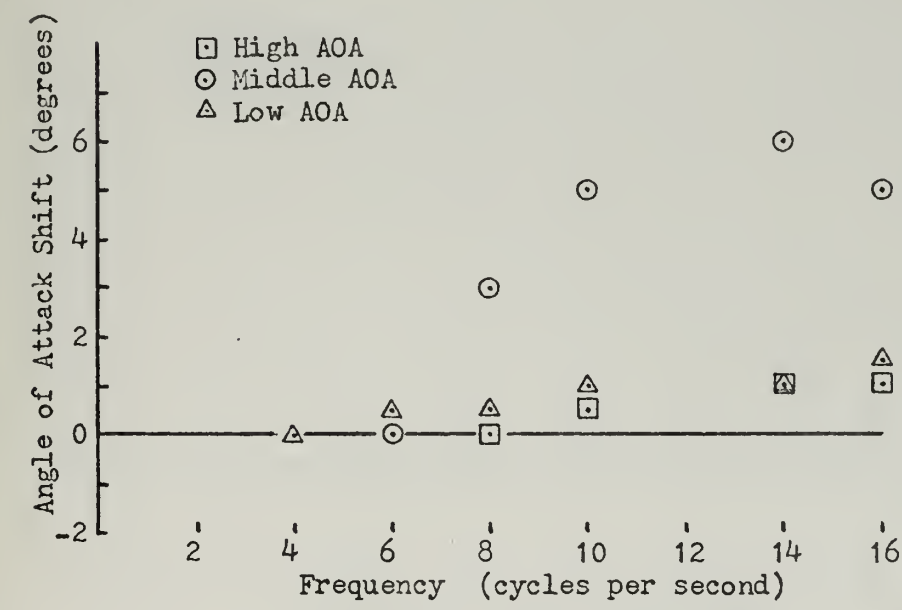

CONE -- ϕ = 225° and 45°, AOA = ± 24°, Tap 5.

FIGURE 22 ANGLE OF ATTACK SHIFT CURVES

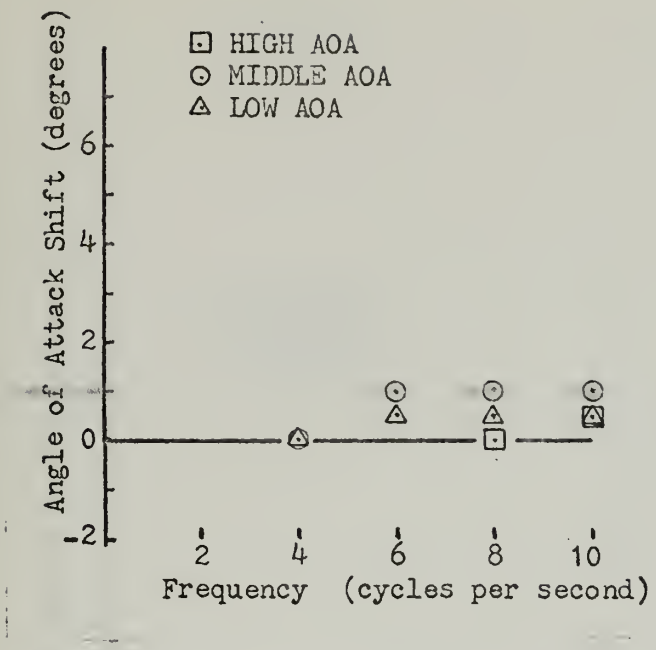

CONE -- ϕ = 90° and 270°, AOA = ± 20°, Tap 6.

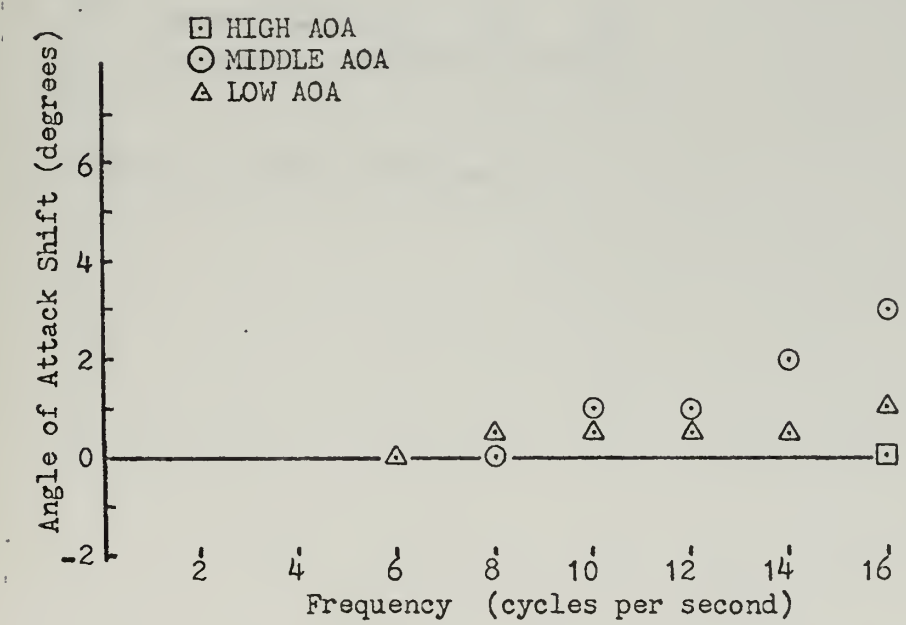

WEDGE -- AOA = ± 20°, Tap 2.

FIGURE 23 ANGLE OF ATTACK SHIFT CURVES

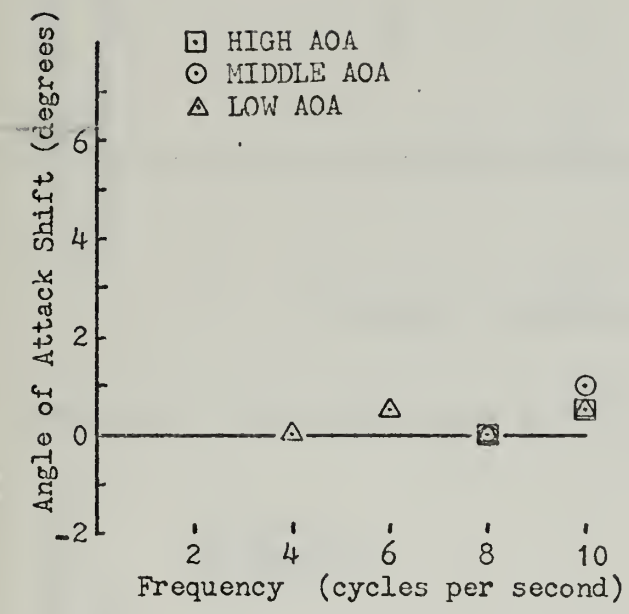

FLAT PLATE -- AOA = ± 5°, Tap 2.

FIGURE 24 ANGLE OF ATTACK SHIFT CURVE

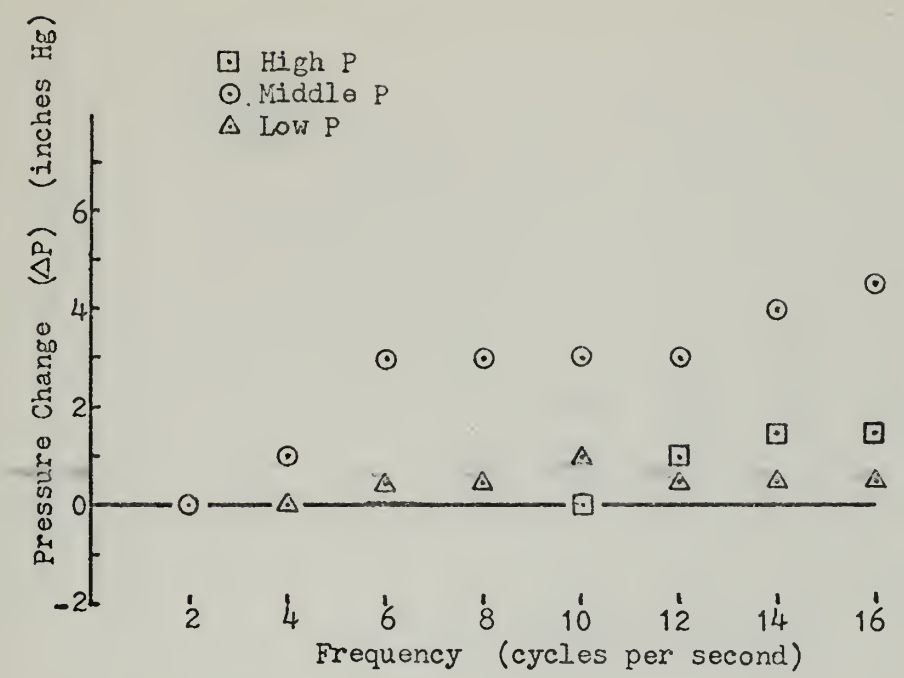

CONE -- $\phi = 0°$ and $180°$, AOA = $\pm$ $20°$, Tap 6.

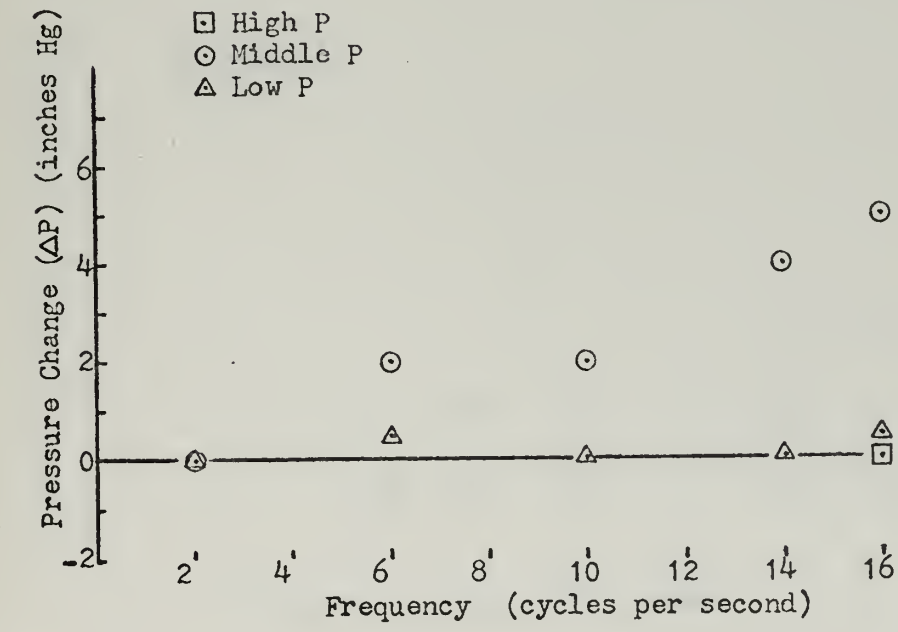

CONE -- $\phi = 0°$ and $180°$, AOA = $\pm$ $24°$, Tap 6.

FIGURE 25 PRESSURE CHANGE CURVES

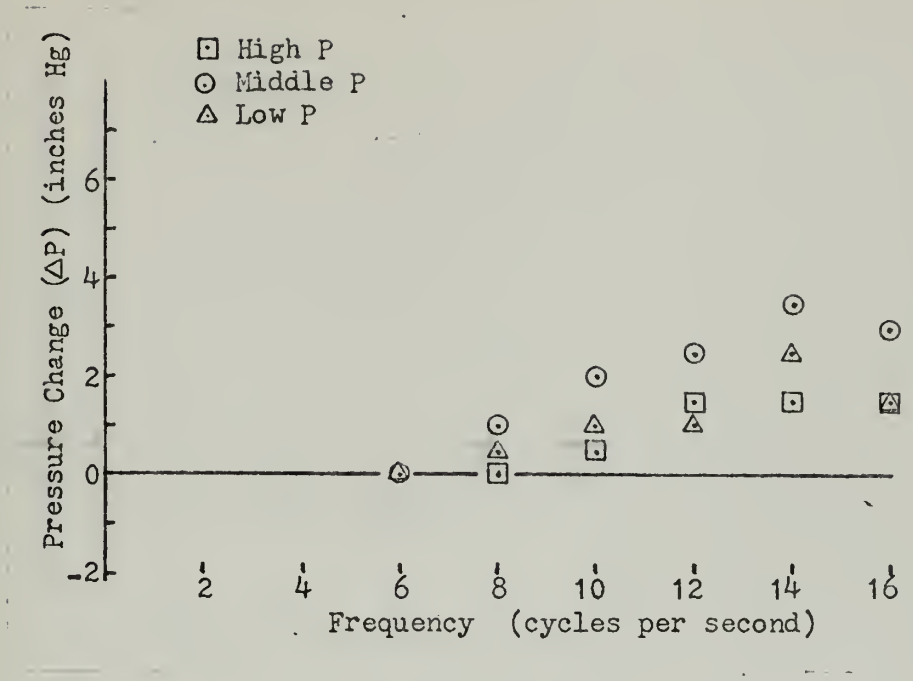

CONE -- ϕ = 225° and 45°, AOA = ± 20°, Tap 5.

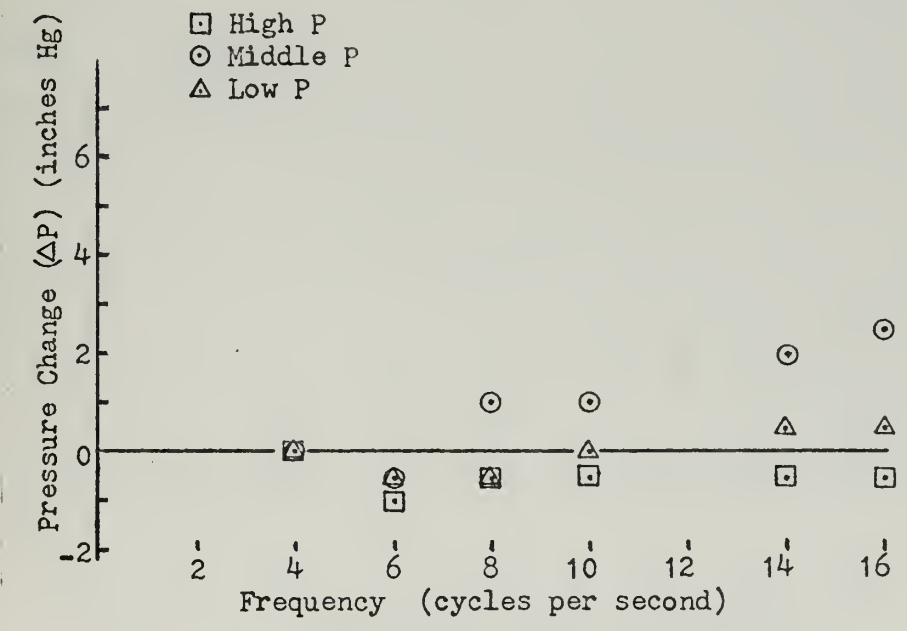

CONE -- ϕ = 225° and 45°, AOA = ± 24°, Tap 5.

FIGURE 26 PRESSURE CHANGE CURVES

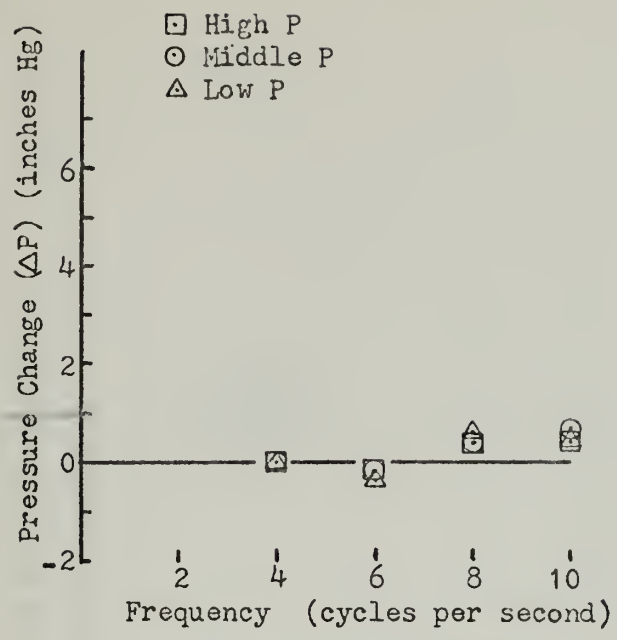

CONE -- $\phi = 90^\circ$ and 270°, AOA = $\pm$ 20°, Tap 6.

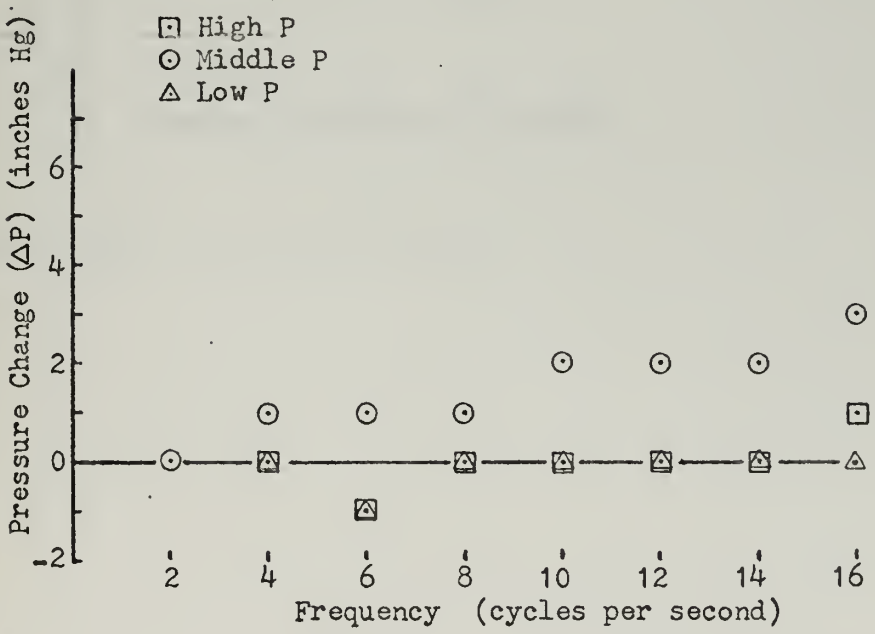

WEDGE -- AOA = $\pm$ 20°, Tap 2.

FIGURE 27 PRESSURE CHANGE CURVES

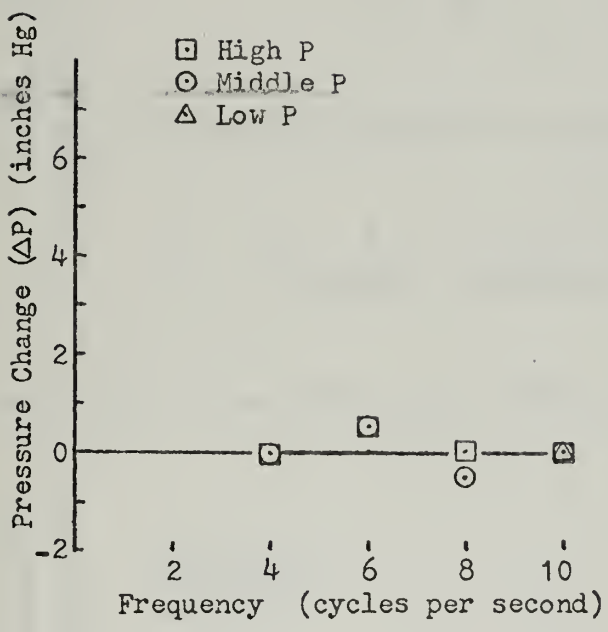

FLAT PLATE -- AOA = ± 5°, Tap 2.

FIGURE 28 PRESSURE CHANGE CURVE

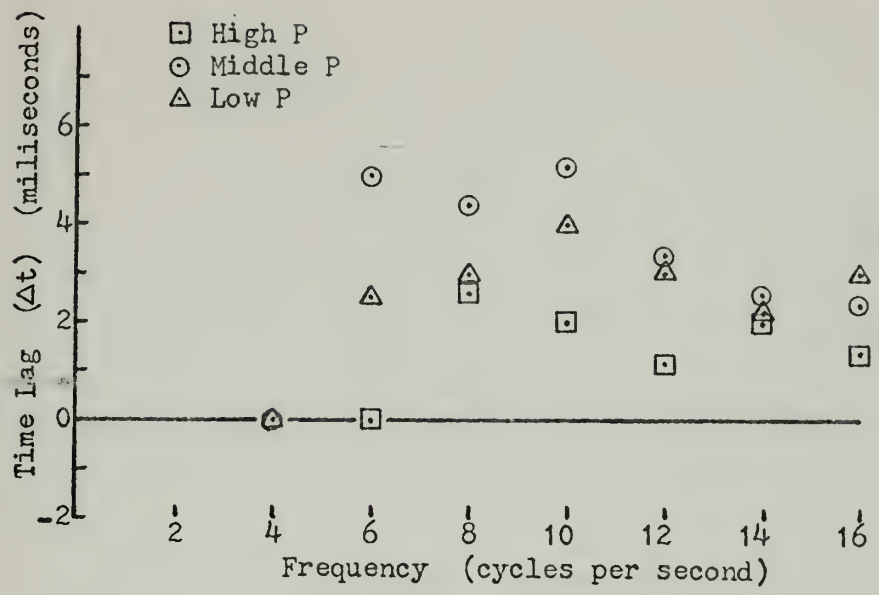

CONE -- ϕ = 0° and 180°, AOA = ± 20°, Tap 6.

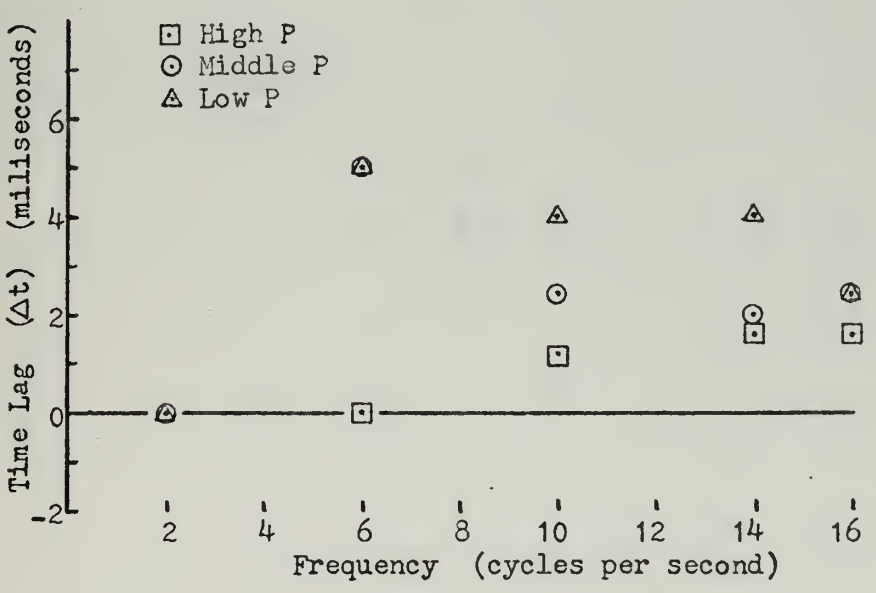

CONE -- ϕ = 0° and 180°, AOA = ± 24°, Tap 6.

FIGURE 29 TIME LAG CURVES

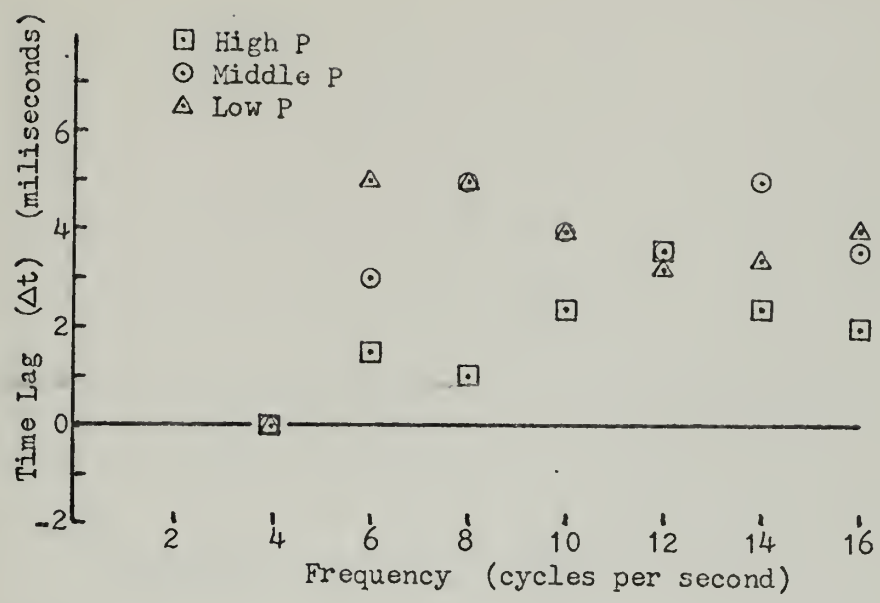

CONE -- ϕ = 225° and 45°, AOA = ± 20°, Tap 5.

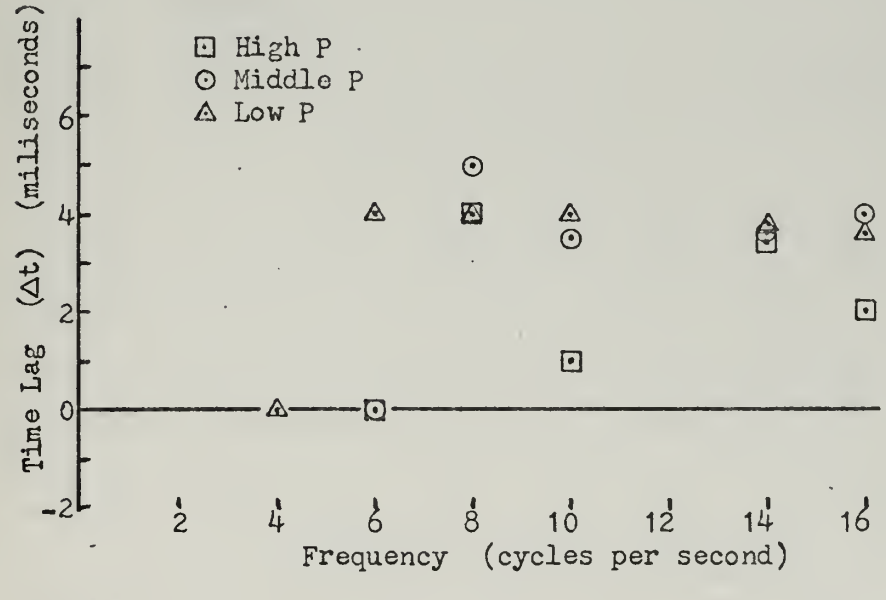

CONE -- ϕ = 225° and 45°, AOA = ± 24°, Tap 5.

FIGURE 30 TIME LAG CURVES

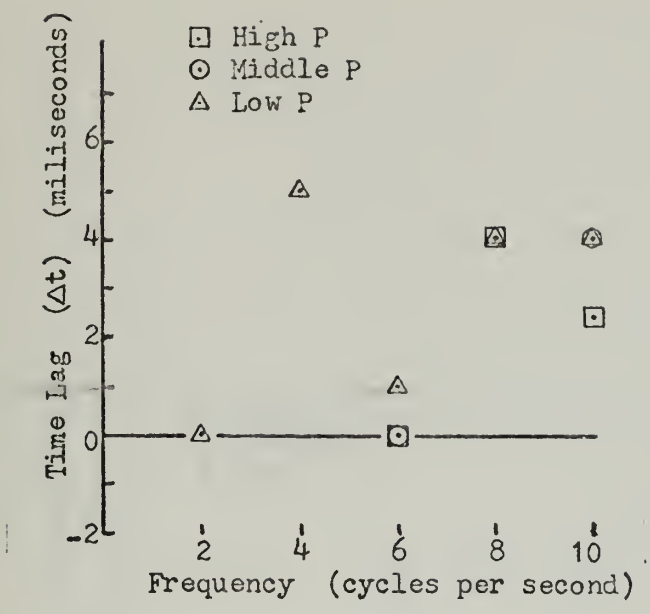

CONE -- $\phi = 90^\circ$ and 270°, AOA = $\pm$ 20°, Tap 6.

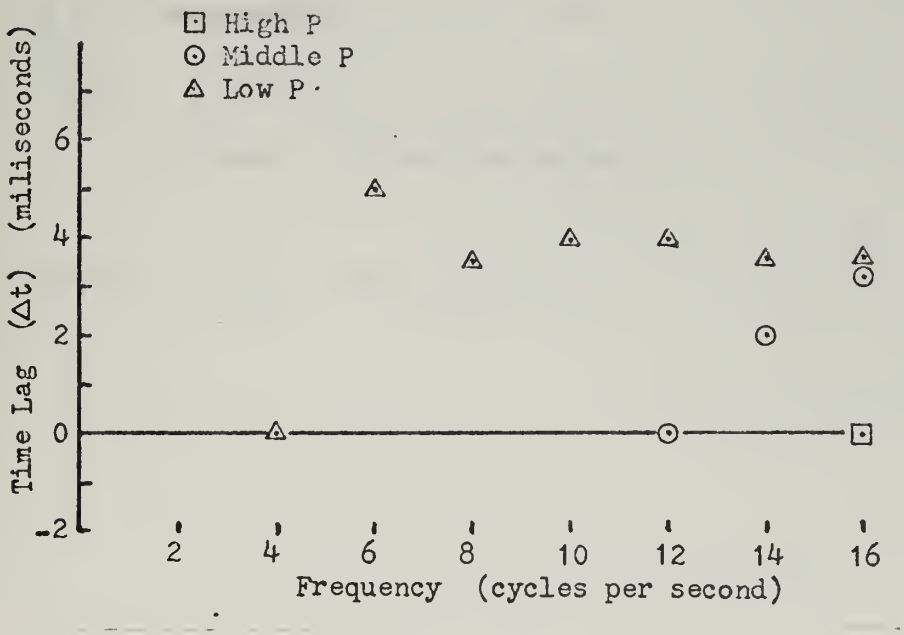

WEDGE -- AOA = $\pm$ 20°, Tap 2.

FIGURE 31 TIME LAG CURVES

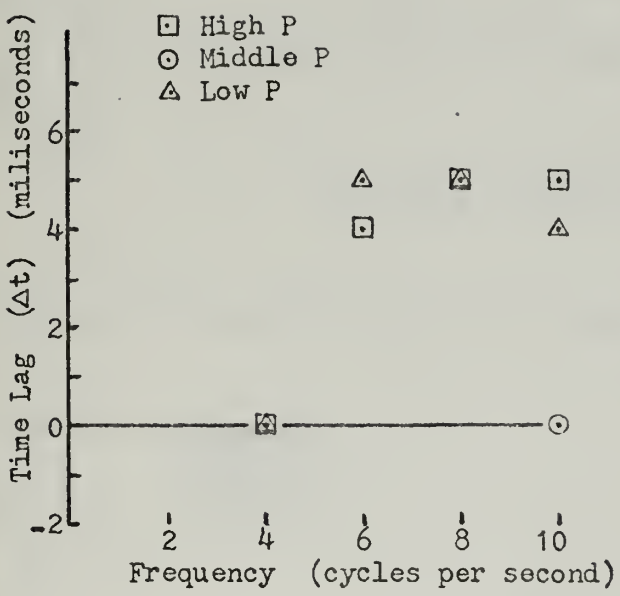

FLAT PLATE -- AOA = ± 5°, Tap 2.

FIGURE 32 TIME LAG CURVE

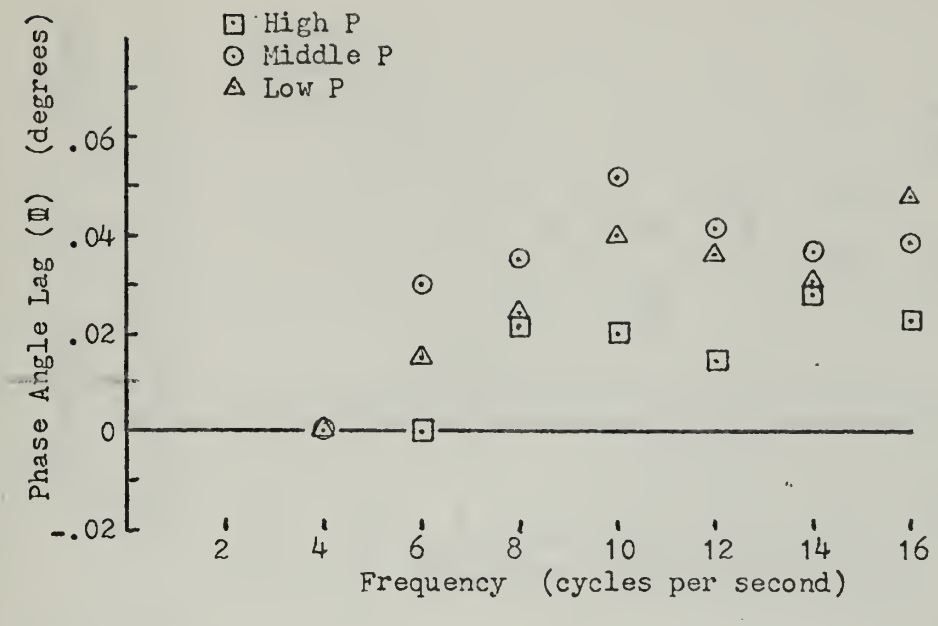

CONE -- $\phi = 0°$ and $180°$, AOA = $\pm$ $20°$, Tap 6.

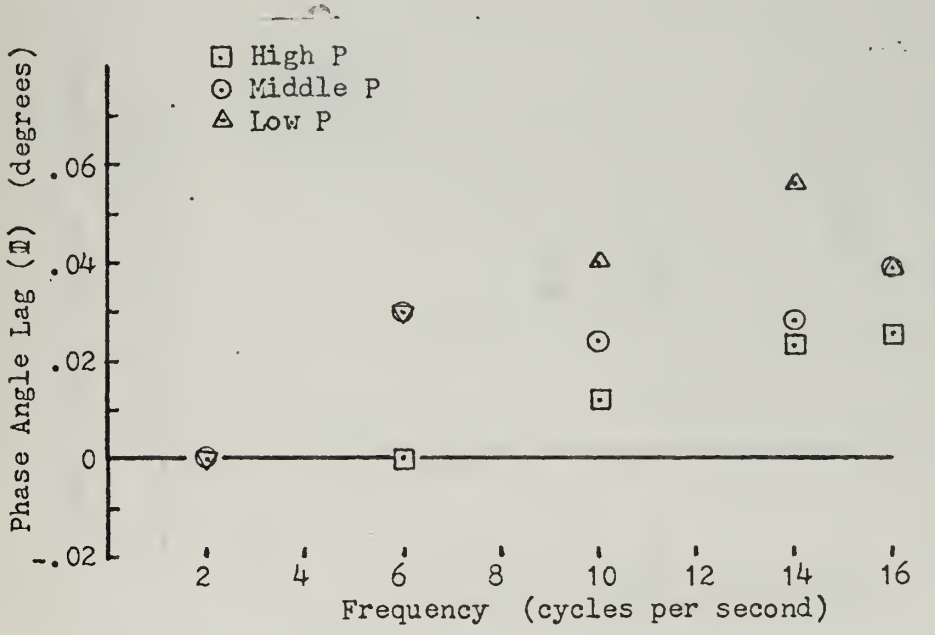

CONE -- $\phi = 0°$ and $180°$, AOA = $\pm$ $24°$, Tap 6.

FIGURE 33 PHASE ANGLE CURVES

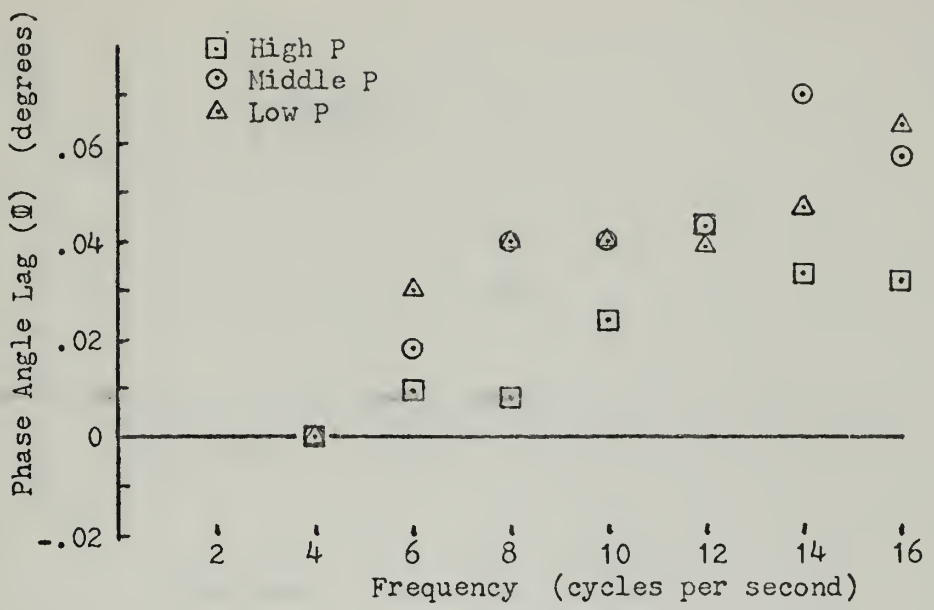

CONE -- ϕ = 225° and 45°, AOA = ± 20°, Tap 5.

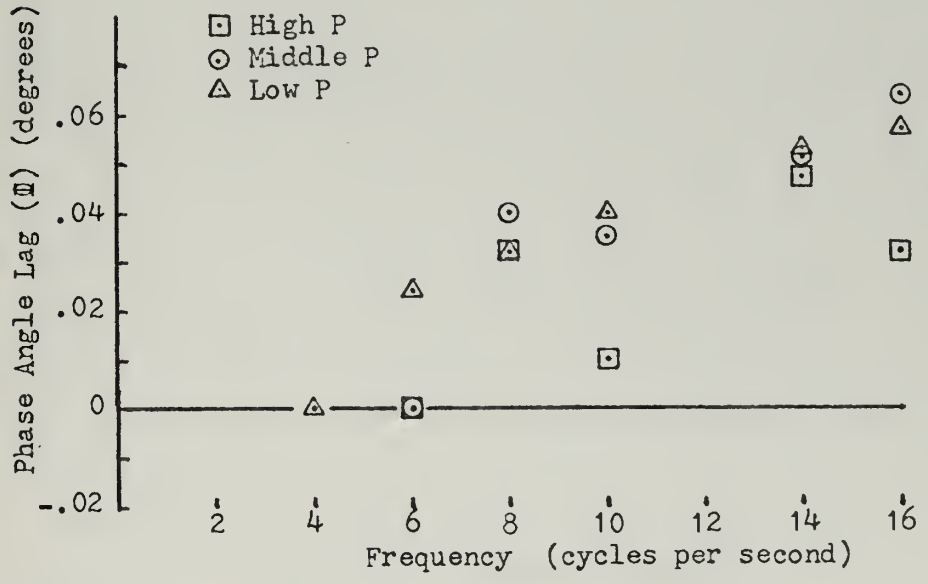

CONE -- ϕ = 225° and 45°, AOA = ± 24°, Tap 5.

FIGURE 34 PHASE ANGLE CURVES

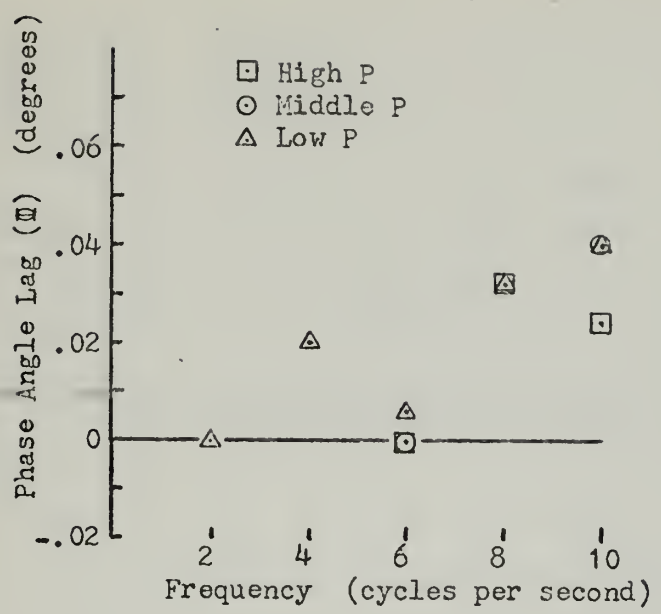

CONE -- ϕ = 90° and 270°, AOA = ± 20°, Tap 6.

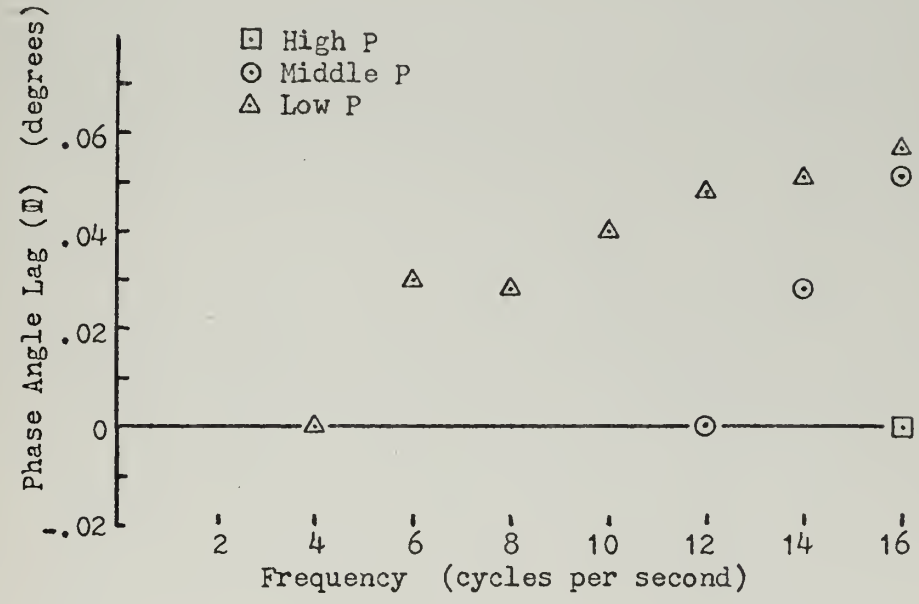

WEDGE -- AOA = ± 20°, Tap 2.

FIGURE 35 PHASE ANGLE CURVES

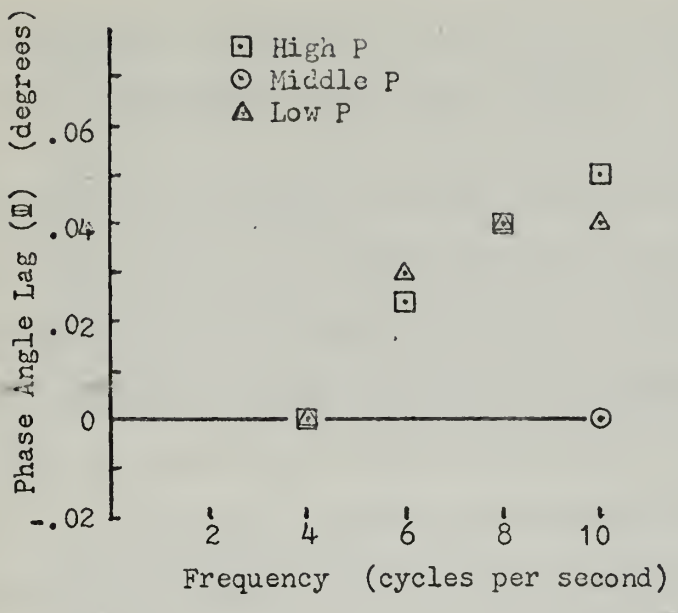

FLAT PLATE -- AOA = ± 5°, Tap 2.

FIGURE 36 PHASE ANGLE CURVE

APPENDIX A

NATURAL FREQUENCY MEASUREMENT OF THE PRESSURE TRANSDUCER SYSTEM

The pressure transducer system consisted of the pressure transducer, 8.2 inches of 0.045 inch ID tubing, the 12 volt DC power supply and the bridge balance. This system was connected to a vacuum pump and a 551 Dual Beam Oscilloscope. After balancing the bridge, the system was evacuated to 2 inches Hg.; then the slightly stretched tubing was cut at approximately 8.2 inches with a sharp knife. The resulting pressure traces are shown on pages 69 and 70; the lower trace being the 2 inch vacuum reference line. The oscilloscope had a 0.2 microsecond delay, and the time scale was one millisecond per centimeter. Various lengths and types of cutting strokes were recorded as labeled.

In accordance with the method outlined in Reference 6 the normalized observed overshoot yielded the damping ratio h=0.7 and using the formula: $f_n = \frac{2\pi}{T(1-h)^{1/2}}$ where T is the period of oscillations, the natural frequency was found to be 2410. If h was taken as 0.5, f_n would be 2000.

The last pressure trace, page 70, resulted from tapping the transducer which then oscillated at its own natural frequency. The frequency counts out to be approximately 3700 cycles per second which compares favorably with the specification of 4200 cycles per second. Notice that the other traces have the same small oscillations.

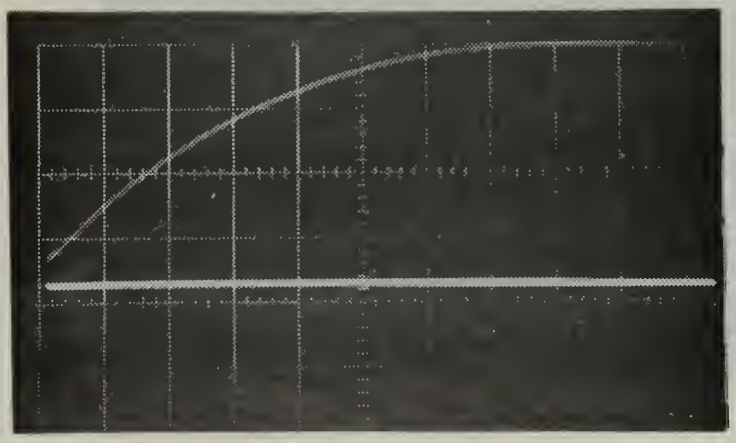

1. 18 inches of tubing, hand disconnected.

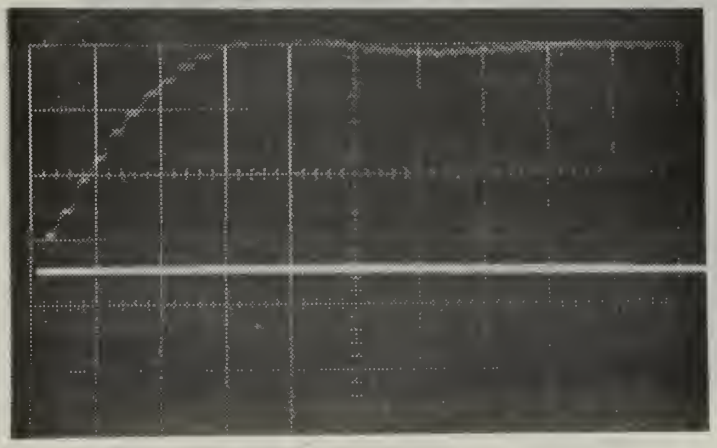

2. 10 inches of tubing, draw cut.

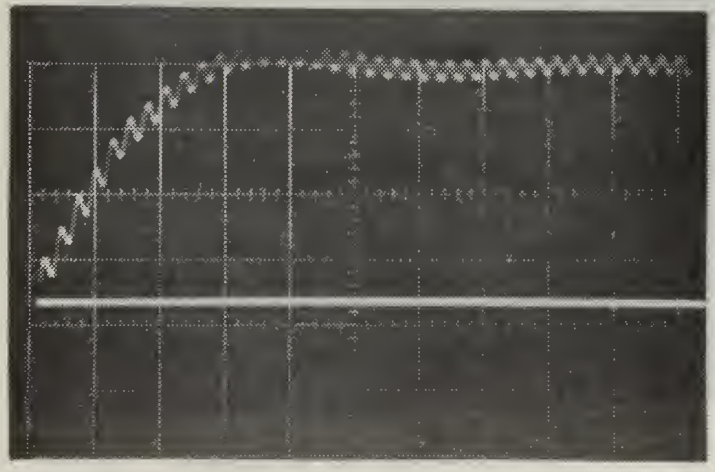

3. $8\frac{1}{2}$ inches of tubing, chopped.

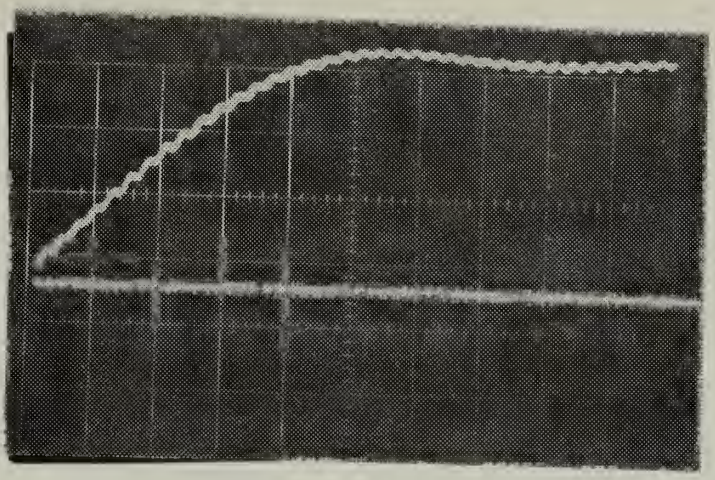

4. 8 inches of tubing, draw cut.

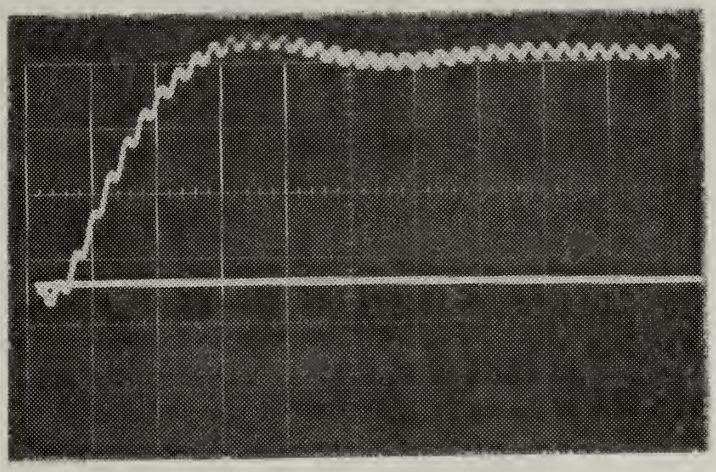

5. 8 inches of tubing, chopped.

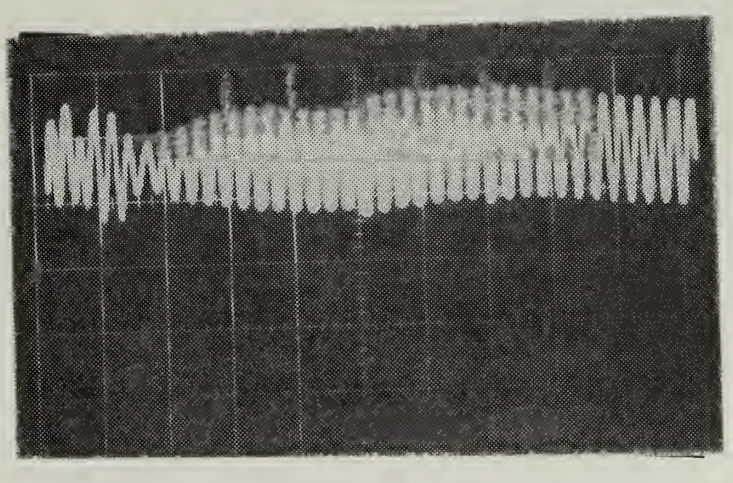

6. Response to tapping the transducer.

APPENDIX B

CONE DATA

OUTLINE:

A. PRESSURE TAP AND PHI ANGLE DIAGRAM

B. PRESSURE TAP COMPARISON DATA

C. PRESSURE TAP ANGLE PHI = 0° AND 180°

   I. Angle of Attack = ± 20°

   II. Angle of Attack = ± 24°

   III. Non-Oscillatory Data

D. PRESSURE TAP ANGLE PHI = 225° AND 45°

   I. Angle of Attack = ± 20°

   II. Angle of Attack = ± 24°

   III. Non-Oscillatory Data

E. PRESSURE TAP ANGLE PHI = 90° AND 270°

APPENDIX B

CONE DATA

A. PRESSURE TAP AND PHI ANGLE DIAGRAM

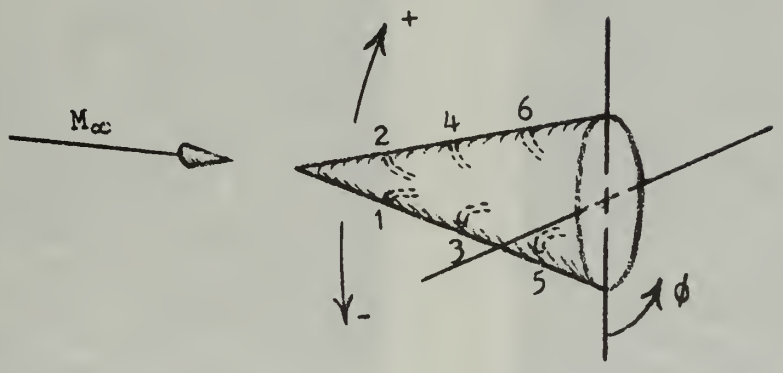

$\theta_c = 20^\circ$

B. PRESSURE TAP COMPARRISON DATA

1. M = 2.8
2. P_∞ = 52.7 psi
3. AOA = $\pm$ 20°
4. ϕ = 0° and 180°
6. Grid Scales as Indicated

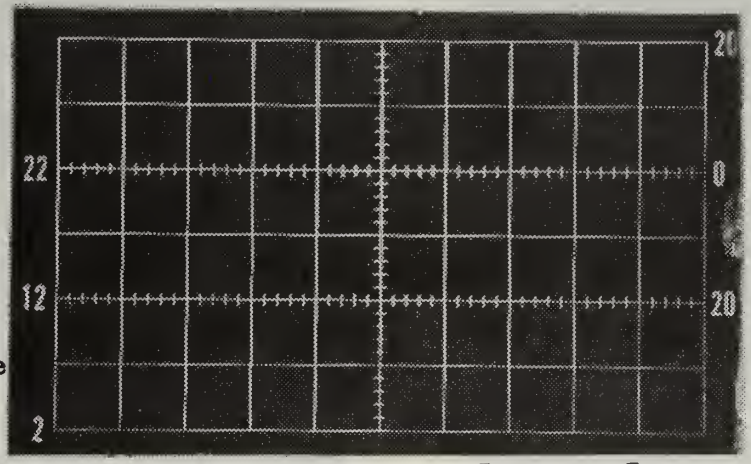

Upper Trace

Angle of Attack (degrees)

Lower Trace

Pressure (inches Hg)

Pressure Tap ___

f = 0.5 c/s, t = 0.5 s/cm

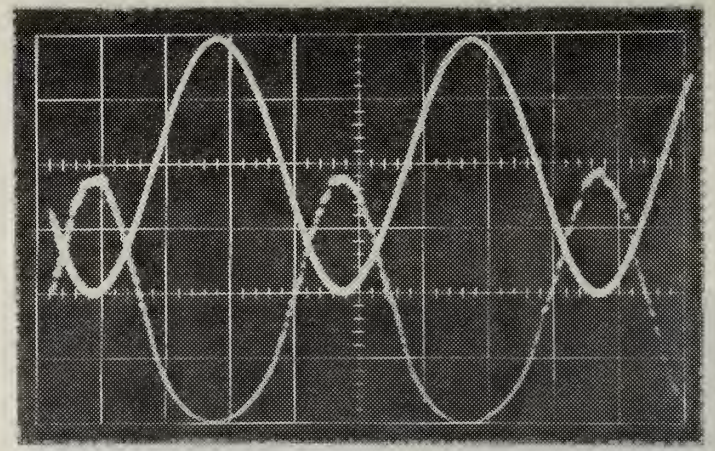

Tap 1

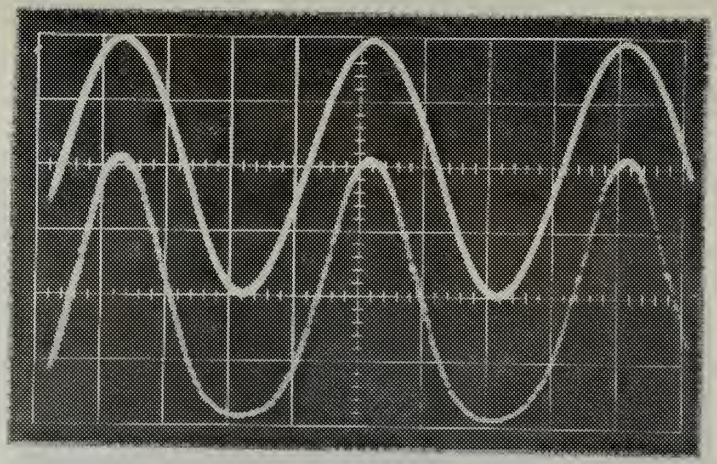

Tap 2

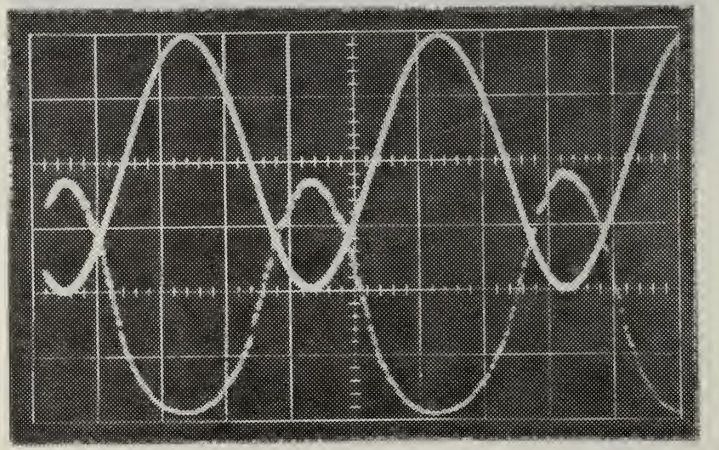

Tap 3

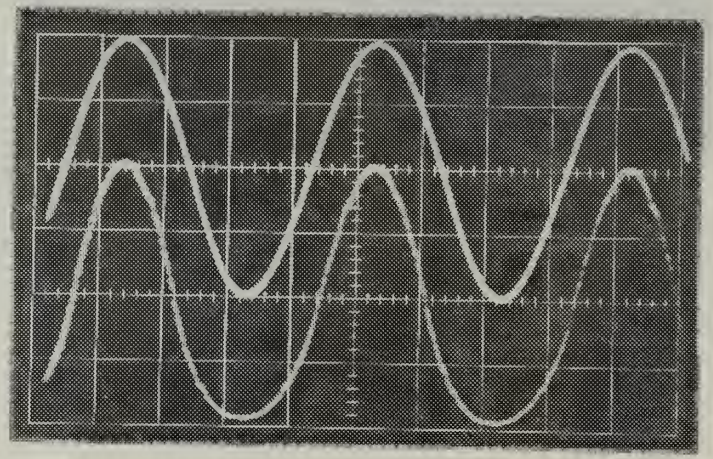

Tap 4

Tap 6

Tap 5

C. PRESSURE TAP ANGLE PHI = 0° AND 180°

I. Angle of Attack = ± 20°

a. M = 2.8

b. P_∞ = 52.7 psi

c. Grid Scales (unless otherwise specified)

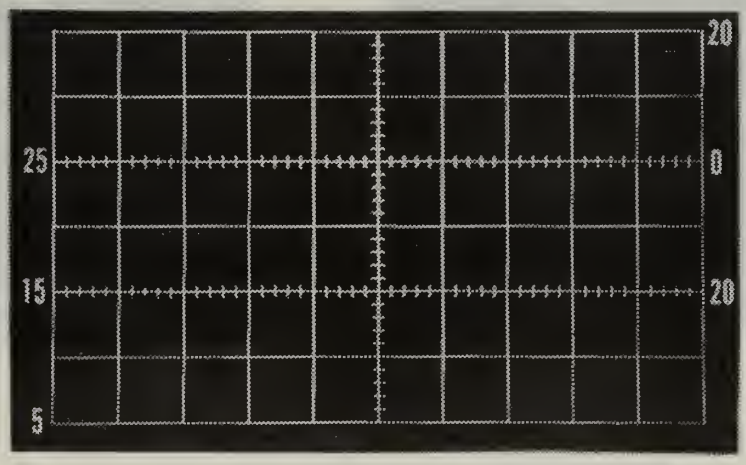

Pressure Tap ___

f = ___ c/s, t = ___ s/cm

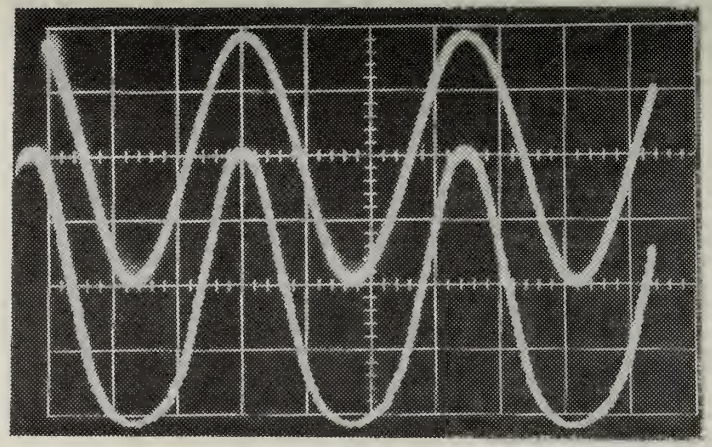

Tap 2

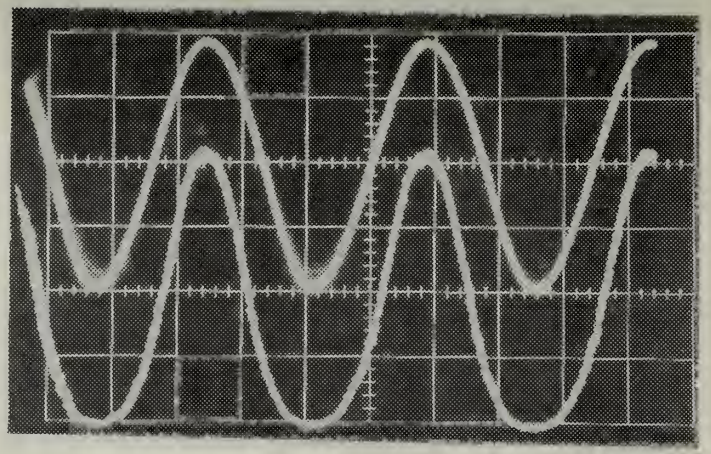

Tap 6

1.0 c/s, 0.5 s/cm

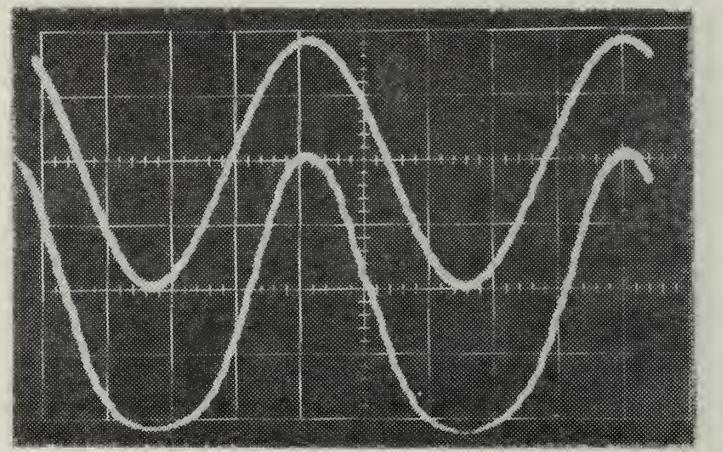

Tap 2

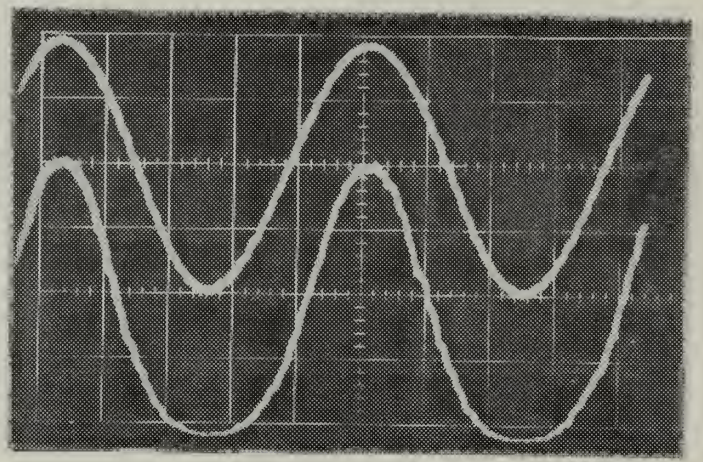

Tap 6

2.0 c/s, 0.1 s/cm

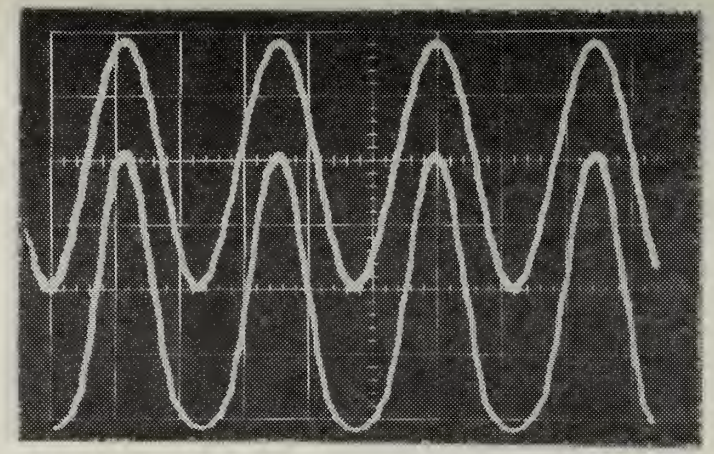

Tap 2

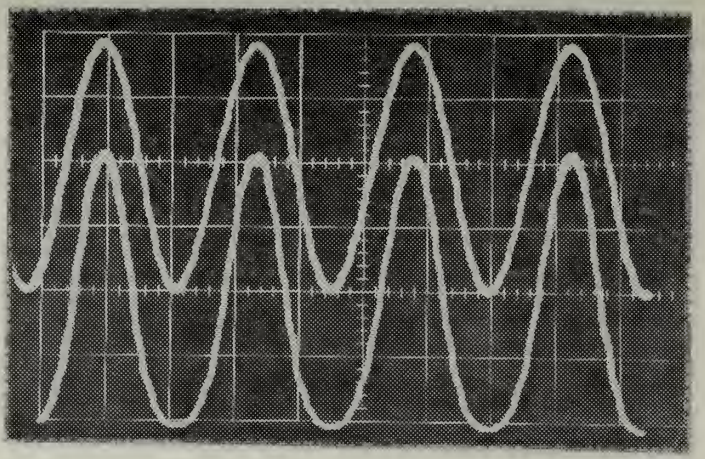

Tap 6

4.0 c/s, 0.1 s/cm

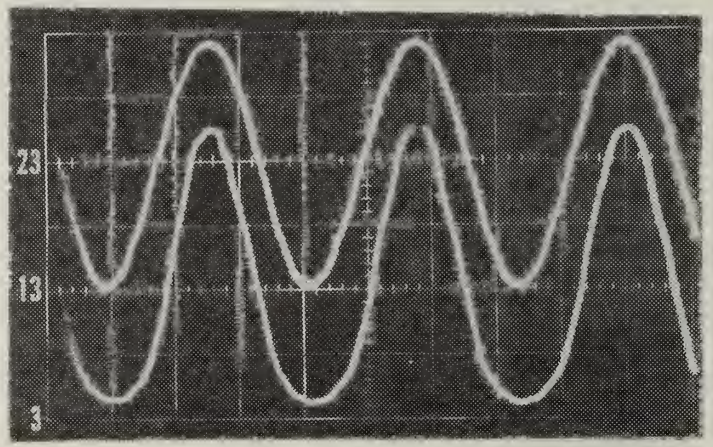

Tap 2

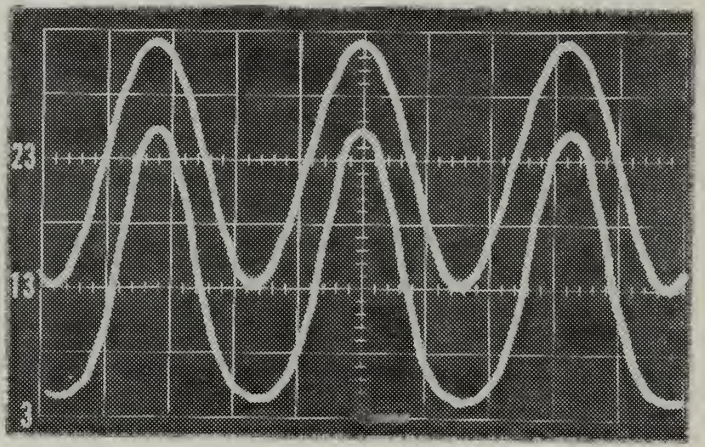

Tap 6

6.0 c/s, 0.05 s/cm

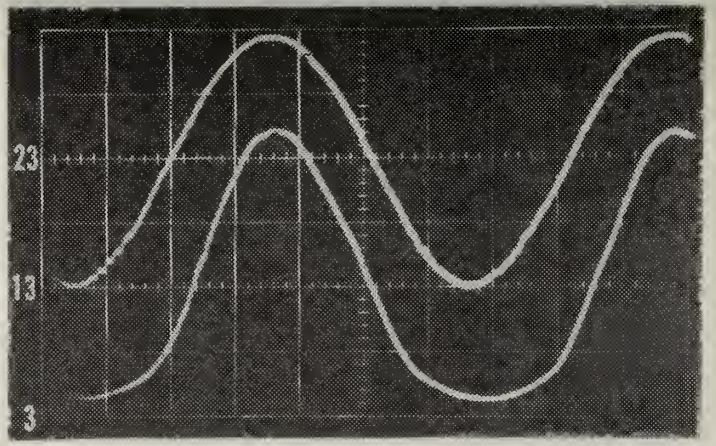

Tap 2

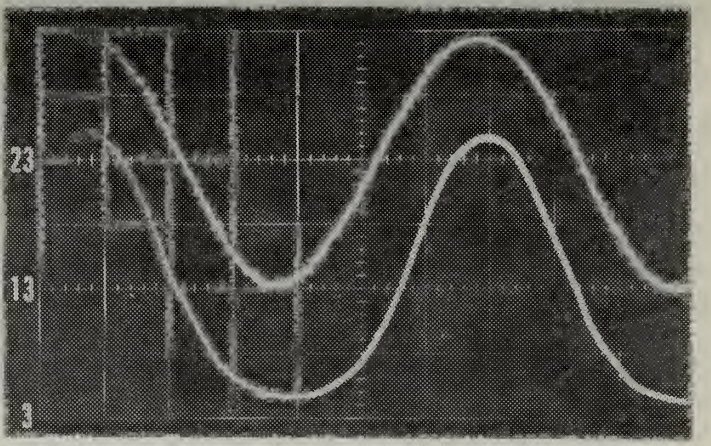

Tap 6

8.0 c/s, 0.02 s/cm

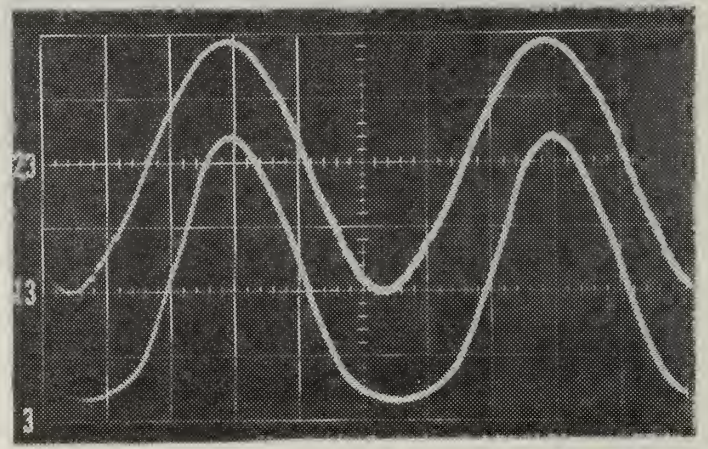

Tap 2

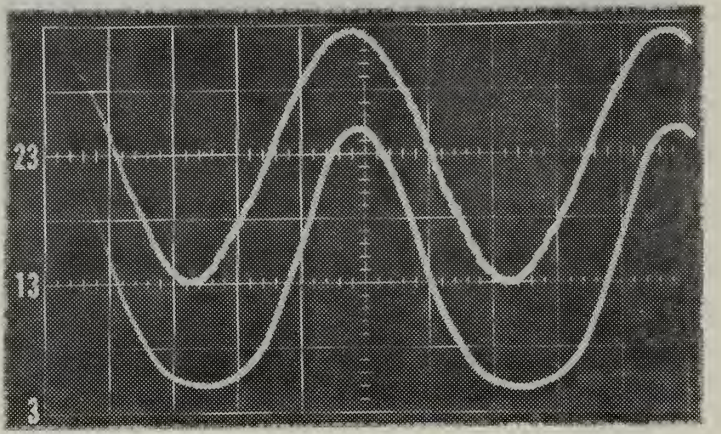

Tap 6

10.0 c/s, 0.02 s/cm

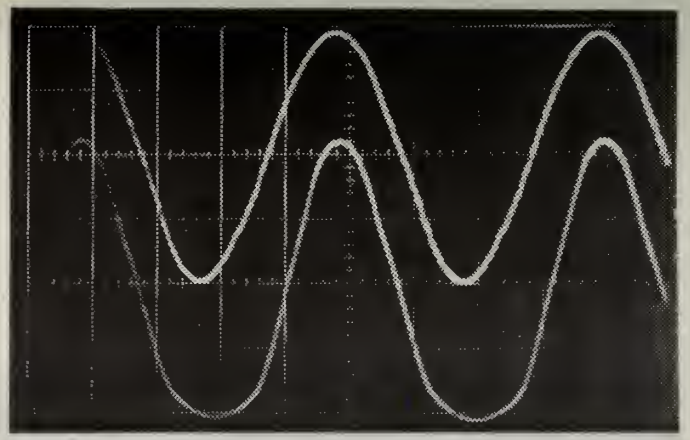

Tap 2

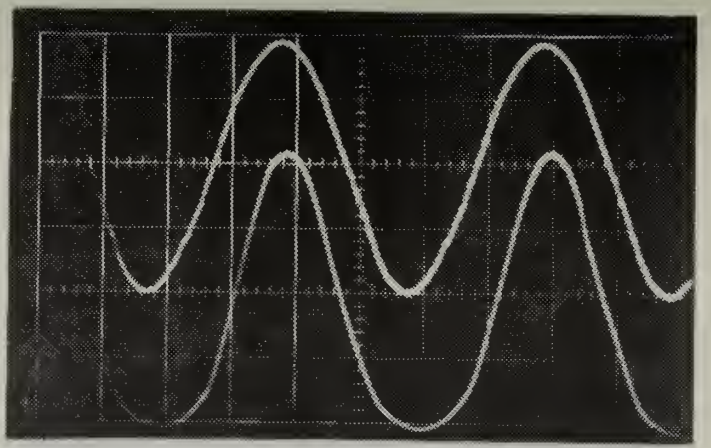

Tap 6

12.0 c/s, 0.02 s/cm

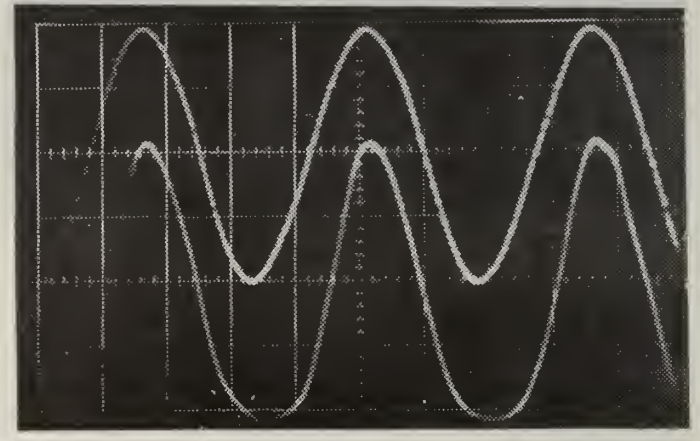

Tap 2

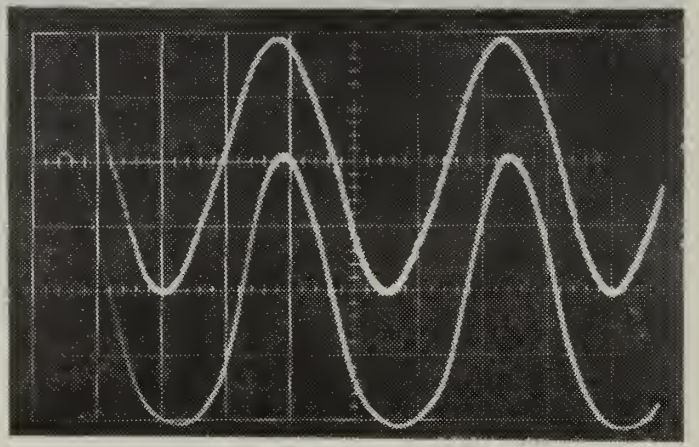

Tap 6

14.0 c/s, 0.02 s/cm

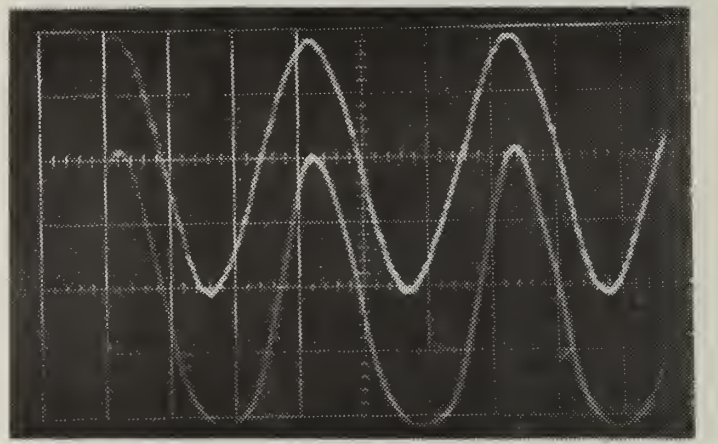

Tap 2

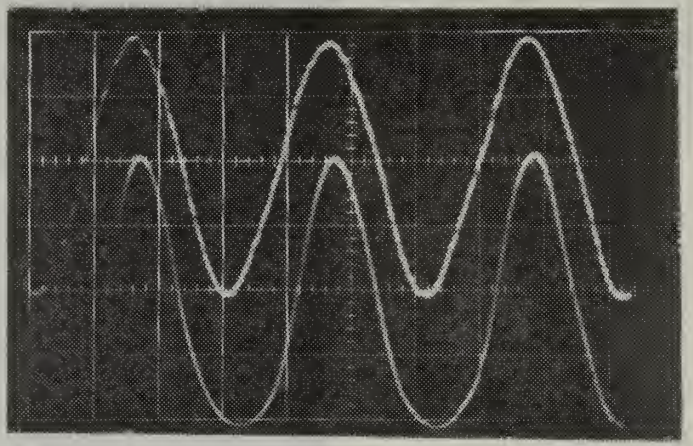

Tap 6

16.0 c/s, 0.02 s/cm

II. Angle of Attack = ± 24°

a. M = 2.8

b. P_∞ = 52.7

c. ϕ = 0° and 180°

d. Grid Scales

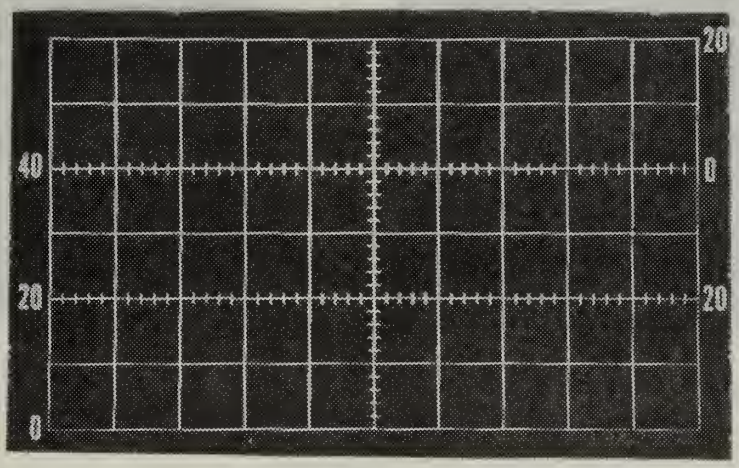

Upper Trace

Angle of Attack (degrees)

Lower Trace

Pressure (inches Hg)

Pressure Tap ___

f = ___ c/s, t = ___ s/cm

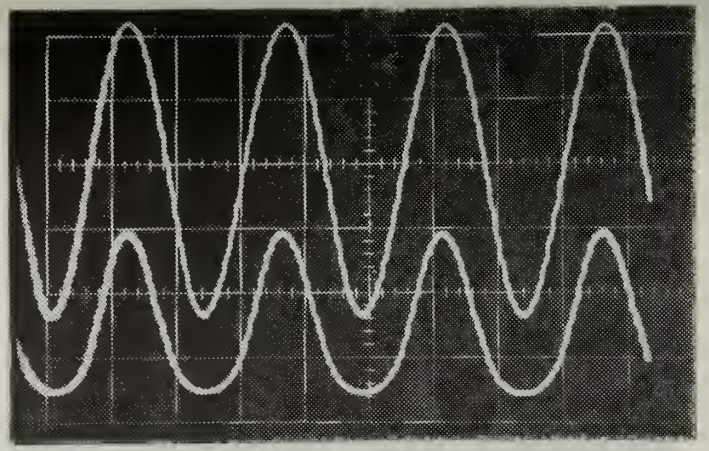

Tap 2

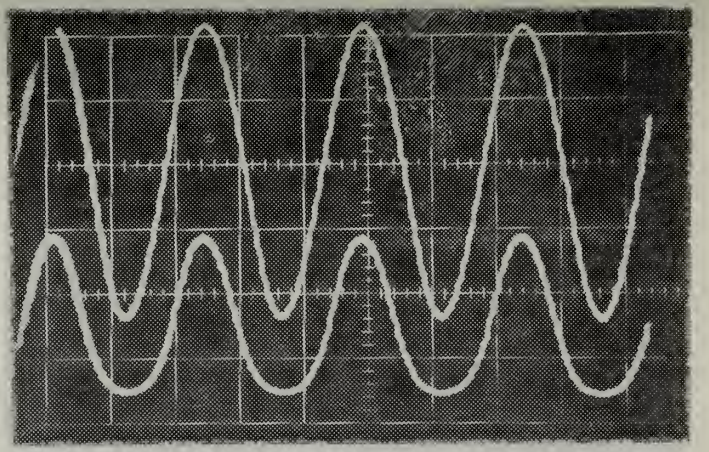

Tap 6

2.0 c/s, 0.2 s/cm

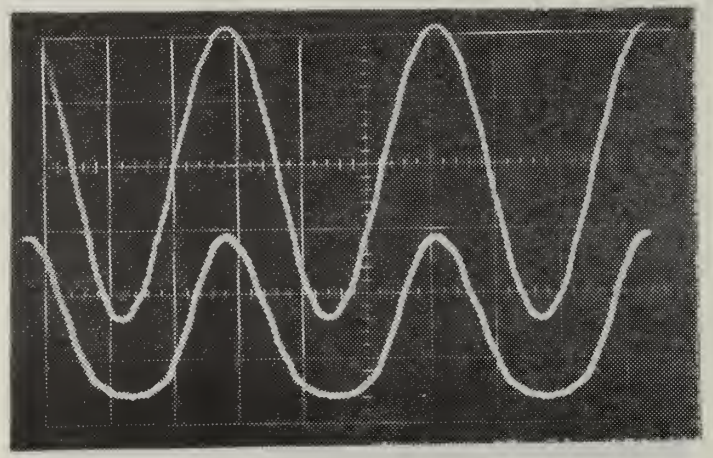

Tap 2

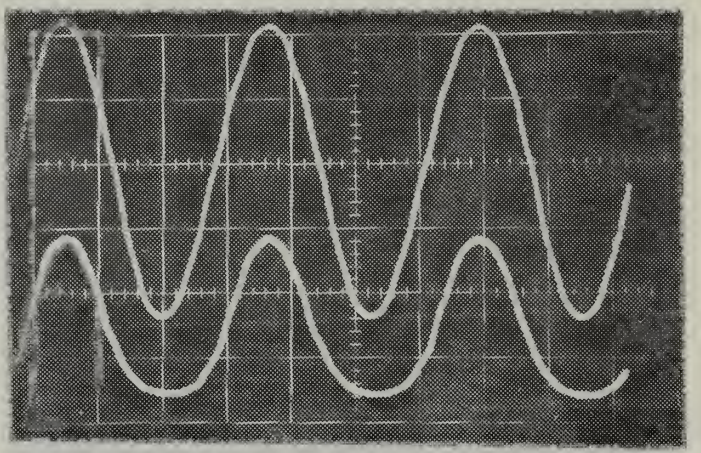

Tap 6

5.0 c/s, 0.05 s/cm

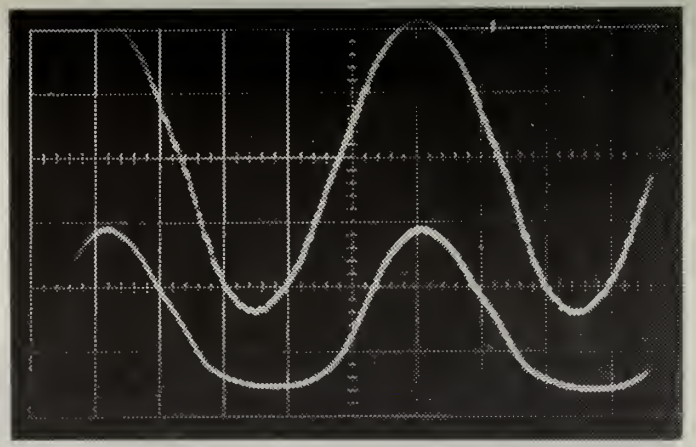

Tap 2

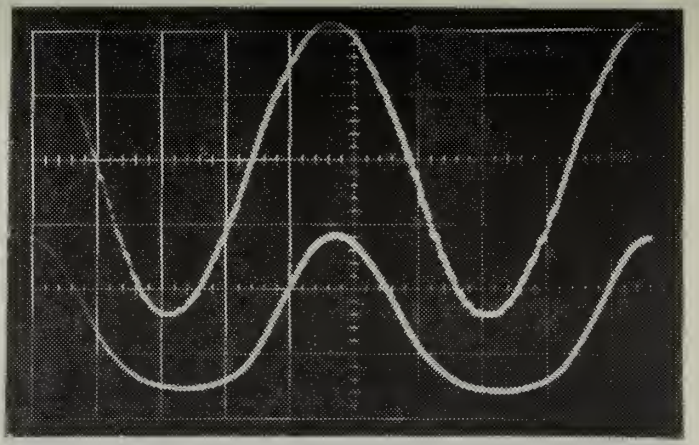

Tap 6

10.0 c/s, 0.02 s/cm

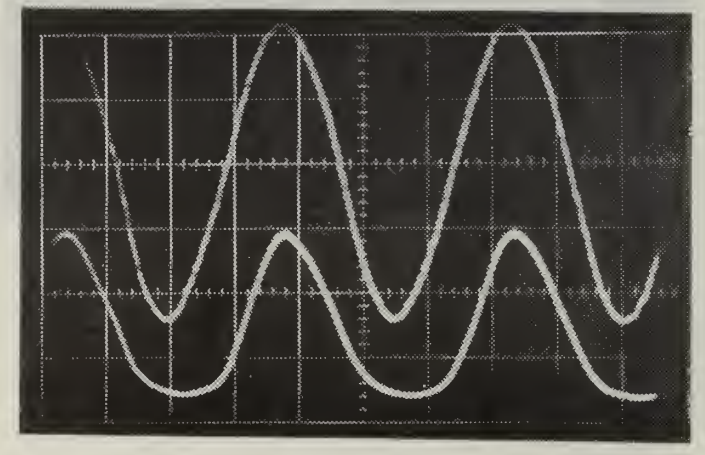

Tap 2

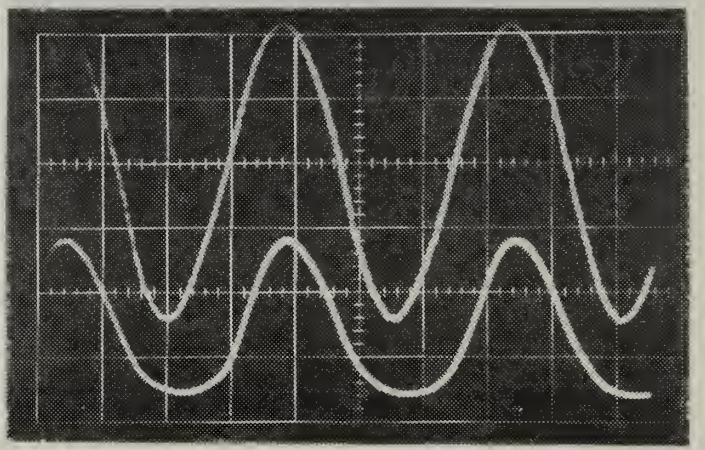

Tap 6

14.0 c/s, 0.02 s/cm

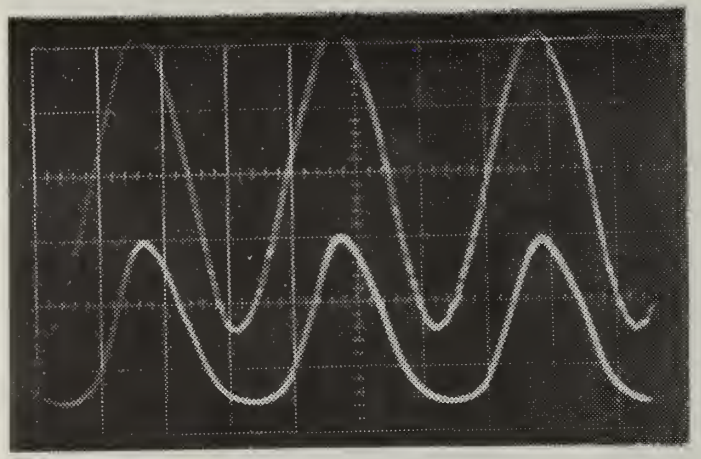

Tap 2

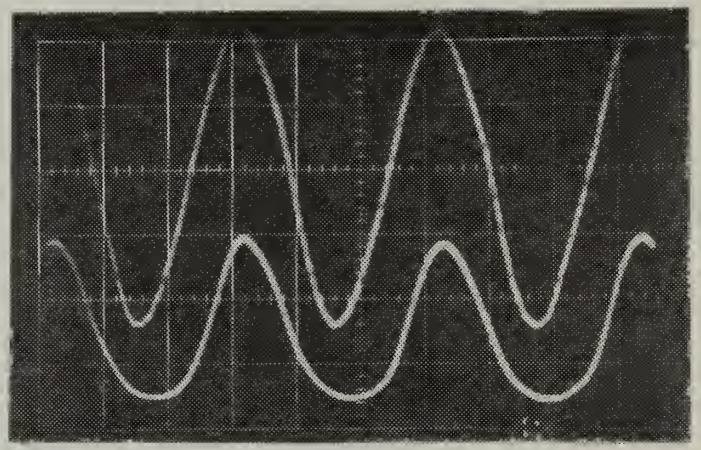

Tap 6

16.0 c/s, 0.02 s/cm

III. Non-Oscillatory Data

a. Angle of Attack = ± 20°

(1) M = 2.8

(2) P_∞ = 52.7 psi

(3) ϕ = 0° and 180°

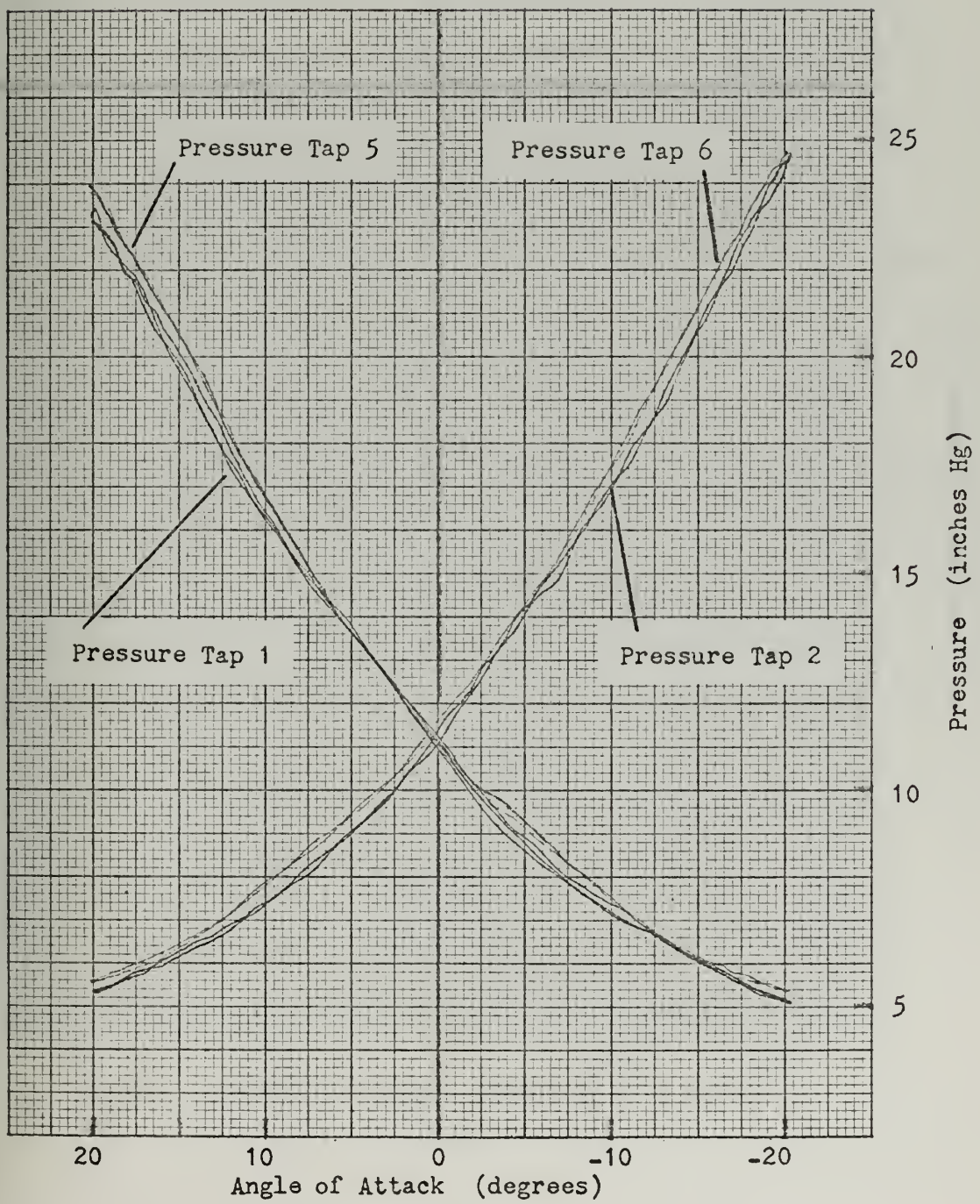

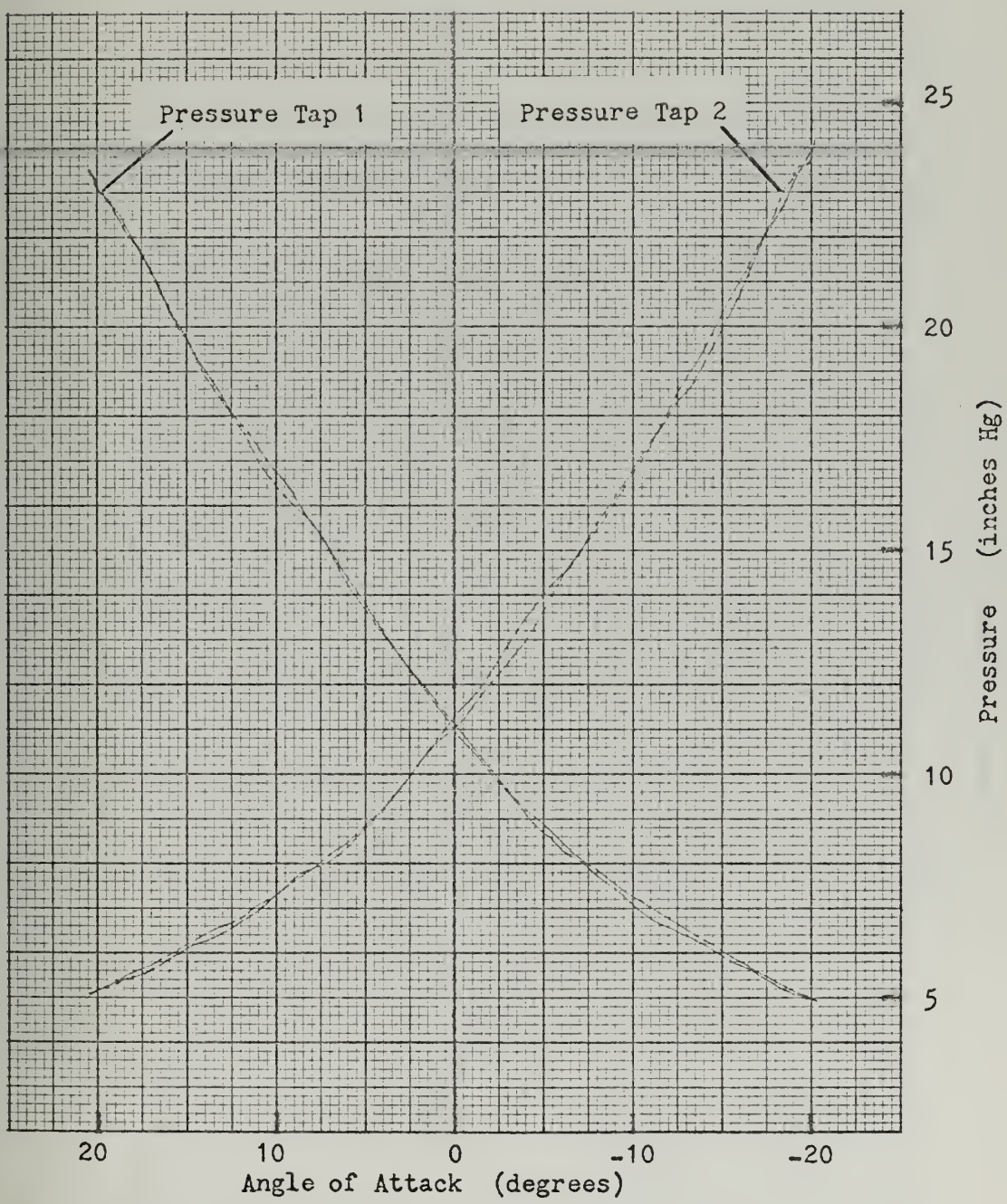
Pressure Tap 1
Pressure Tap 2
25
20
15
10
5
Pressure (inches Hg)
20
10
0
-10
-20
Angle of Attack (degrees)

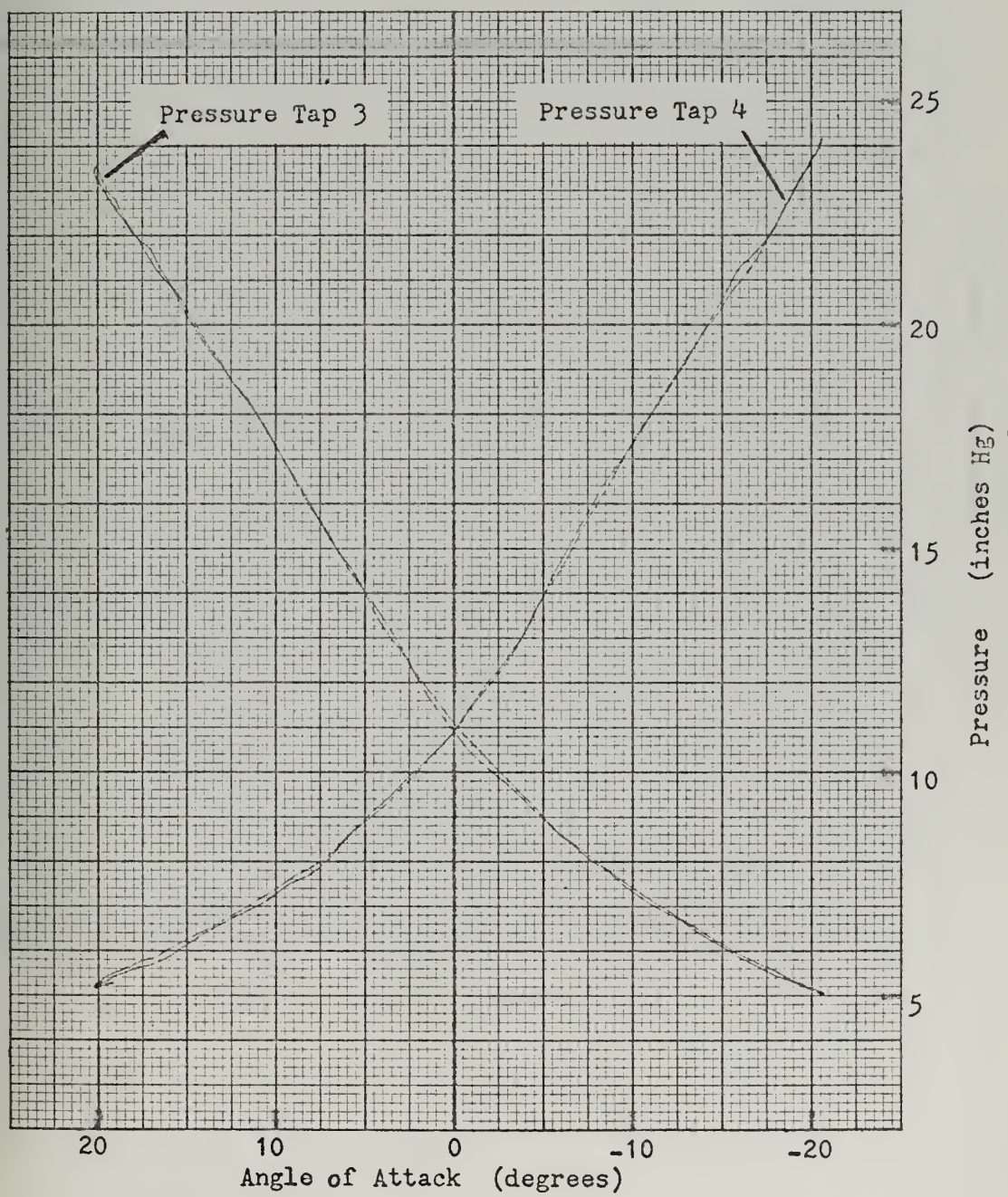
Pressure Tap 3
Pressure Tap 4
25
20
15
10
5
Pressure (inches Hg)
20
10
0
-10
-20
Angle of Attack (degrees)

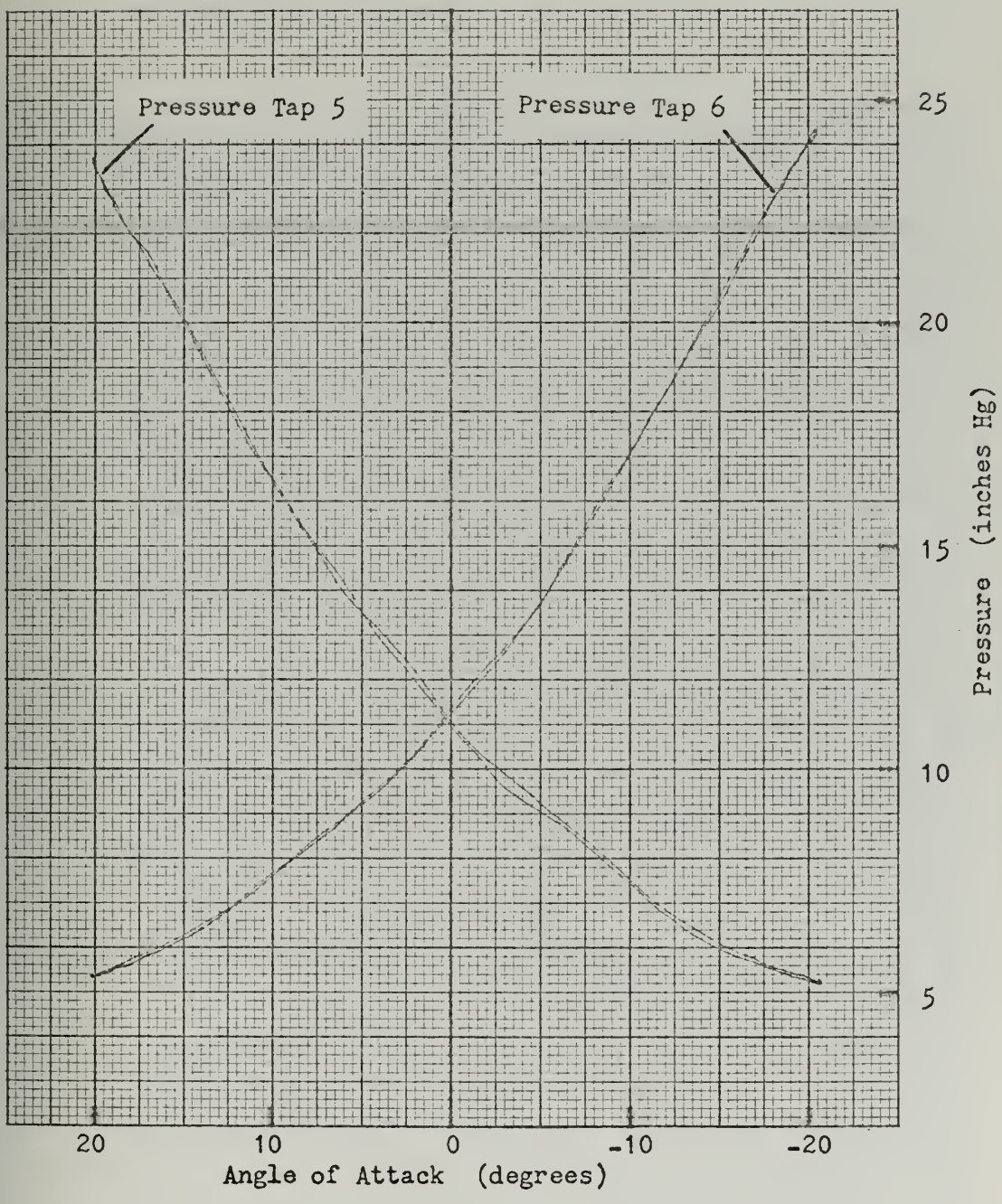
Pressure Tap 5
Pressure Tap 6
25
20
15
10
5
Pressure (inches Hg)
20
10
0
-10
-20
Angle of Attack (degrees)

b. Angle of Attack = ± 24°

(1) M = 2.8

(2) P_∞ = 52.7

(3) ϕ = 0° and 180°

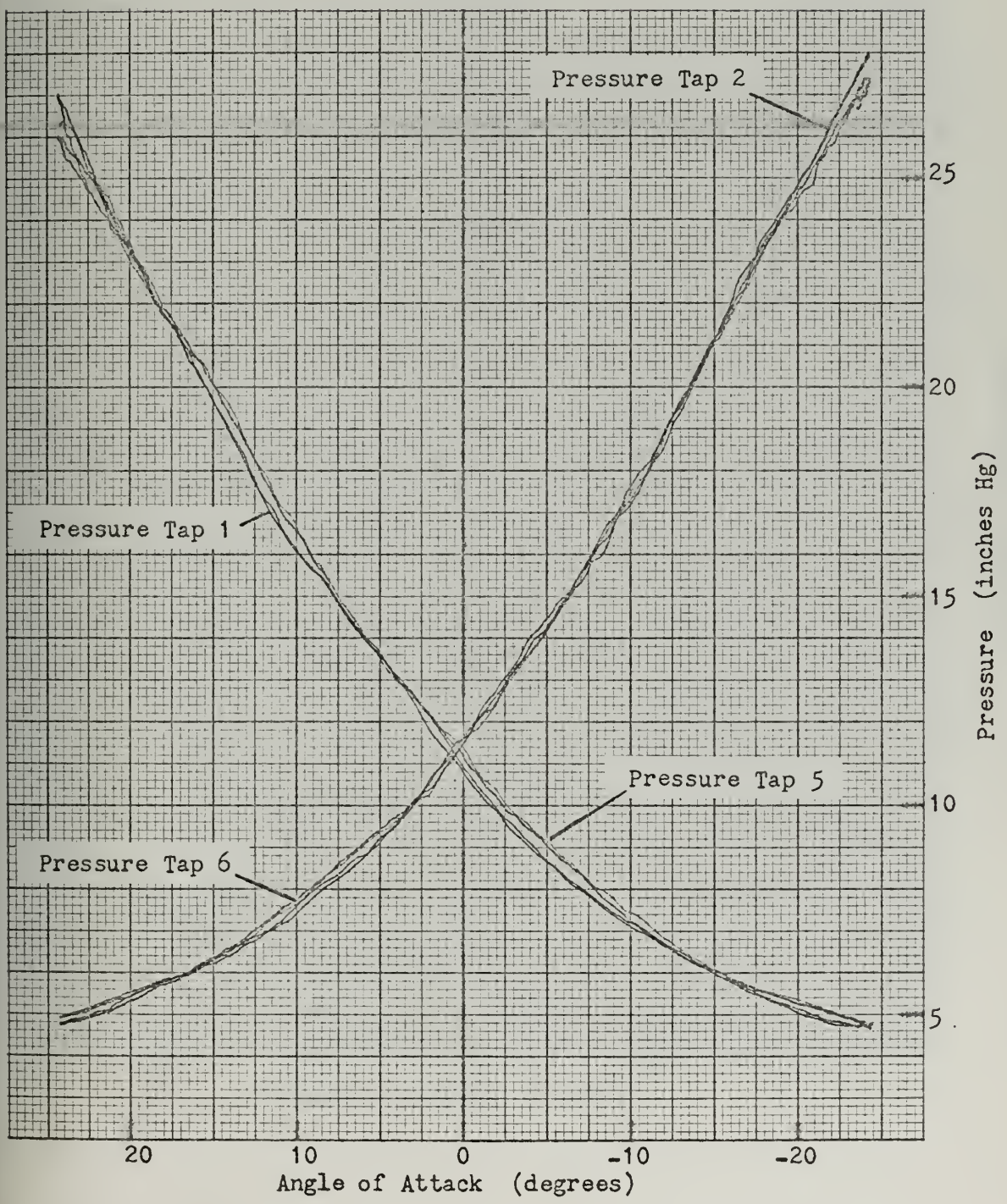

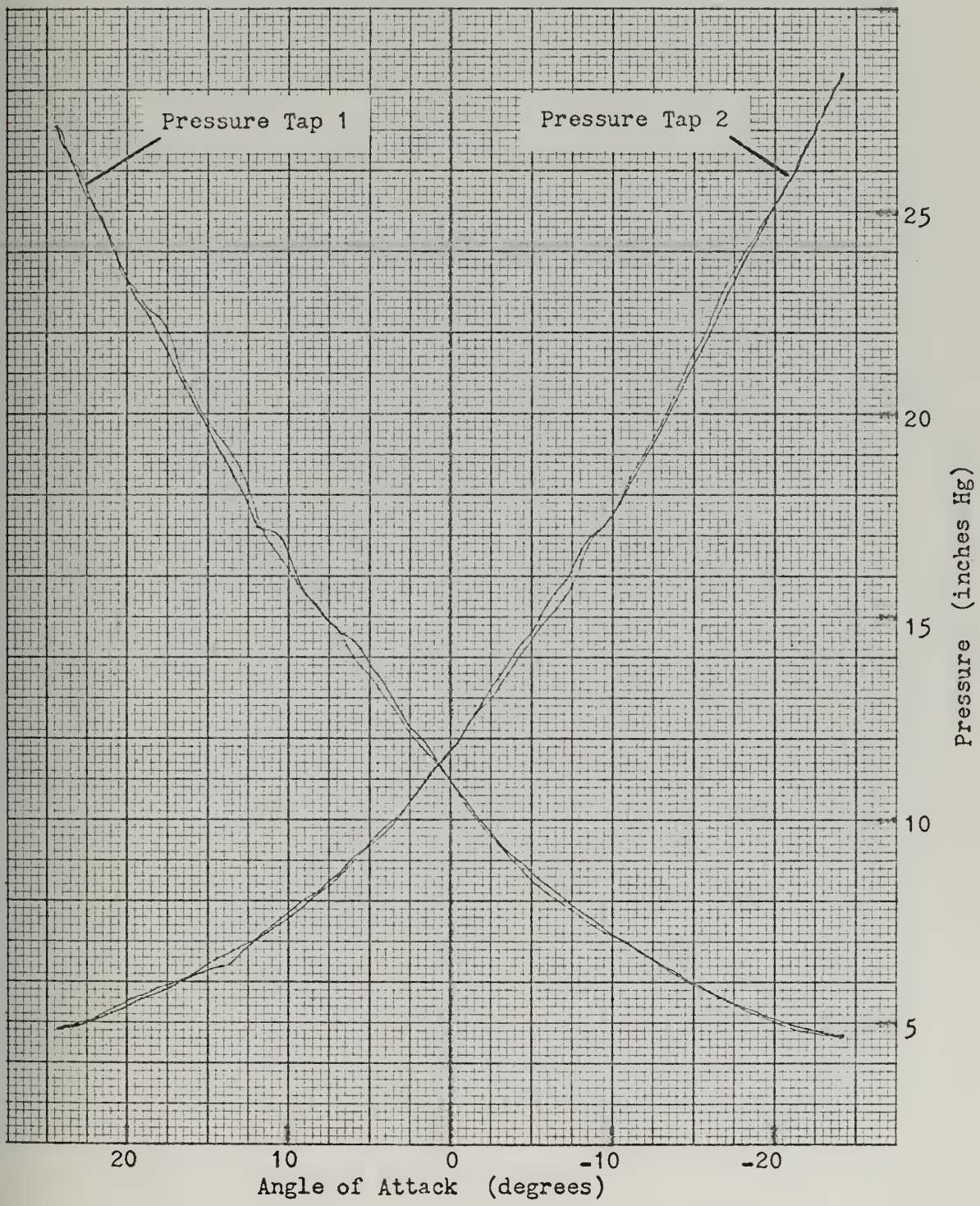
Pressure Tap 1
Pressure Tap 2
25
20
15
10
5
Pressure (inches Hg)
20
10
0
-10
-20
Angle of Attack (degrees)

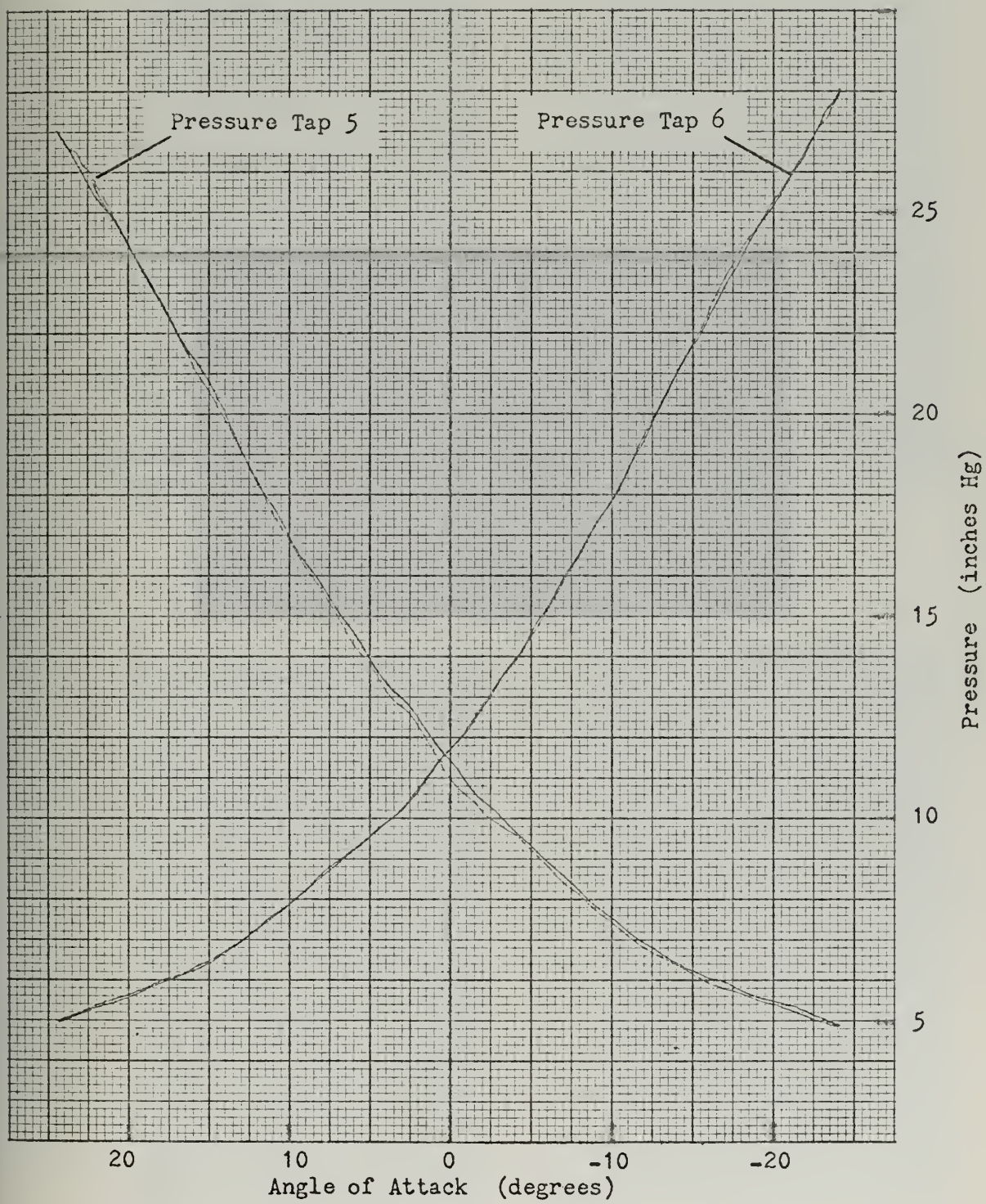
Pressure Tap 5
Pressure Tap 6
25
20
15
10
5
Pressure (inches Hg)
20
10
0
-10
-20
Angle of Attack (degrees)

D. PRESSURE TAP ANGLE PHI = 225° AND 45°

I. Angle of Attack = ± 20°

a. M = 2.8

b. P_∞ = 52.7

c. Grid Scales

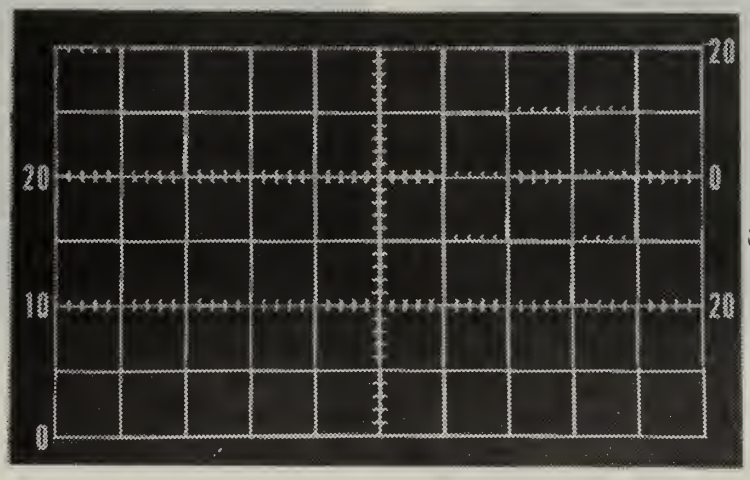

Upper Trace

Angle of Attack (degrees)

Lower Trace

Pressure (inches Hg)

Pressure Tap ___

f = ___ c/s, t = ___ s/cm

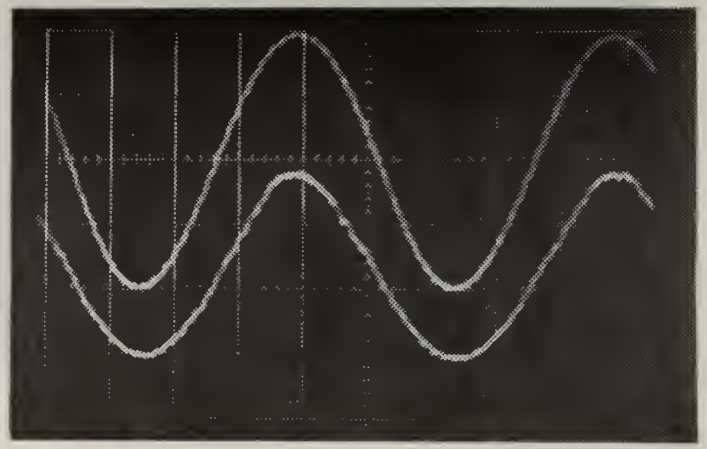

Tap 1

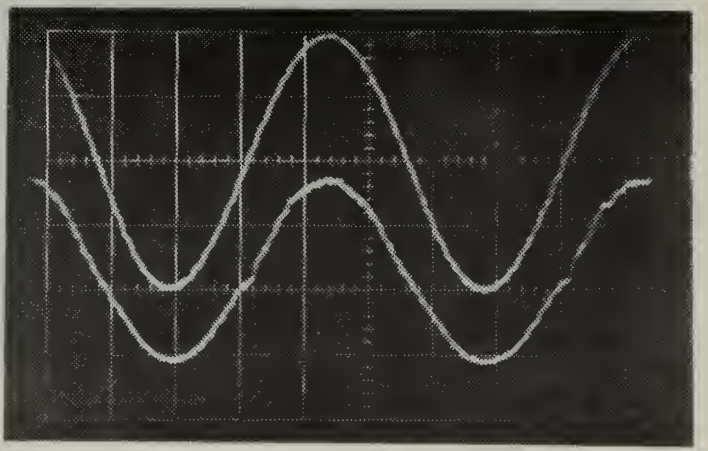

Tap 5

2.0 c/s, 0.1 s/cm

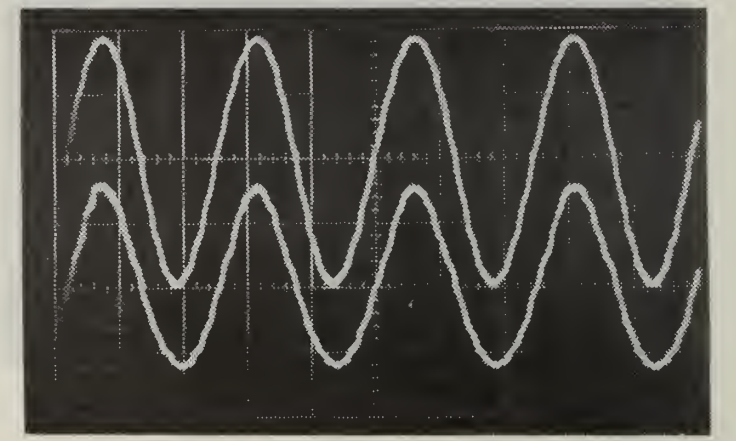

Tap 1

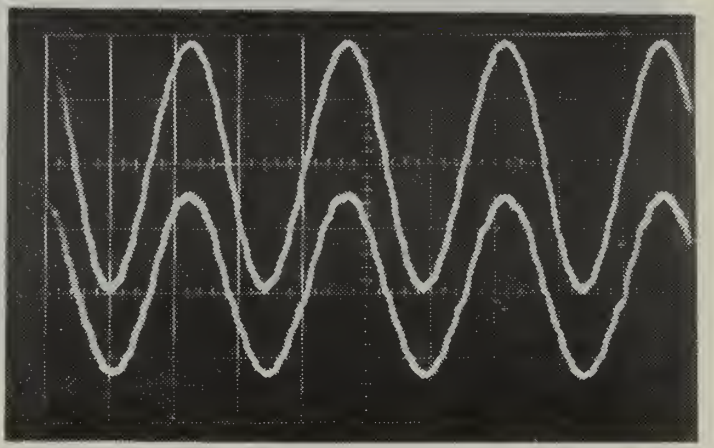

Tap 5

4.0 c/s, 0.1 s/cm

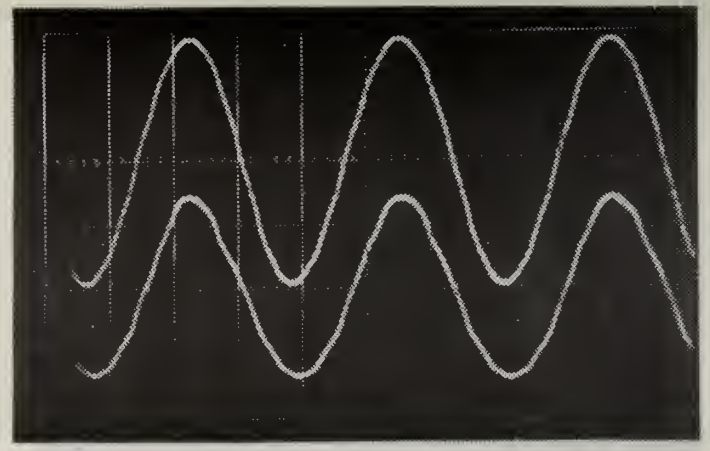

Tap 1

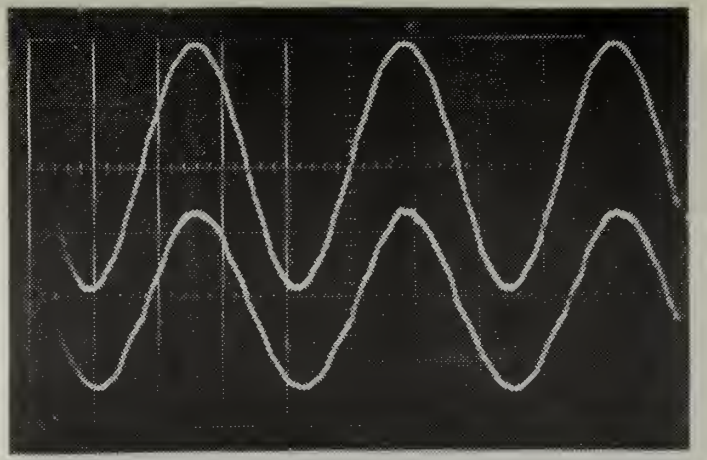

Tap 5

6.0 c/s, 0.05 s/cm

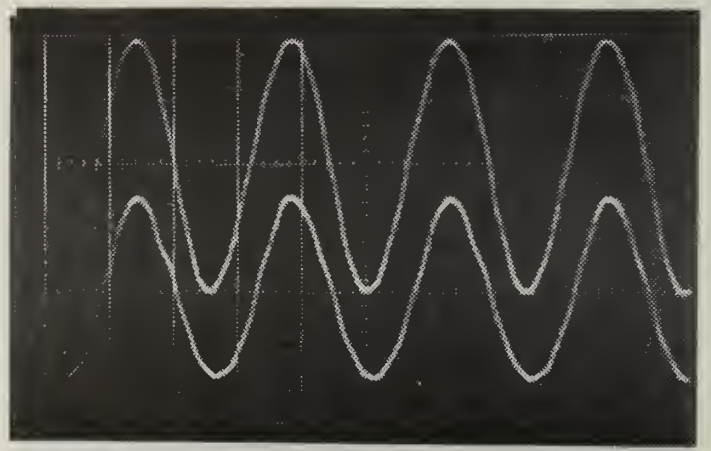

Tap 1

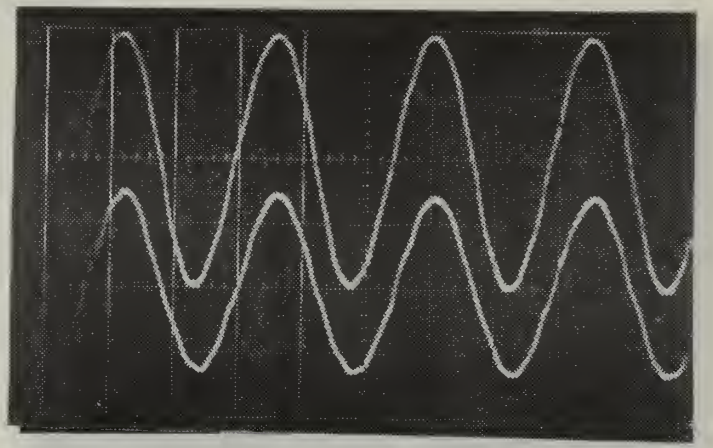

Tap 5

3.0 c/s, 0.05 s/cm

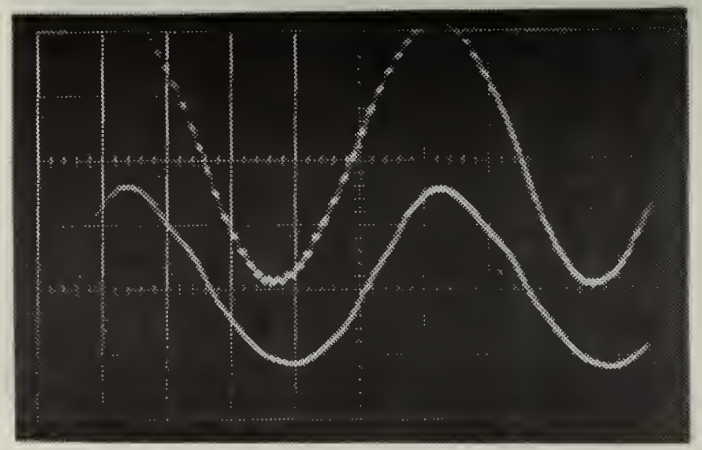

Tap 1

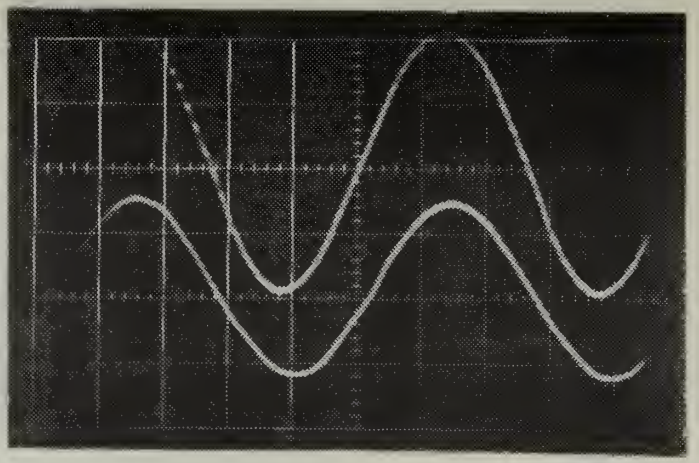

Tap 5

10.0 c/s, 0.02 s/cm

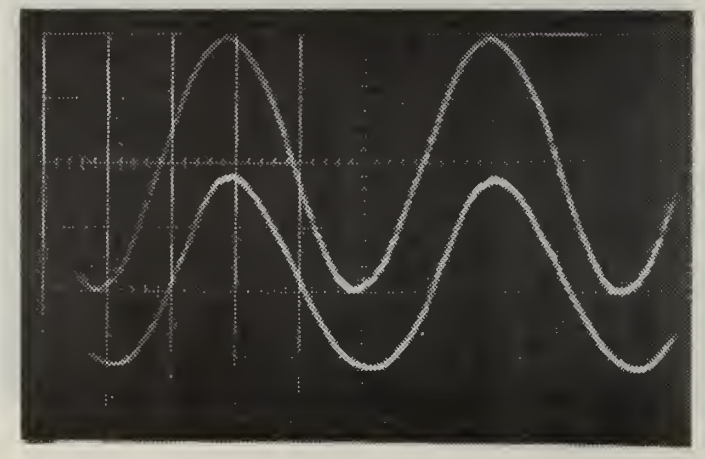

Tap 1

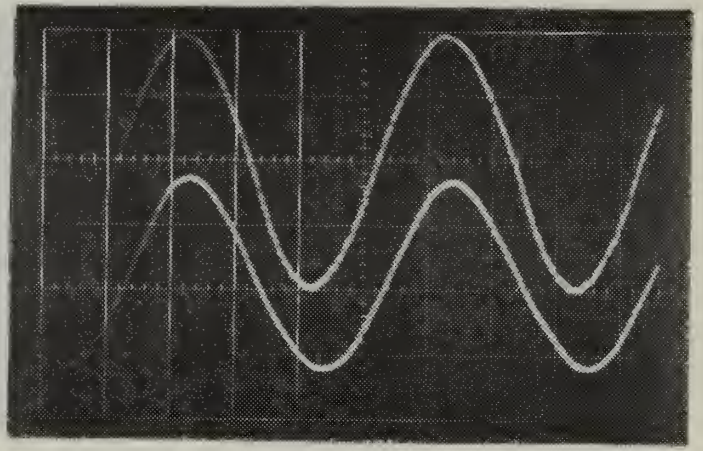

Tap 5

12.0 c/s, 0.02 s/cm

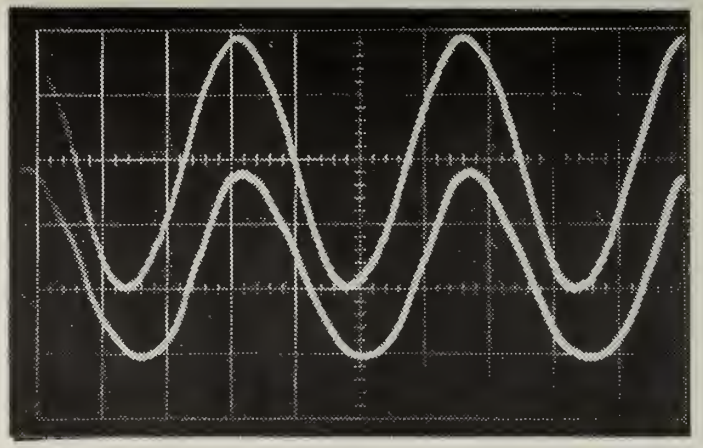

Tap 1

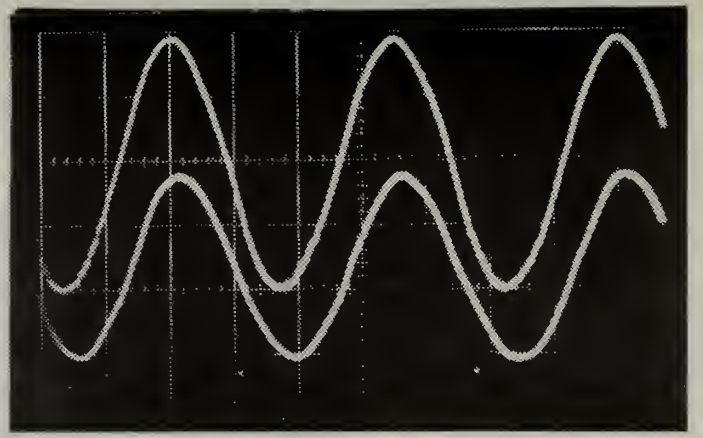

Tap 5

14.0 c/s, 0.02 s/cm

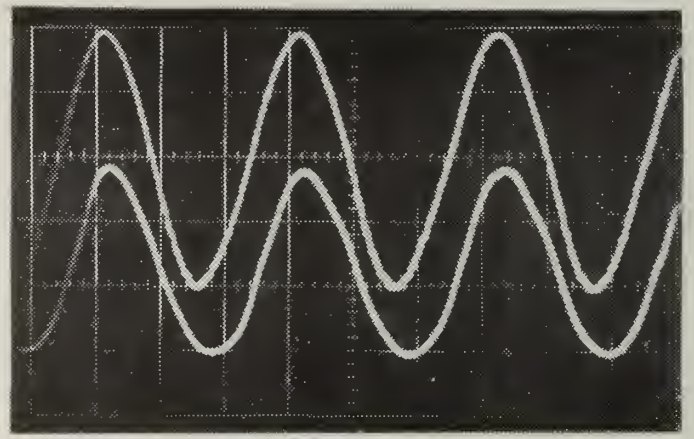

Tap 1

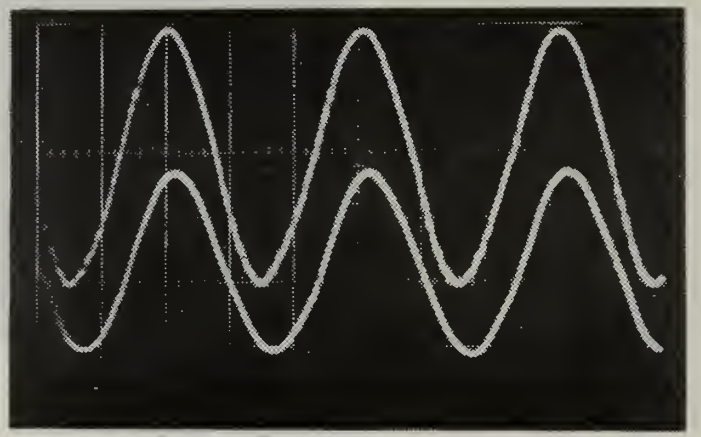

Tap 5

16.0 c/s, 0.02 s/cm

II. Angle of Attack = ± 24°

a. M = 2.8

b. P_{∞} = 52.7

c. ϕ = 225° and 45°

d. Grid Scales

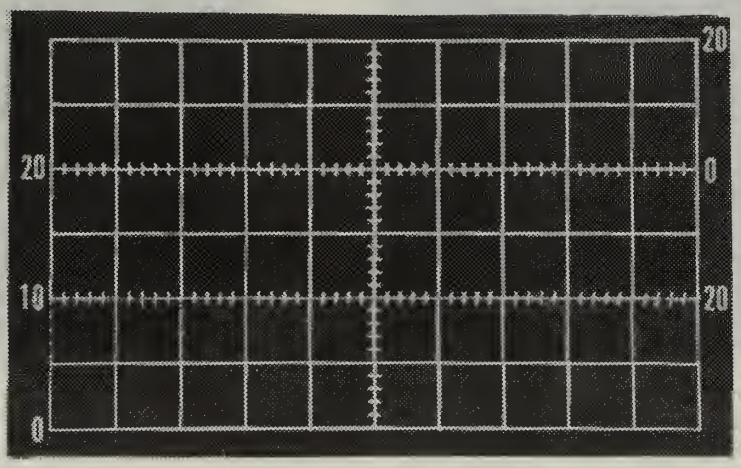

Upper Trace

Angle of Attack (degrees)

Lower Trace

Pressure (inches Hg)

Pressure Tap ___

f = ___ c/s, t = ___ s/cm

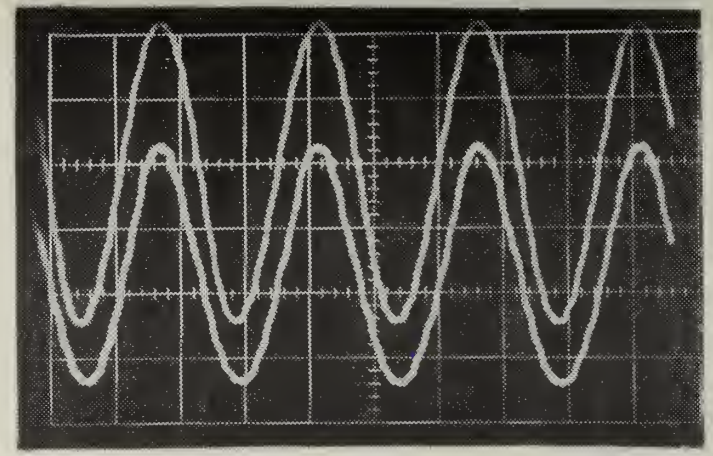

Tap 1

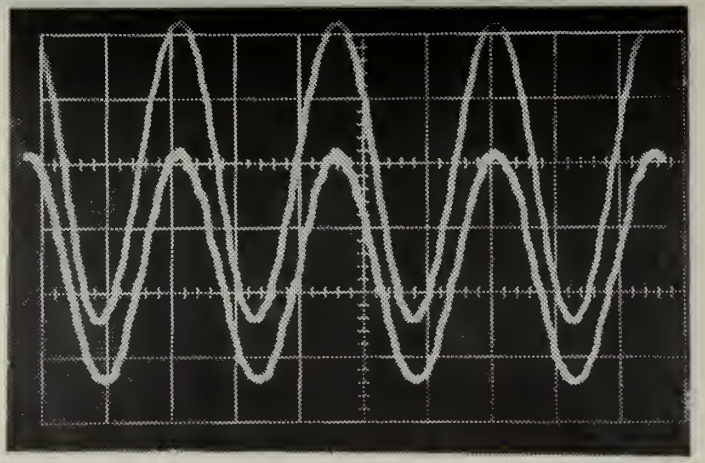

Tap 5

4.0 c/s, 0.1 s/cm

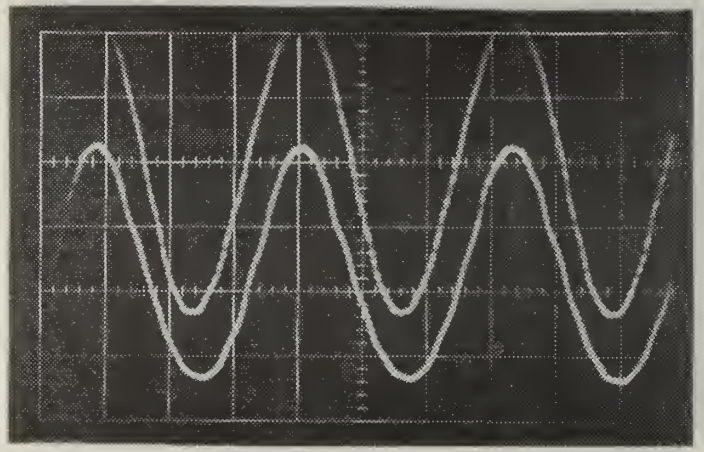

Tap 1

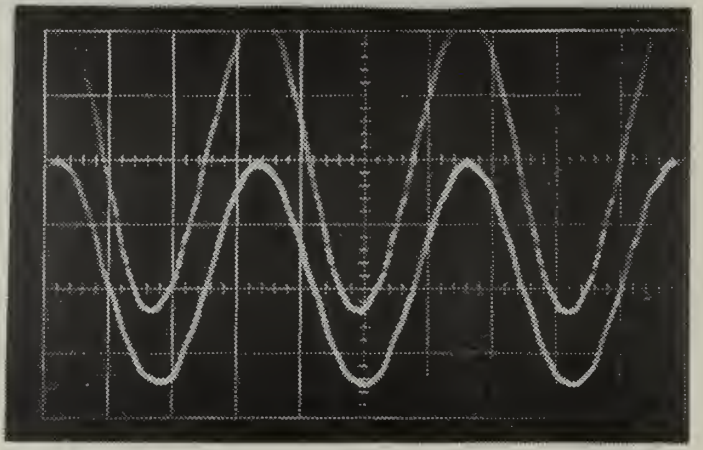

Tap 5

6.0 c/s, 0.05 s/cm

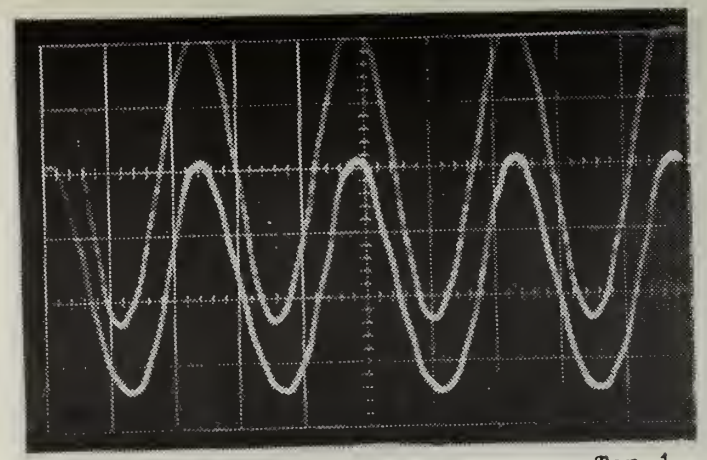

Tap 1

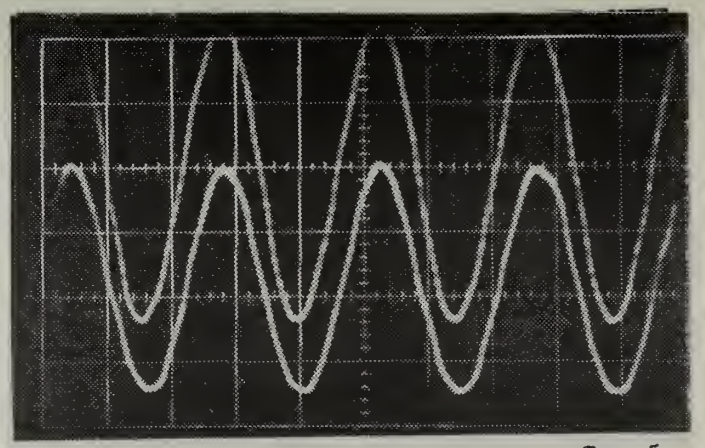

Tap 5

8.0 c/s, 0.05 s/cm

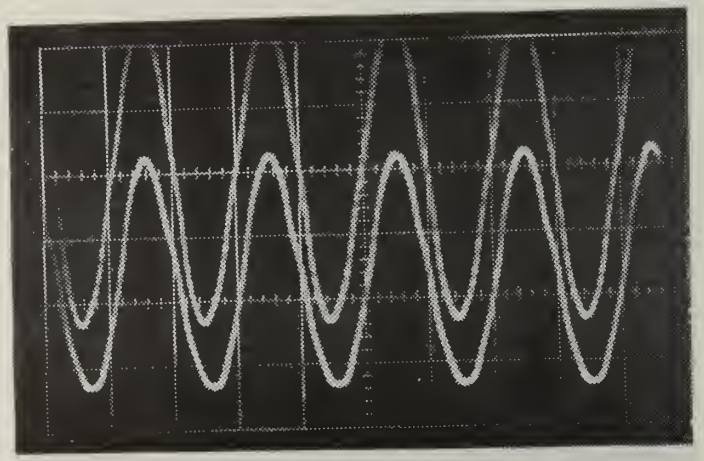

Tap 1

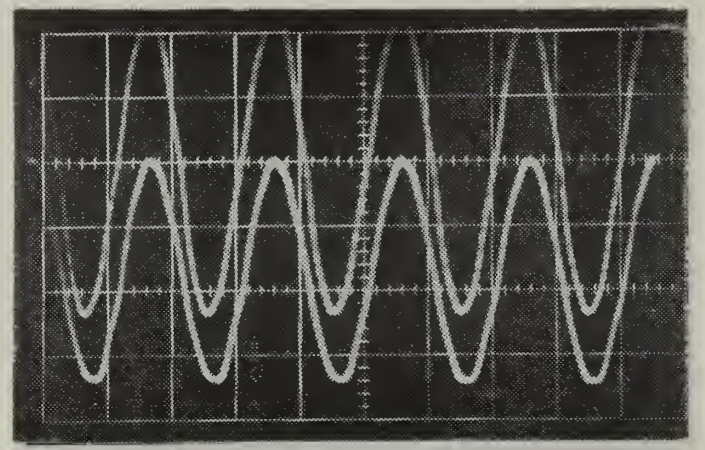

Tap 5

10.0 c/s, 0.05 s/cm

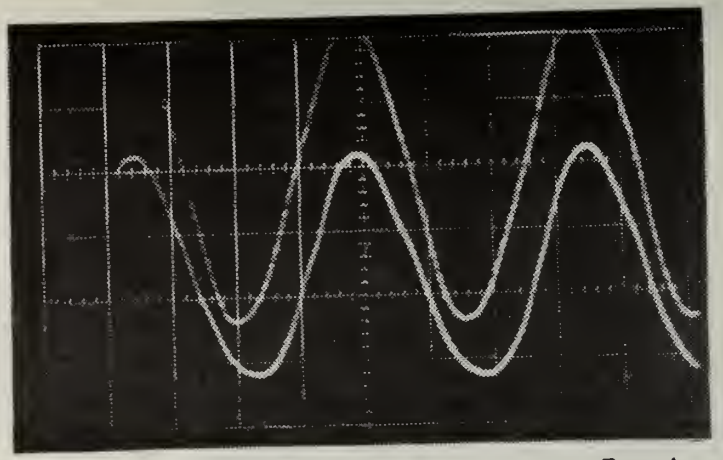

Tap 1

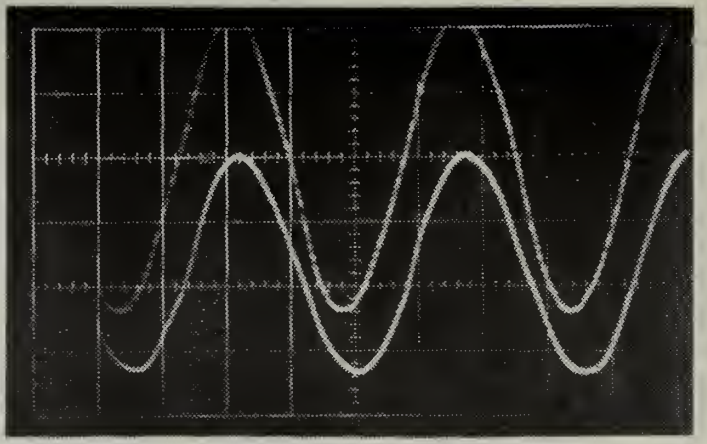

Tap 5

14.0 c/s, 0.02 s/cm

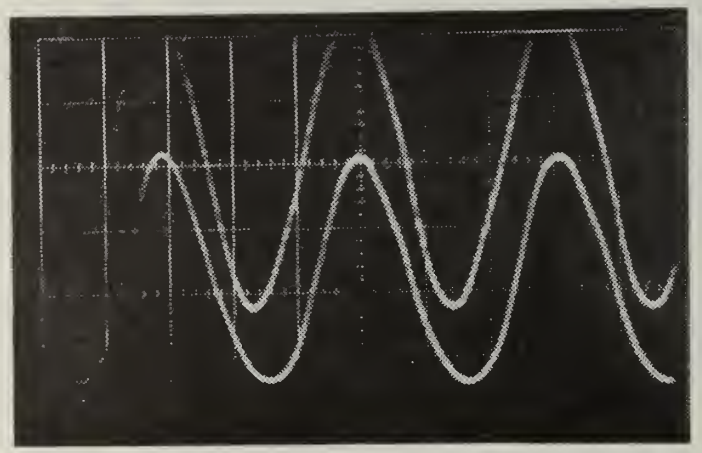

Tap 1

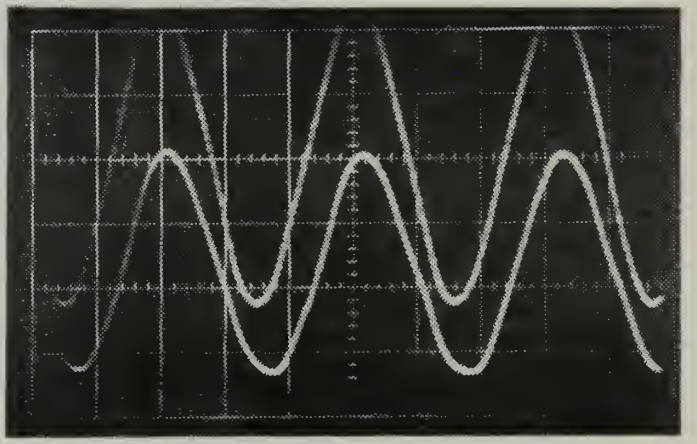

Tap 5

16.0 c/s, 0.02 s/cm

III. Non-Oscillatory Data

a. Angle of Attack = ± 20°

(1) M = 2.8

(2) P_{∞} = 52.7

(3) ϕ = 225° and 45°

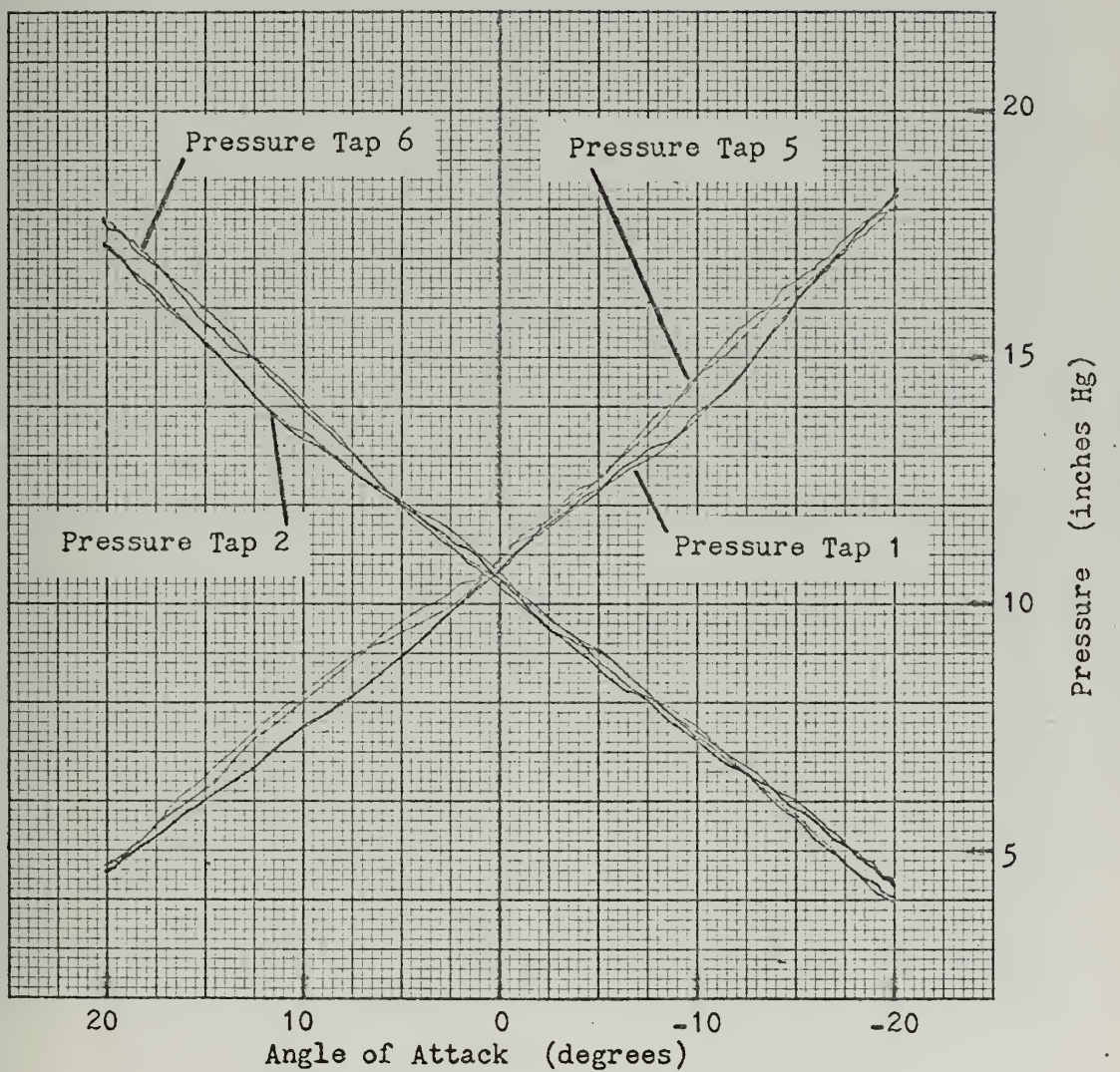

b. Angle of Attack = $\pm$ 24°

(1) M = 2.8

(2) P_{∞} = 52.7

(3) ϕ = 225° and 45°

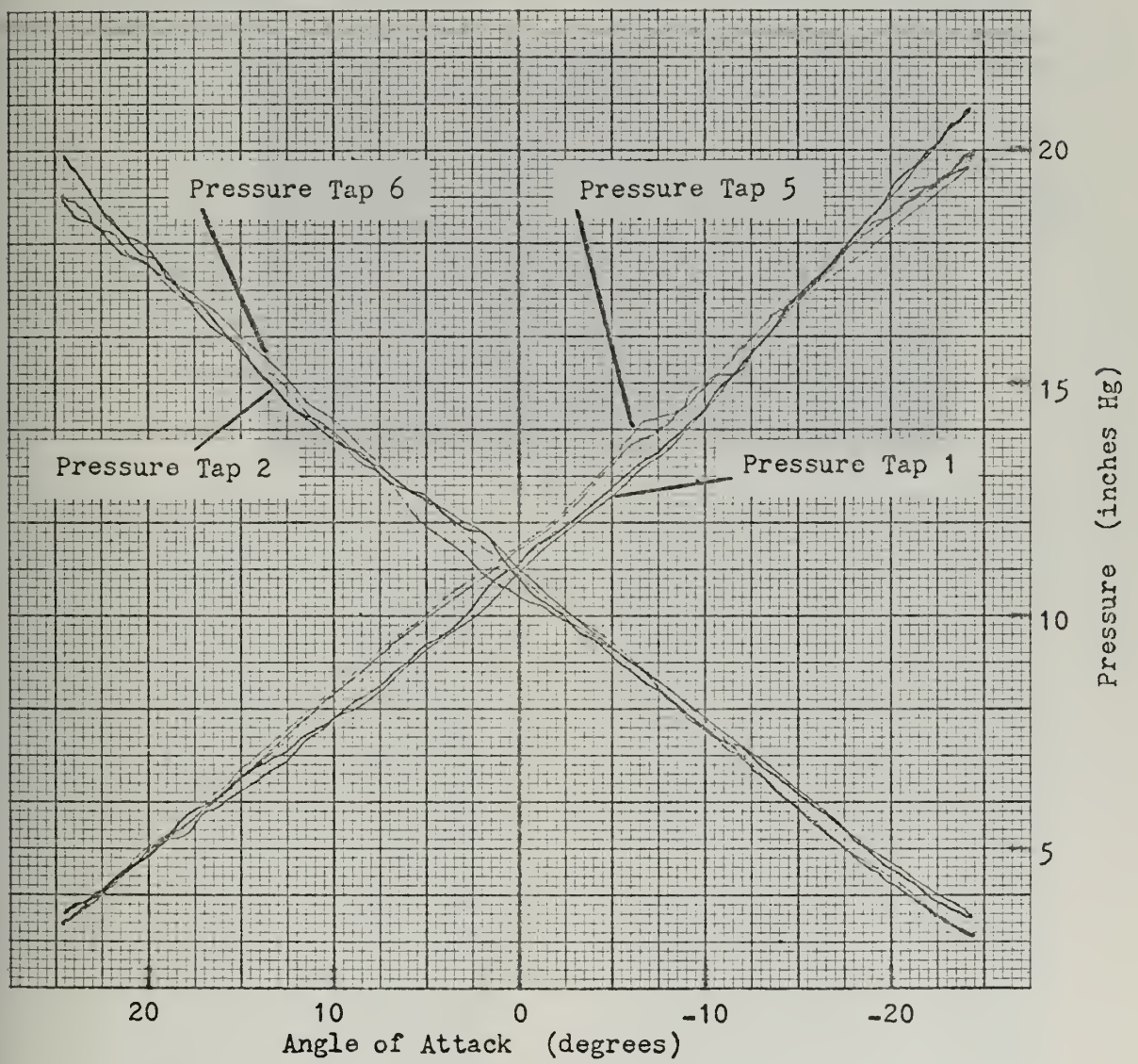

E. PRESSURE TAP ANGLE PHI = 90° AND 270°

1. Common Variables

   a. M = 2.8

   b. P_{∞} = 52.7

   c. AOA = $\pm$ 20°

2. Grid Scales

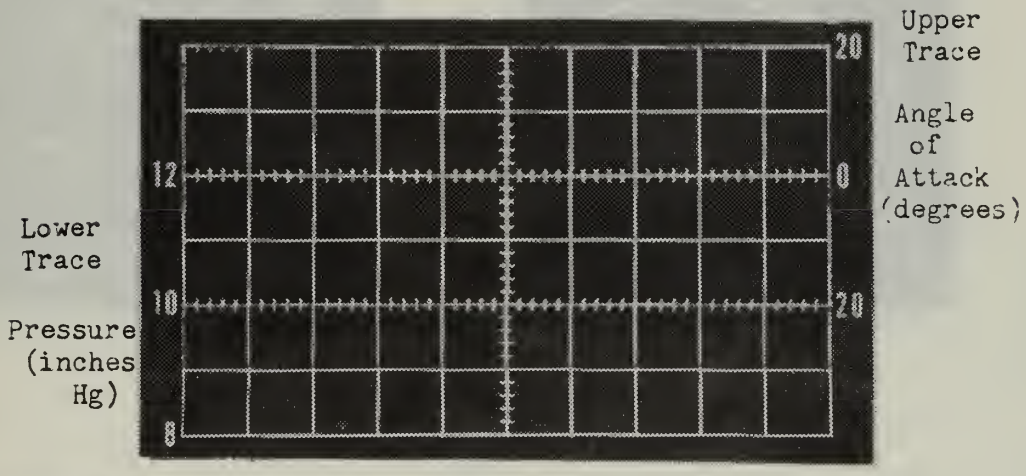

Pressure Tap ___

f = ___ c/s, t = ___ s/cm

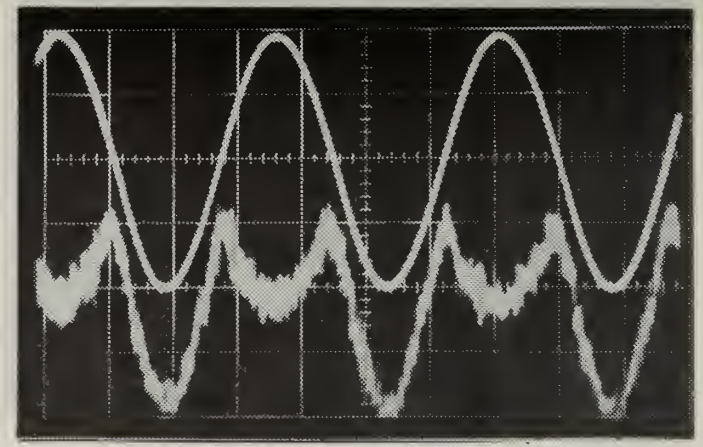

Tap 2

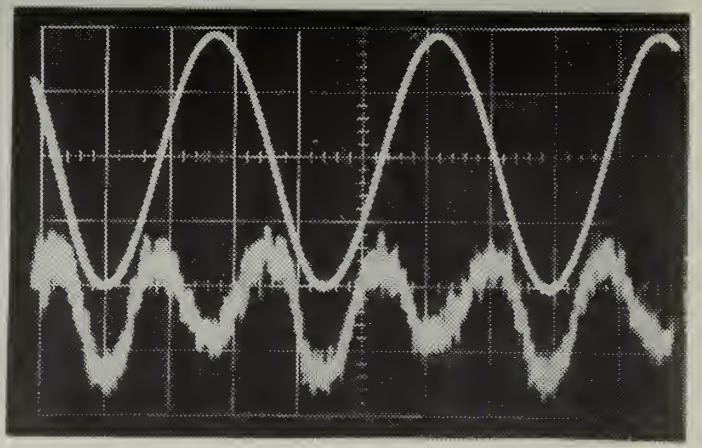

Tap 6

1.0 c/s, 0.5 s/cm

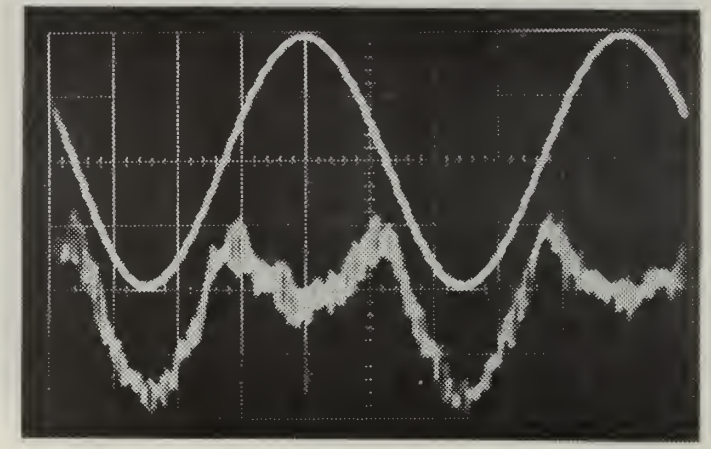

Tap 2

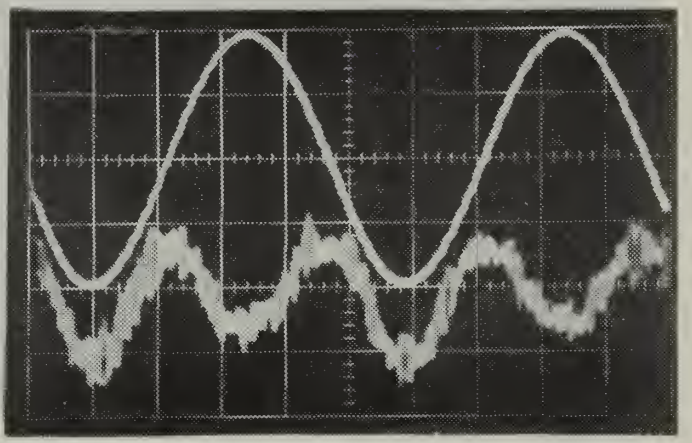

Tap 6

2.0 c/s, 0.1 s/cm

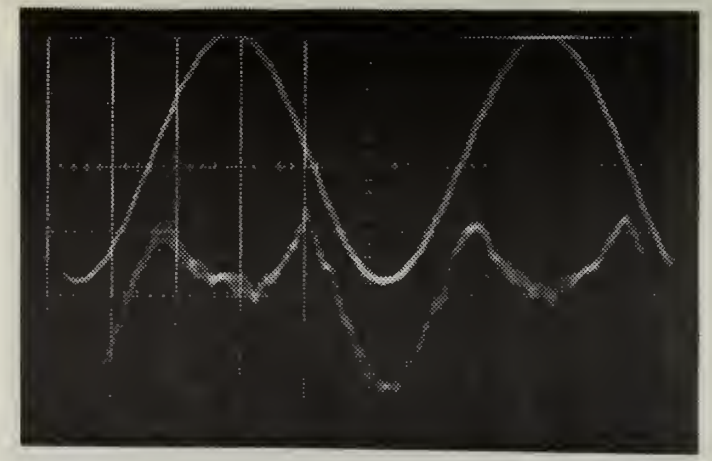

Tap 2

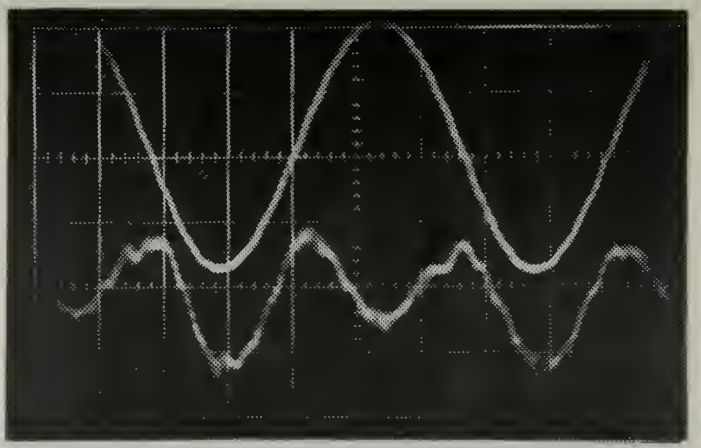

Tap 6

4.0 c/s, 0.05 s/cm

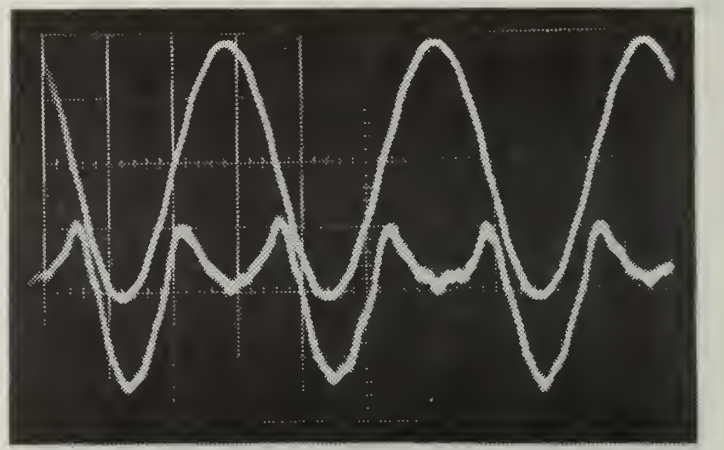

Tap 2

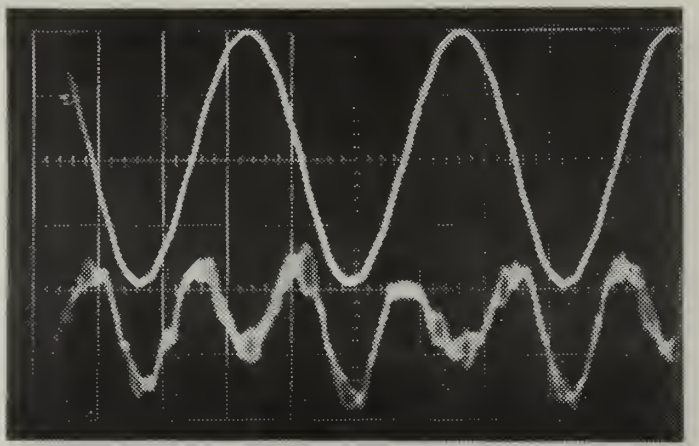

Tap 6

6.0 c/s, 0.05 s/cm

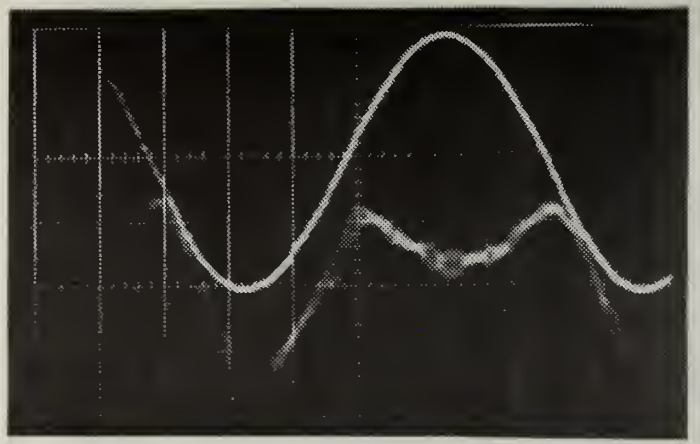

Tap 2

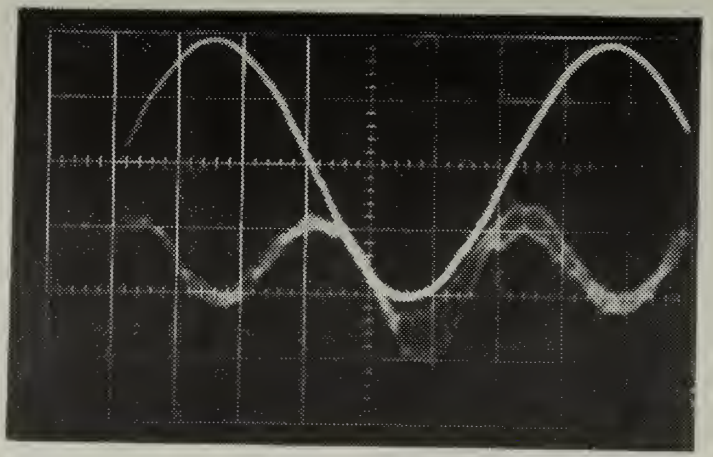

Tap 6

8.0 c/s, 0.02 s/cm

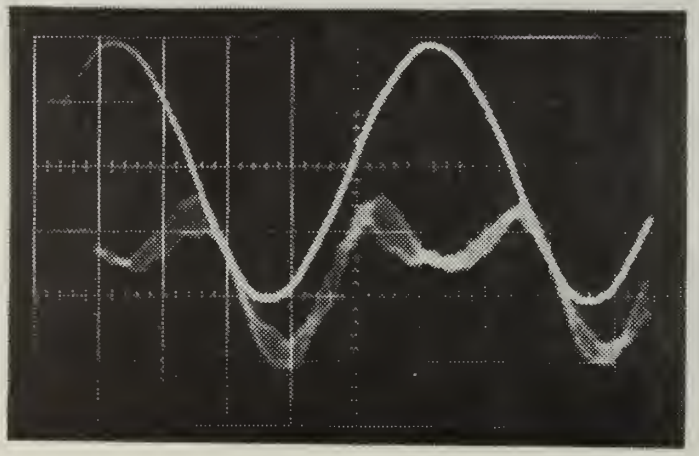

Tap 2

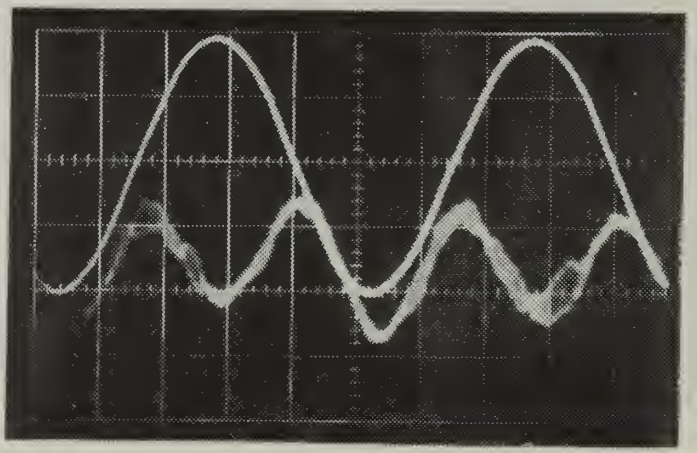

Tap 6

10.0 c/s, 0.02 s/cm

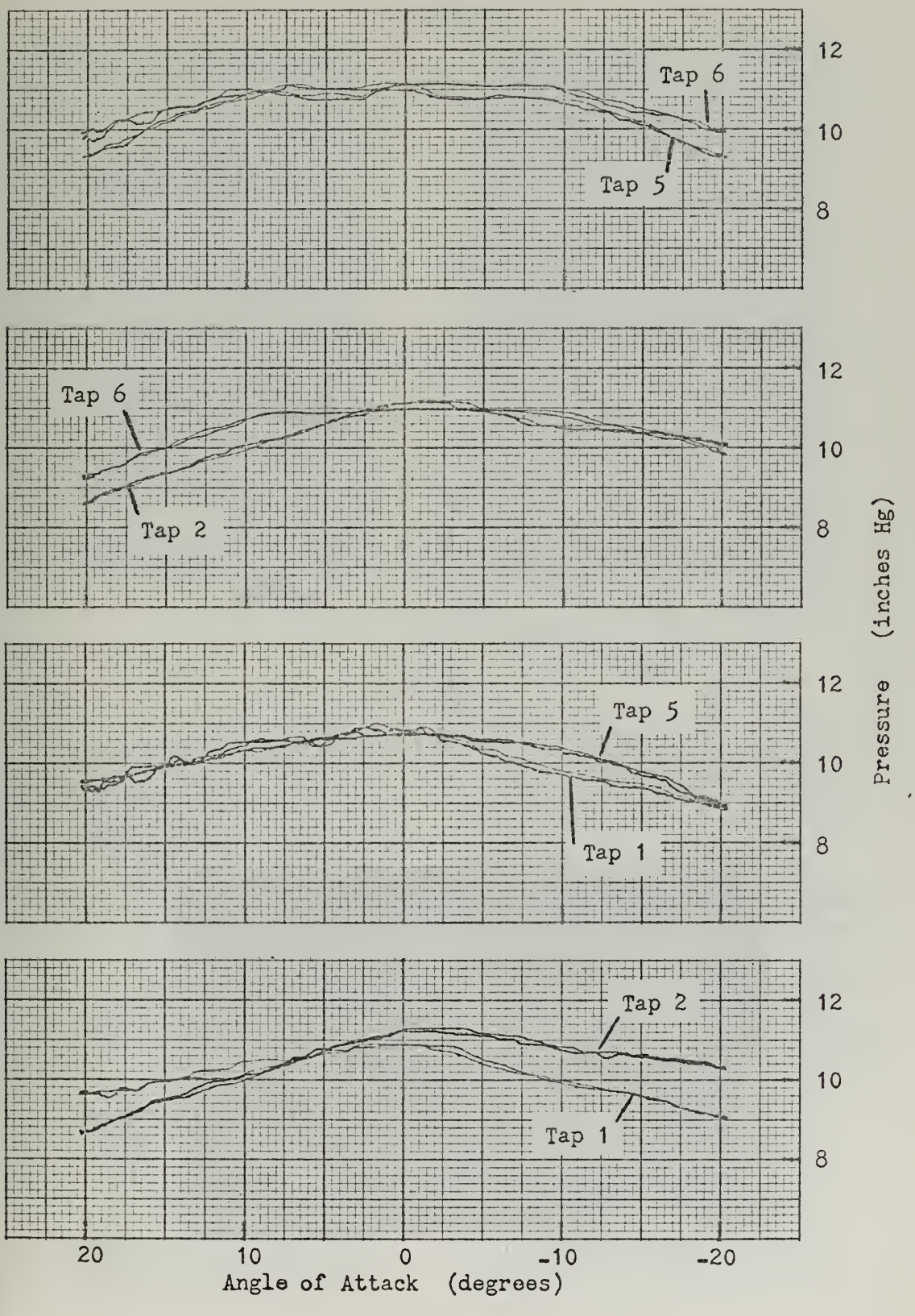

NON-OSCILLATORY CONE DATA (ϕ = 90° and 270°)

APPENDIX C

WEDGE DATA

A. COMMON VARIABLES

1. M = 2.8
2. P_∞ = 52.7 psi
3. AOA = $\pm$ 20°

B. PRESSURE TAP DIAGRAM

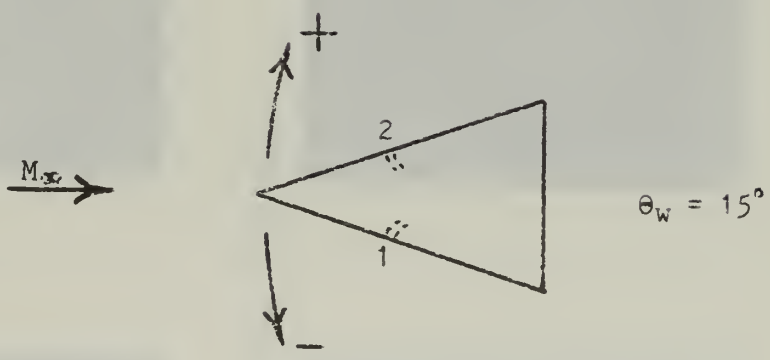

C. GRID SCALES

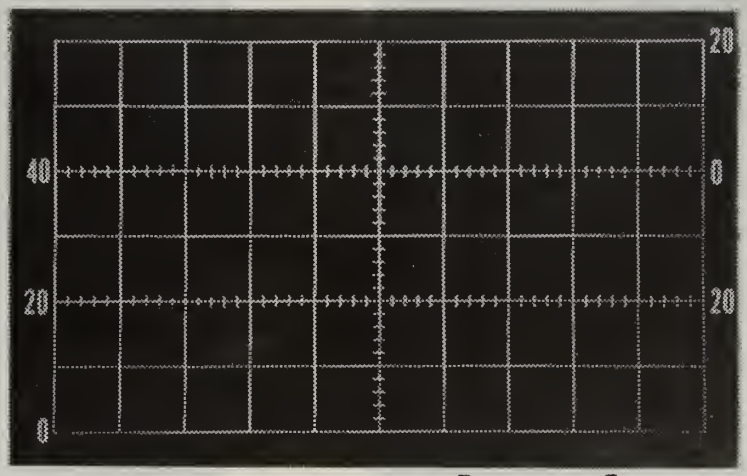

Lower Trace

Pressure (inches Hg)

Upper Trace

Angle of Attack (degrees)

Pressure Tap ___

f = ___ c/s, t = ___ s/cm

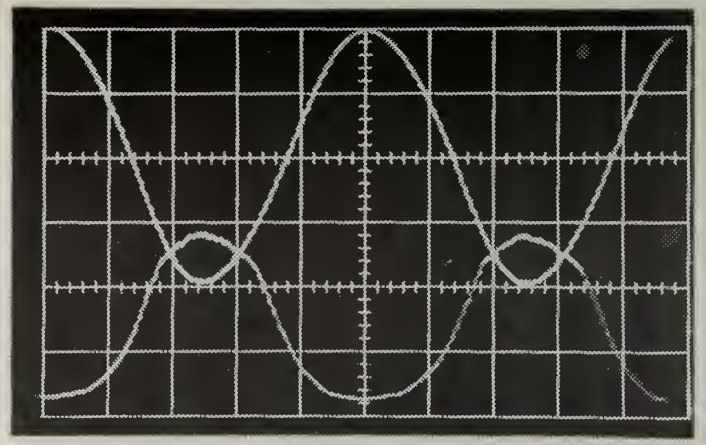

Tap 1

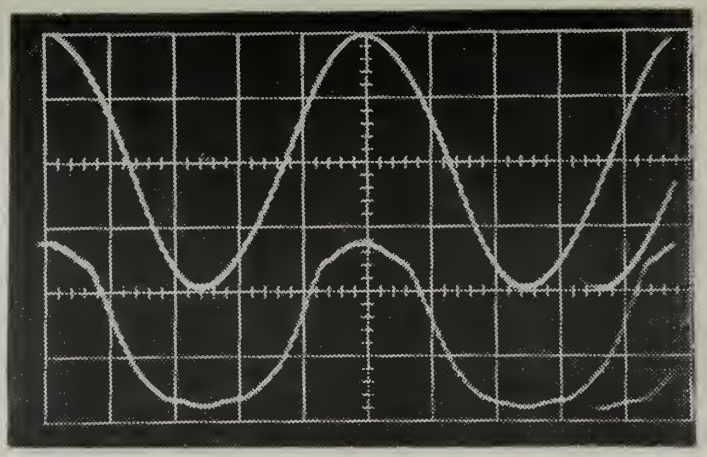

Tap 2

1.0 c/s, 0.2 s/cm

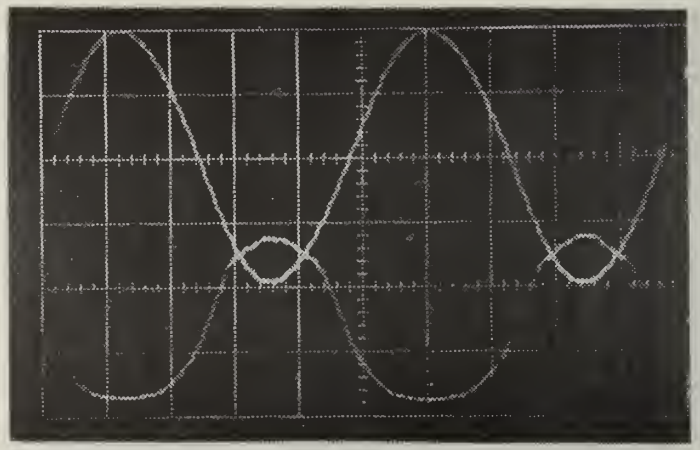

Tap 1

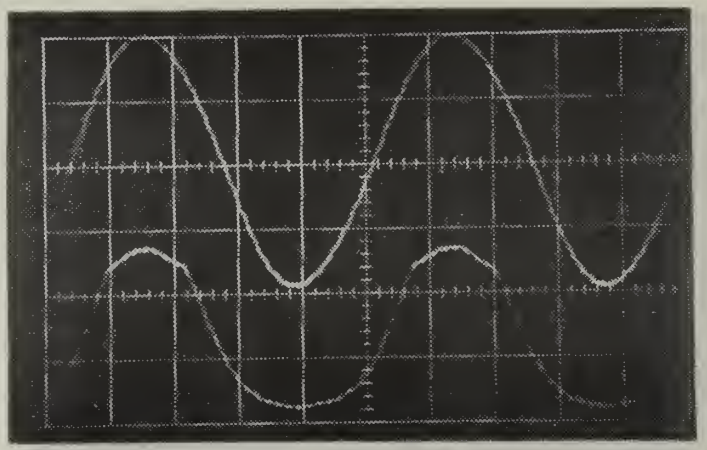

Tap 2

2.0 c/s, 0.1 s/cm

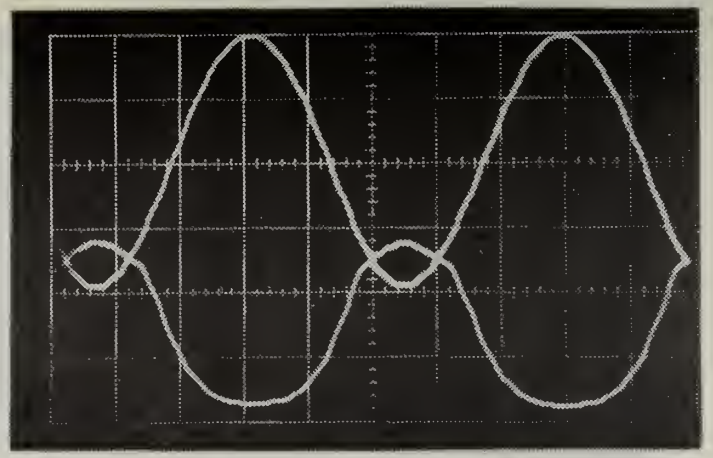

Tap 1

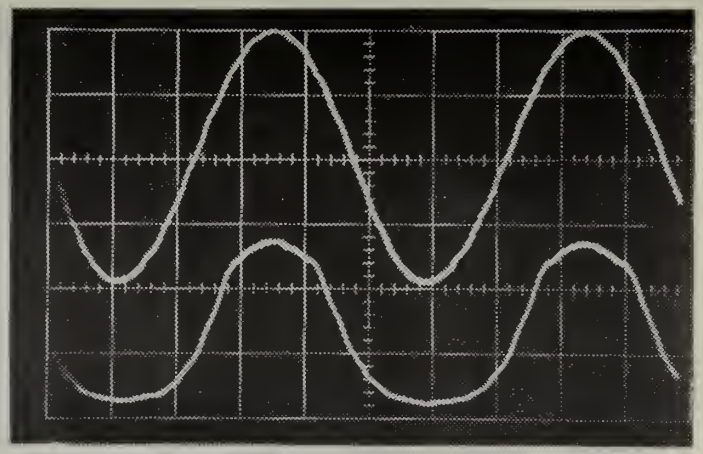

Tap 2

4.0 c/s, 0.05 s/cm

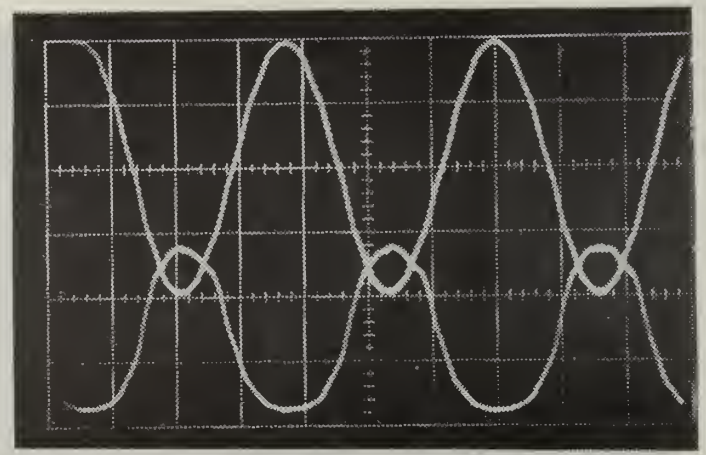

Tap 1

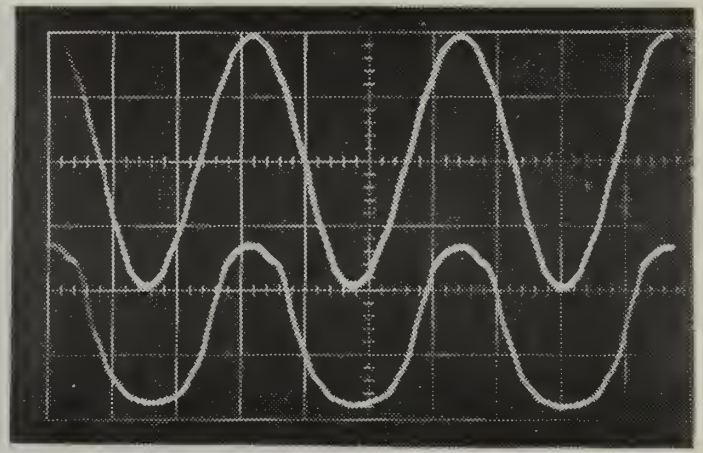

Tap 2

6.0 c/s, 0.05 s/cm

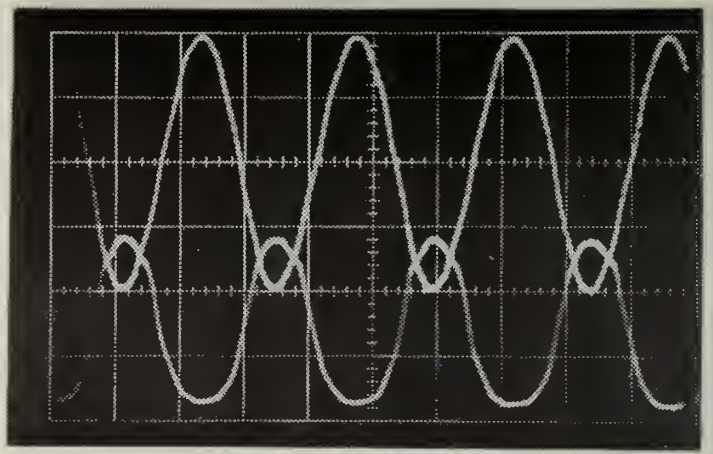

Tap 1

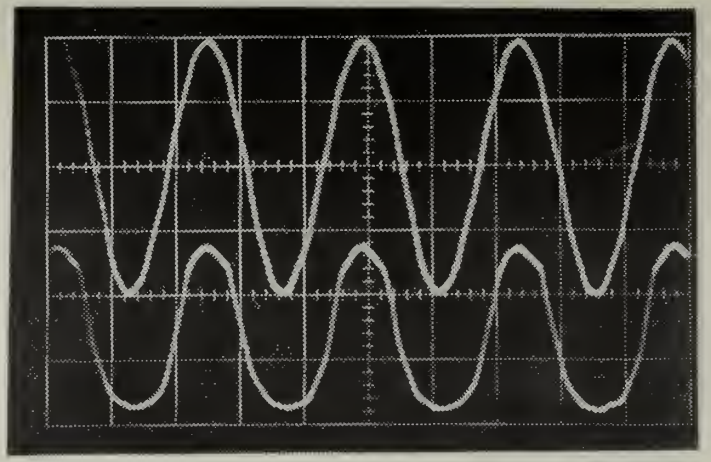

Tap 2

8.0 c/s, 0.05 s/cm

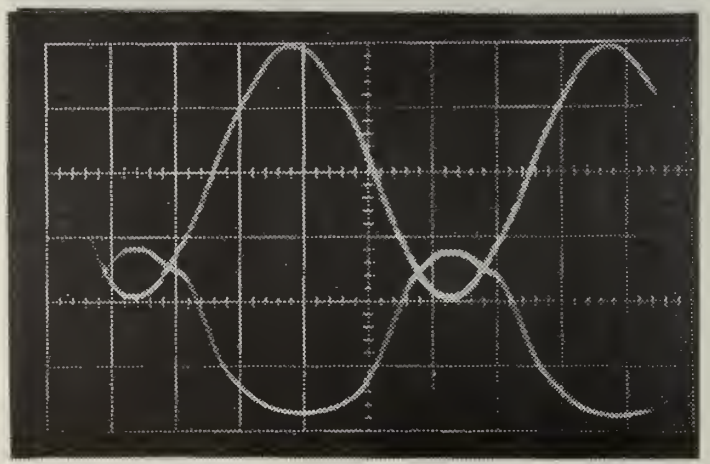

Tap 1

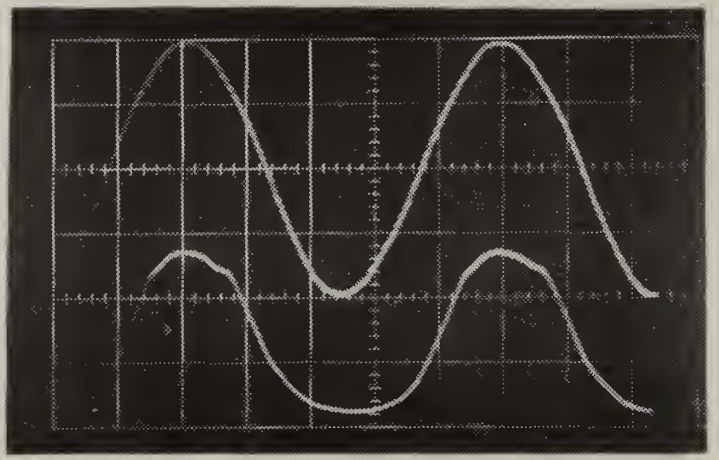

Tap 2

10.0 c/s, 0.02 s/cm

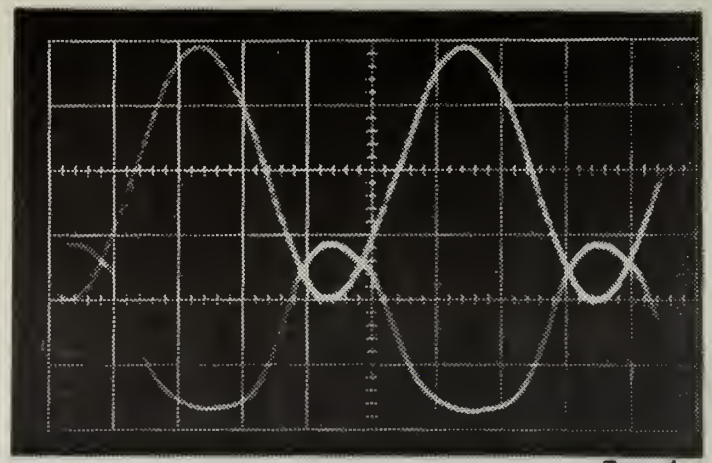

Tap 1

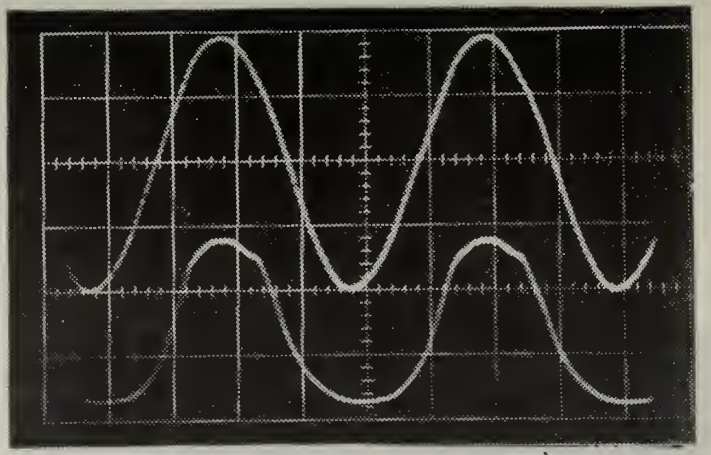

Tap 2

12.0 c/s, 0.02 s/cm

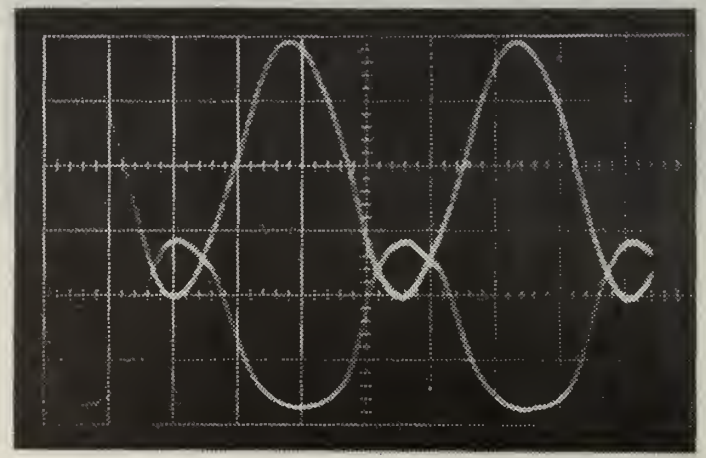

Tap 1

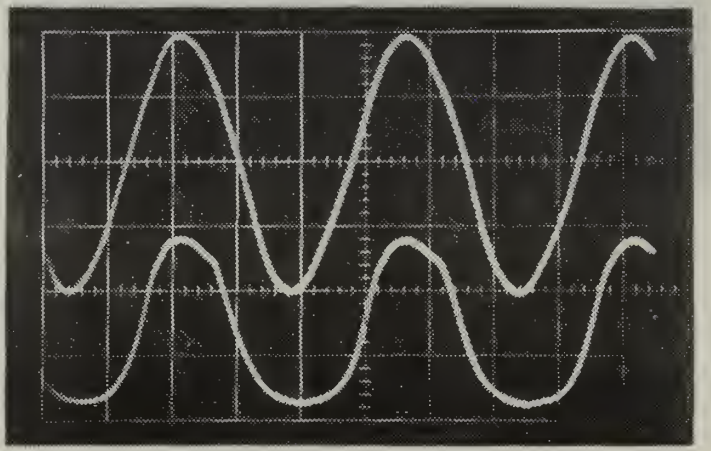

Tap 2

14.0 c/s, 0.02 s/cm

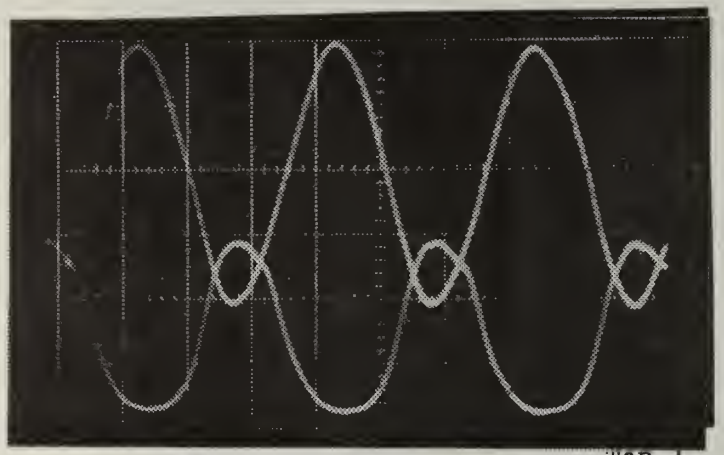

Tap 1

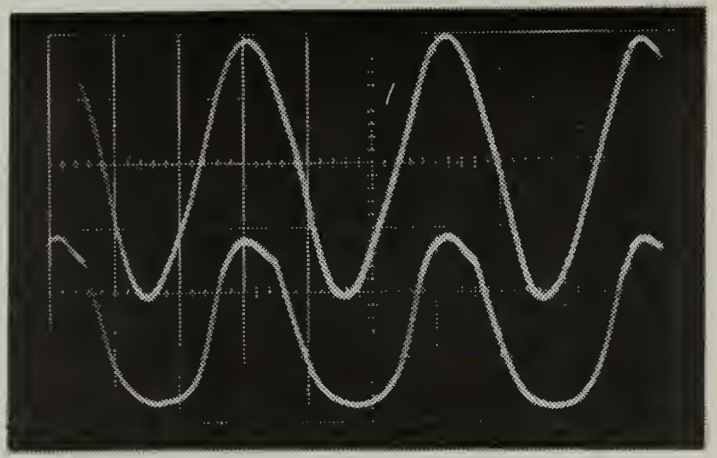

Tap 2

16.0 c/s, 0.02 s/cm

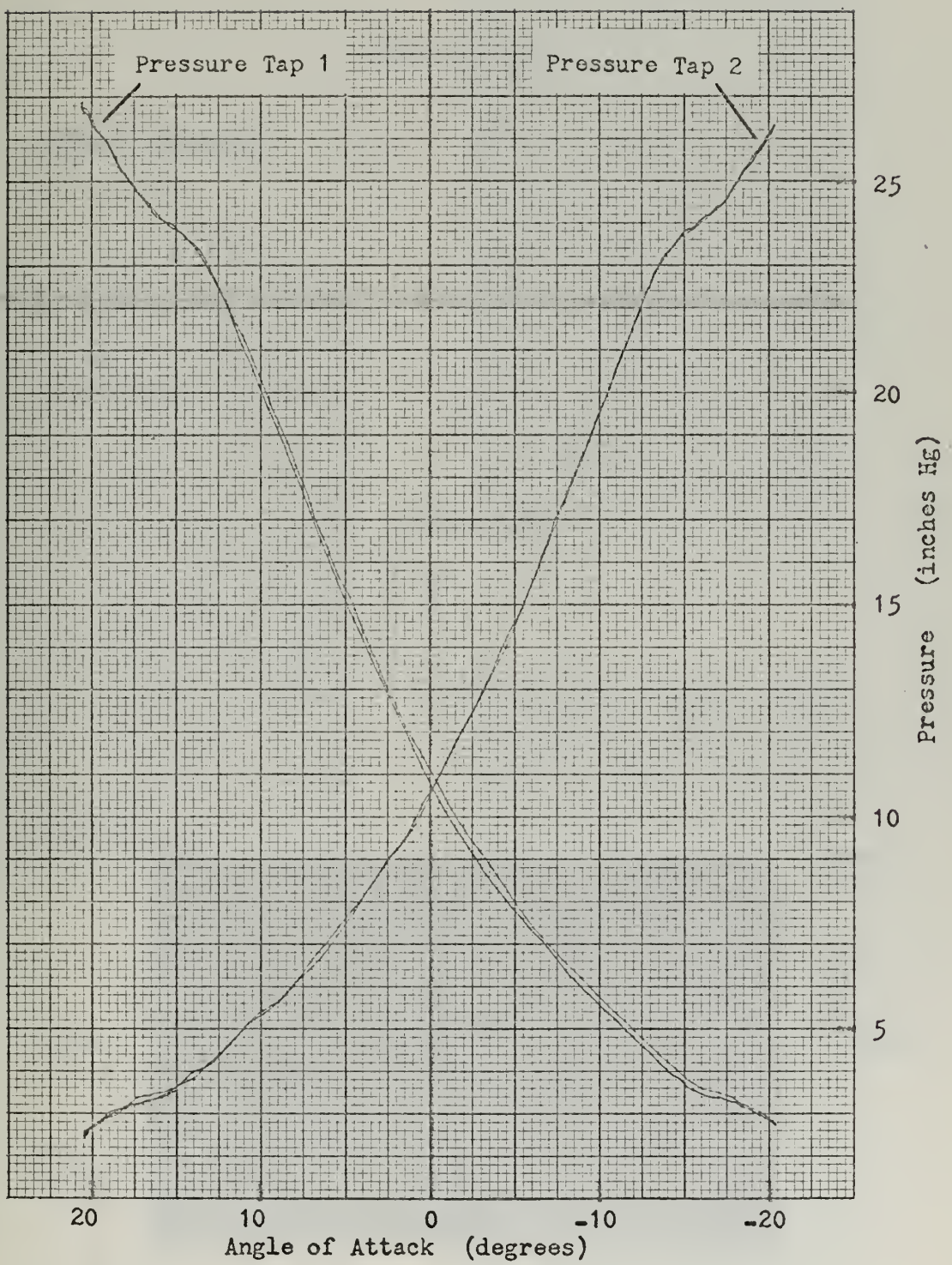

WEDGE NON-OSCILLATORY DATA

APPENDIX D

FLAT PLATE DATA

A. COMMON VARIABLES

1. M = 2.8

2. P_∞ = 52.7 psi

3. AOA = ± 5°

B. PRESSURE TAP DIAGRAM

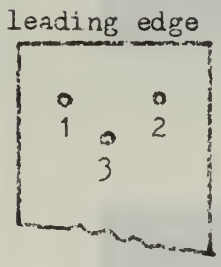

C. GRID SCALES

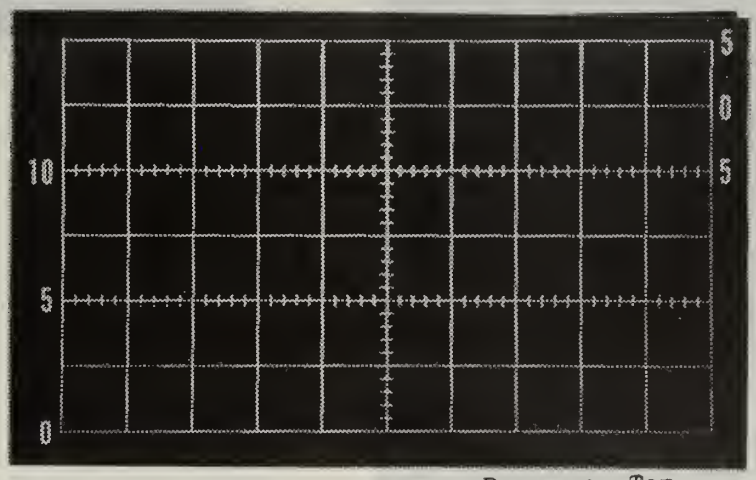

Upper Trace

Angle of Attack (degrees)

Lower Trace

Pressure (inches Hg)

Pressure Tap ___

f = ___ c/s, t = ___ s/cm

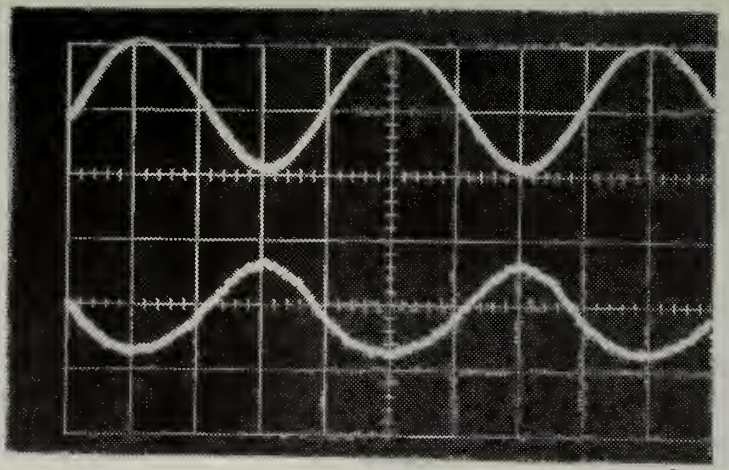

Tap 1

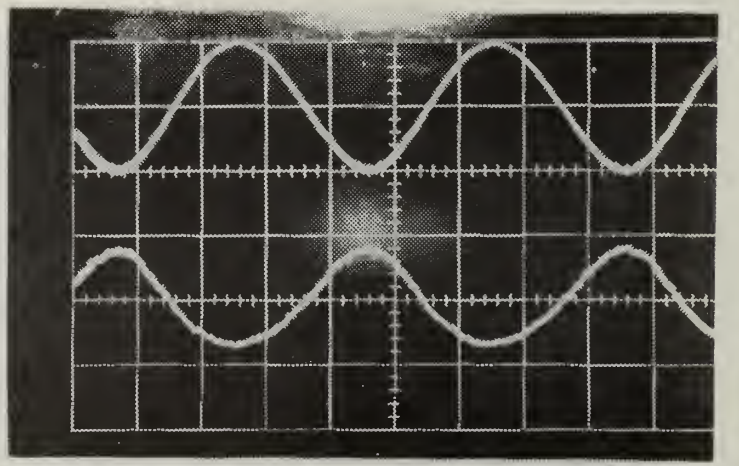

Tap 2

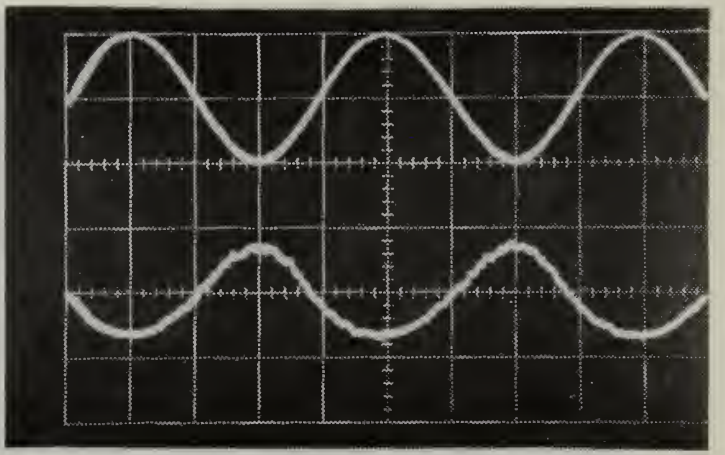

Tap 3

0.5 c/s, 0.5 s/cm

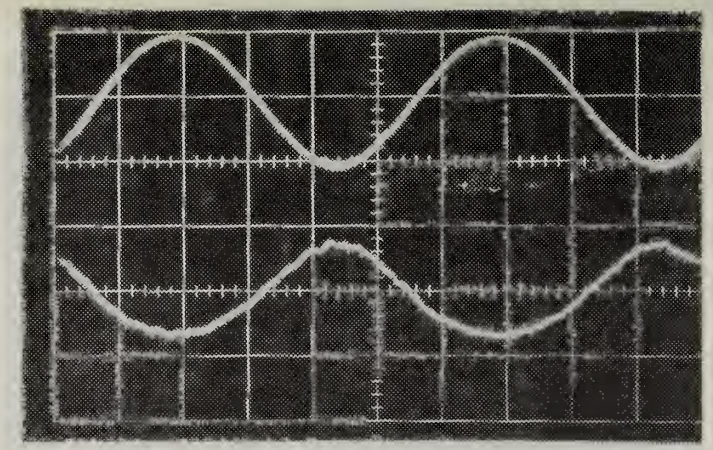

Tap 1

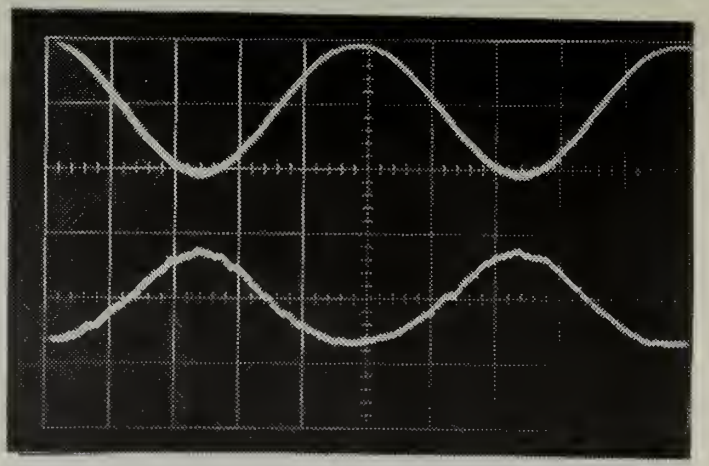

Tap 3

1.0 c/s, 0.2 s/cm

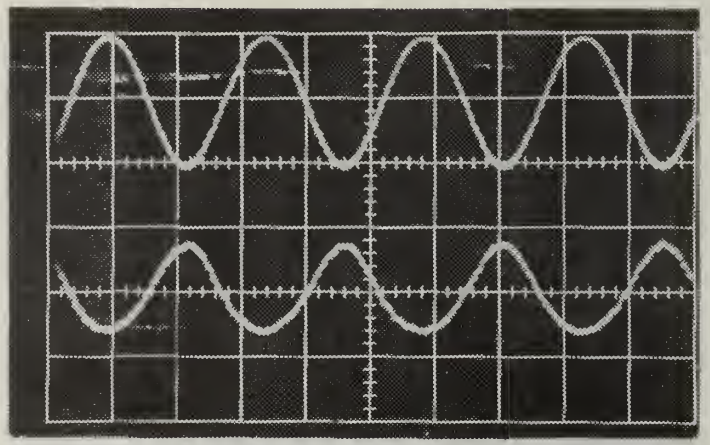

Tap 1

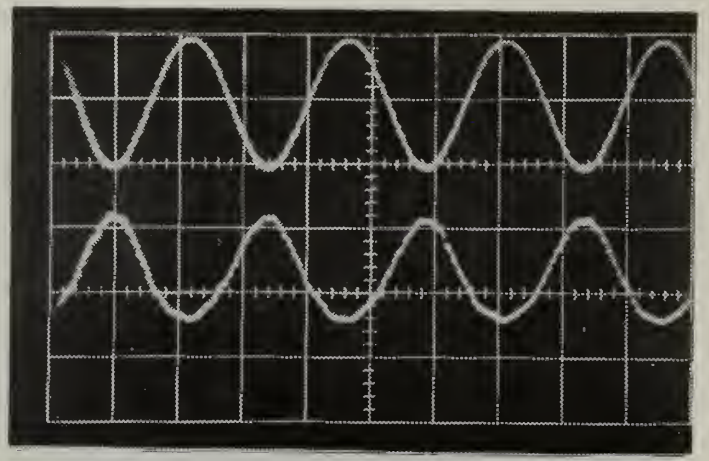

Tap 2

2.0 c/s, 0.2 s/cm

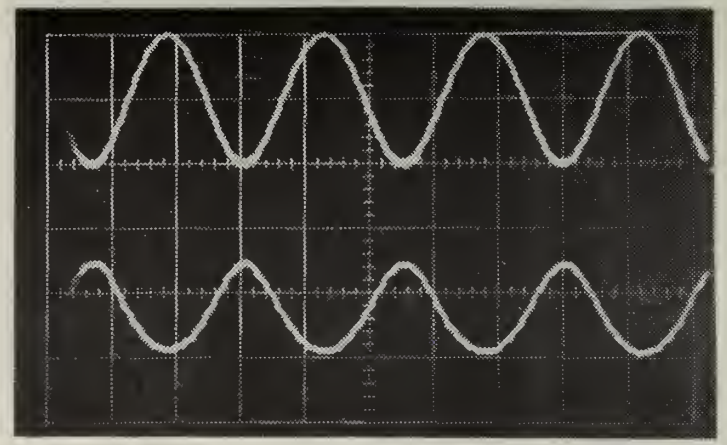

Tap 1

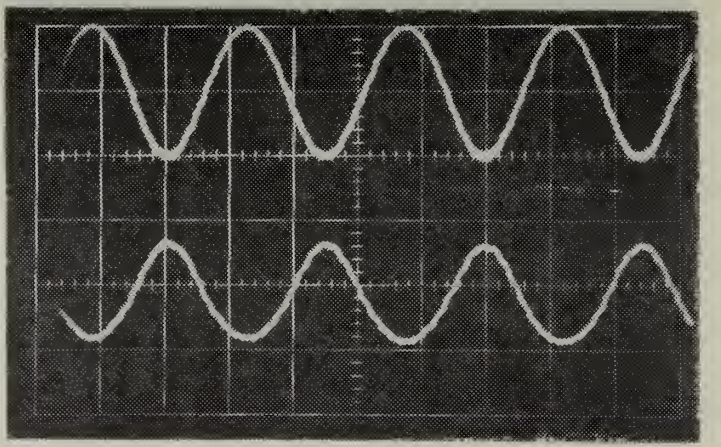

Tap 2

4.0 c/s, 0.1 s/cm

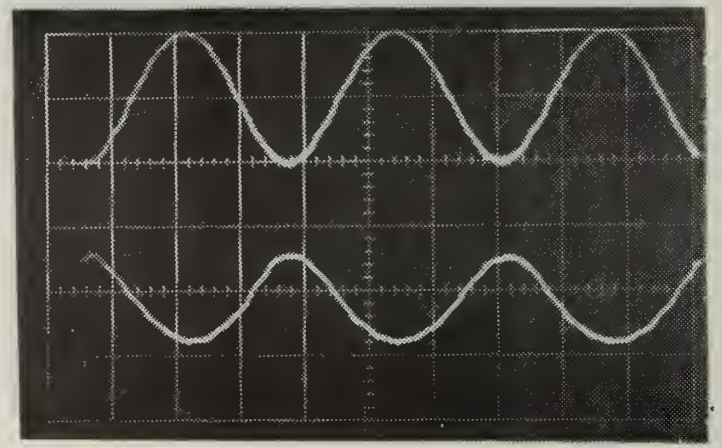

Tap 1

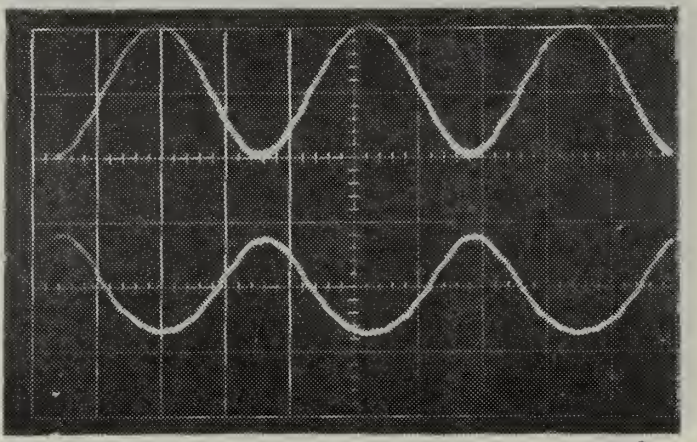

Tap 2

6.0 c/s, 0.05 s/cm

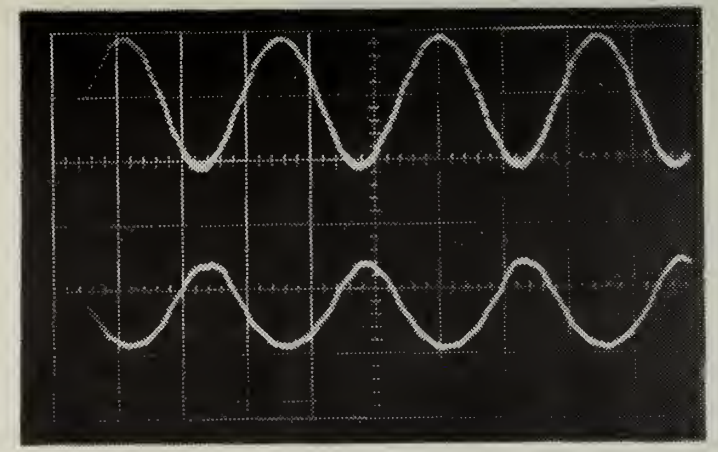

Tap 1

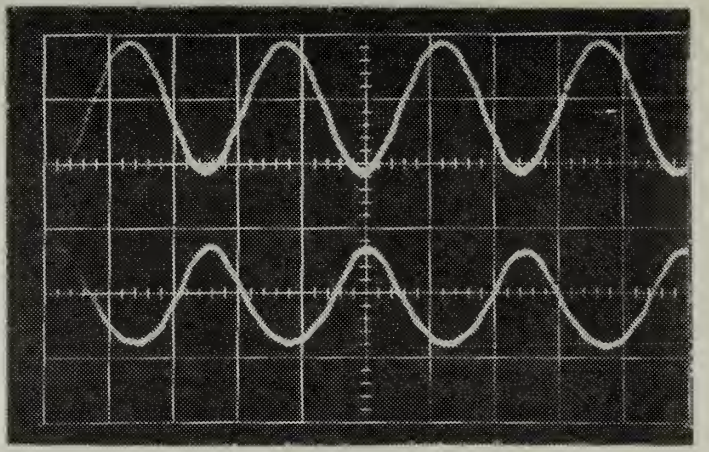

Tap 2

3.0 c/s, 0.05 s/cm

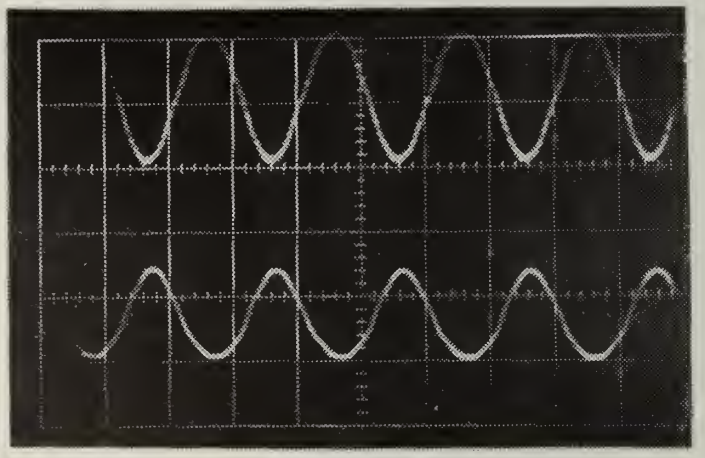

Tap 1

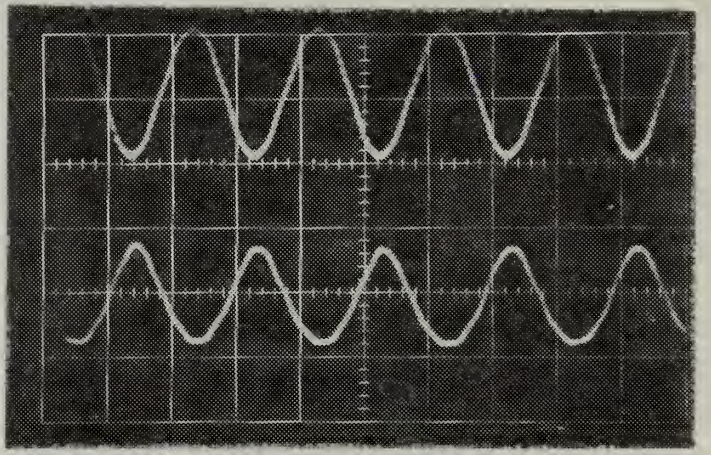

Tap 2

10.0 c/s, 0.05 s/cm

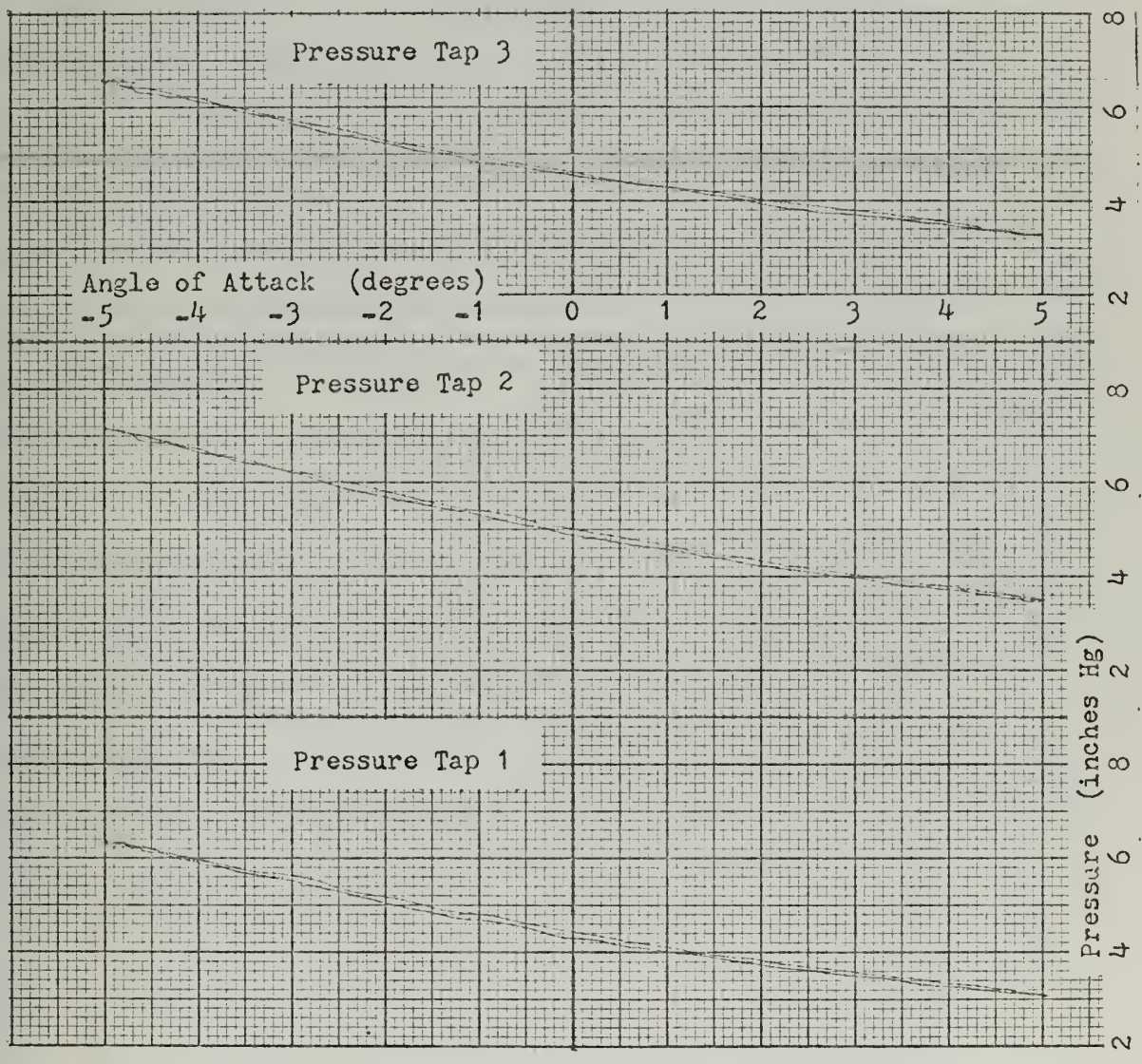

FLAT PLATE NON-OSCILLATORY DATA

APPENDIX E

SCHLIEREN PHOTOGRAPHY DATA

The photographs on the following pages were taken with a Hycam Model K2004E 16 mm high speed movie camera, and individual frames were reproduced. The frames selected were the top and bottom of the cycle of the oscillating wind tunnel model, and the approximate zero angle of attack position as the model was passing through in both directions. The same position, relative to the wind tunnel vertical bar, was selected for each of the zero angle of attack pictures. The wind tunnel model was oscillating at 2, 4, 8, and 16 cycles per second, and the camera speed was always 100 times the frequency, thereby taking 100 frames per cycle. The cone pictures are presented first, followed by the wedge pictures. Each model's pictures are in the order: top, bottom, going up, and going down through zero angle of attack, with frequency increasing as labeled.

2 cycles per second

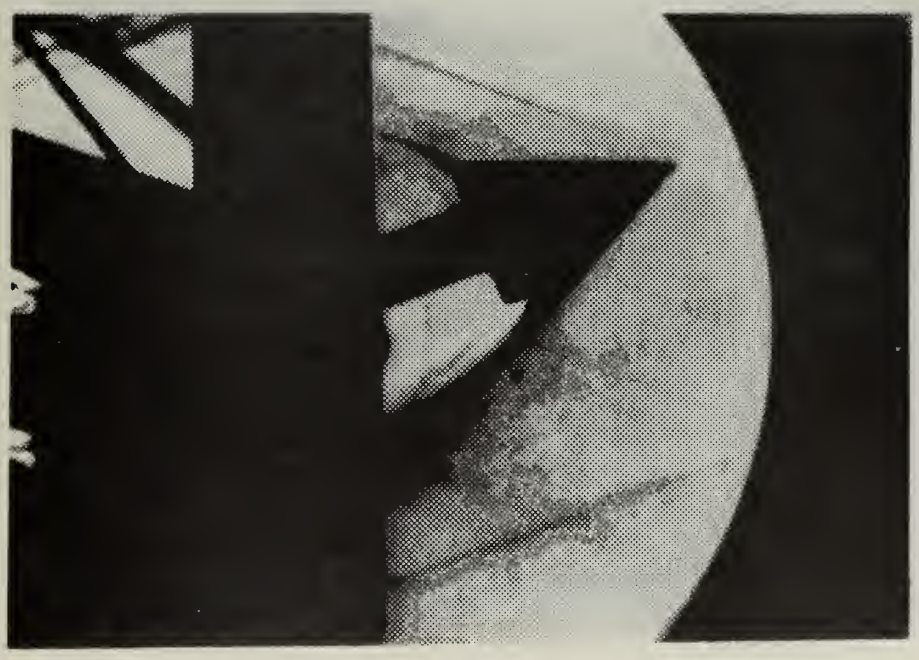

4 cycles per second

CONE AT TOP OF CYCLE

8 cycles per second

16 cycles per second

CONE AT TOP OF CYCLE

2 cycles per second

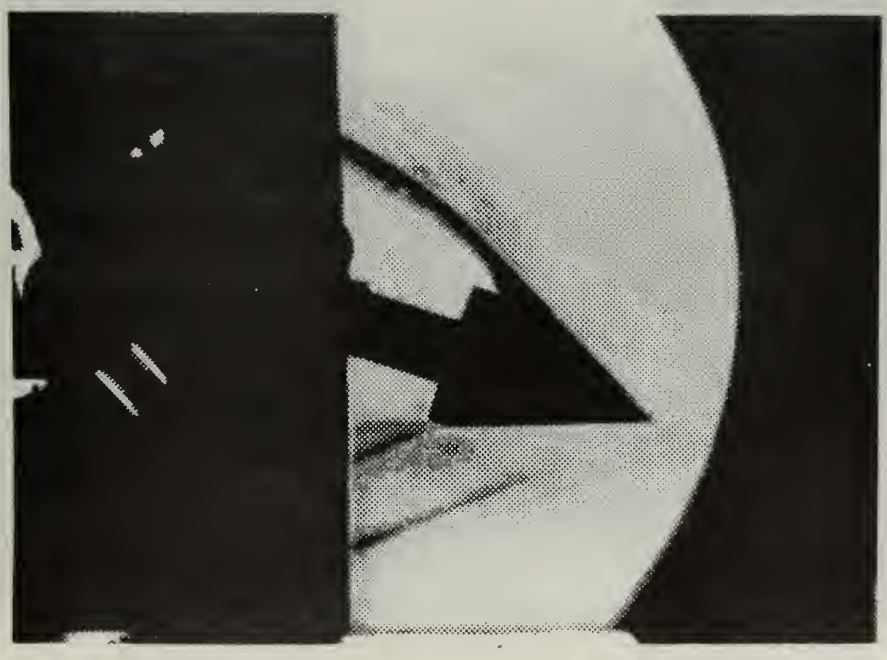

4 cycles per second

CONE AT BOTTOM OF CYCLE

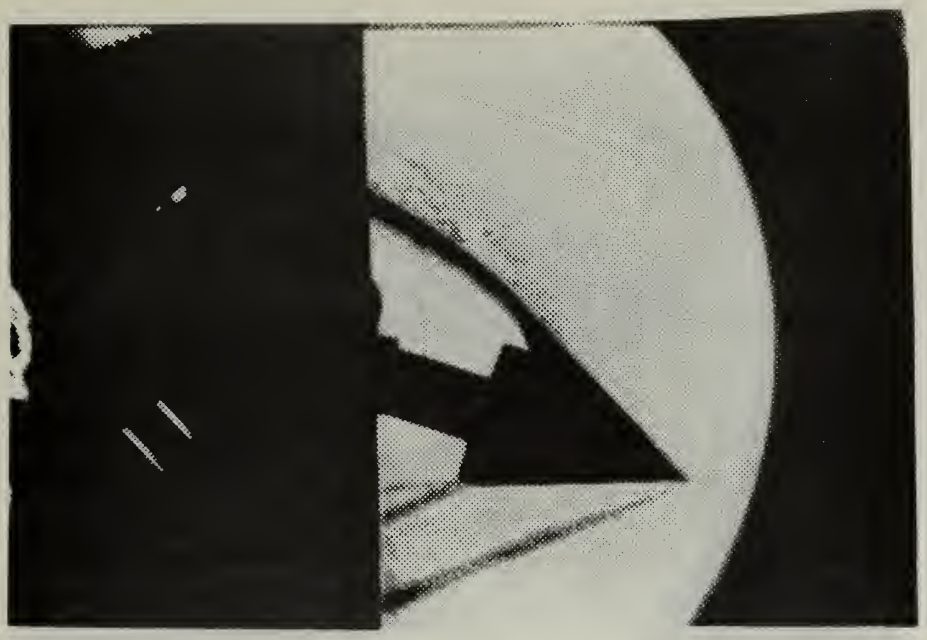

3 cycles per second

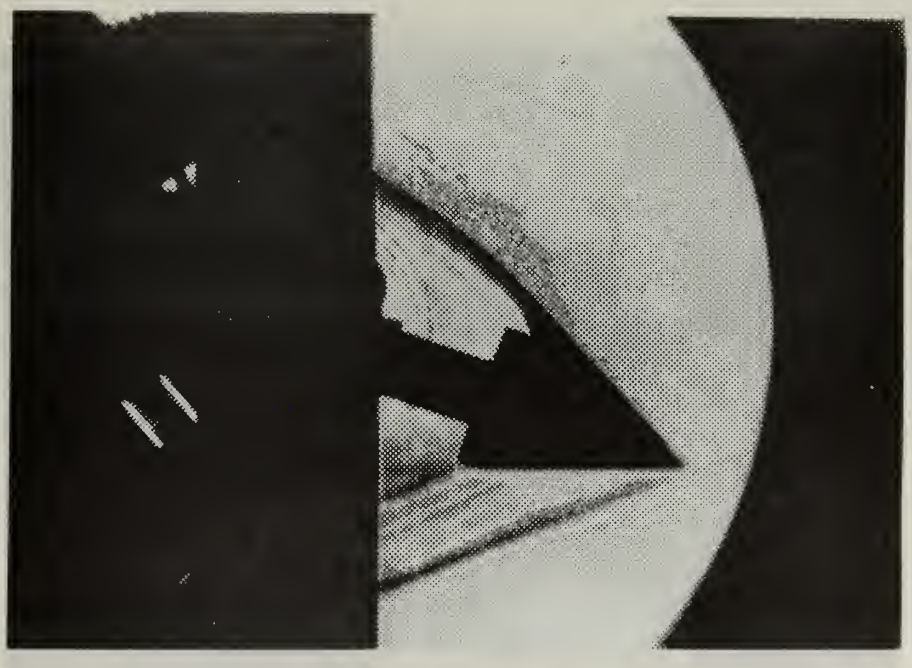

16 cycles per seconds

CONE AT BOTTOM OF CYCLE

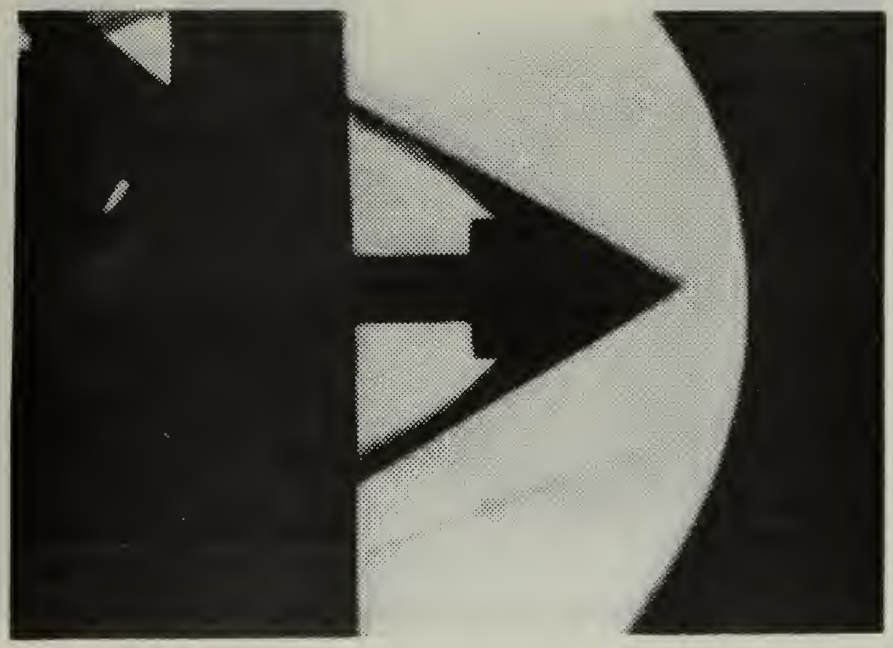

2 cycles per second

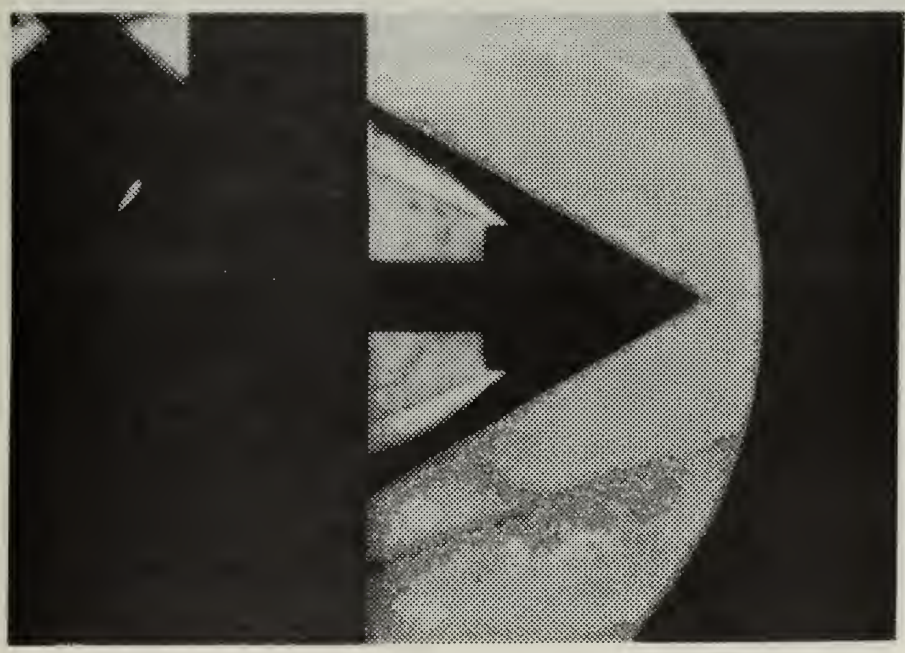

4 cycles per second

CONE GOING UP THRU ZERO AOA

8 cycles per second

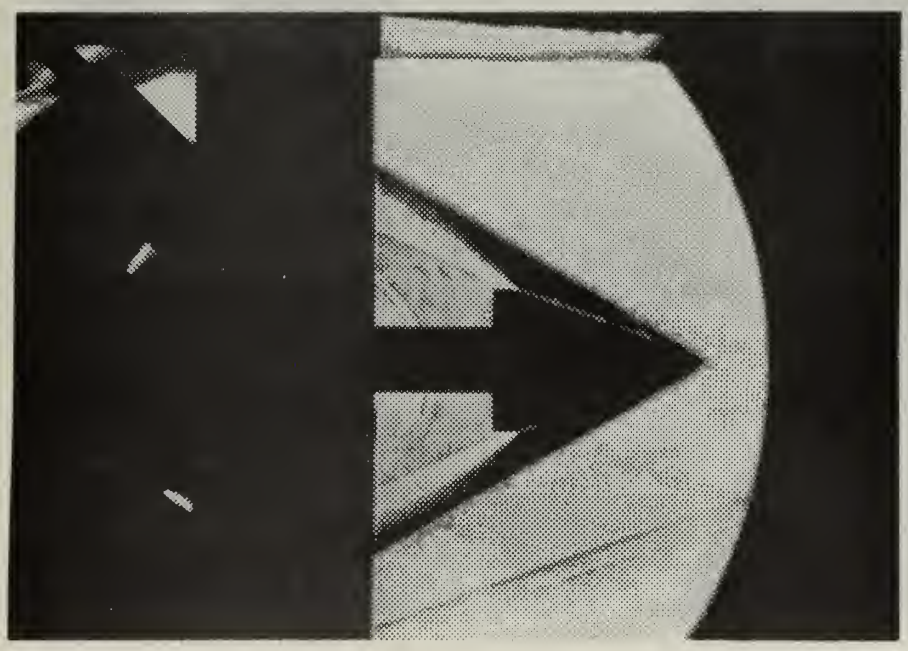

16 cycles per second

CONE GOING UP THRU ZERO AOA

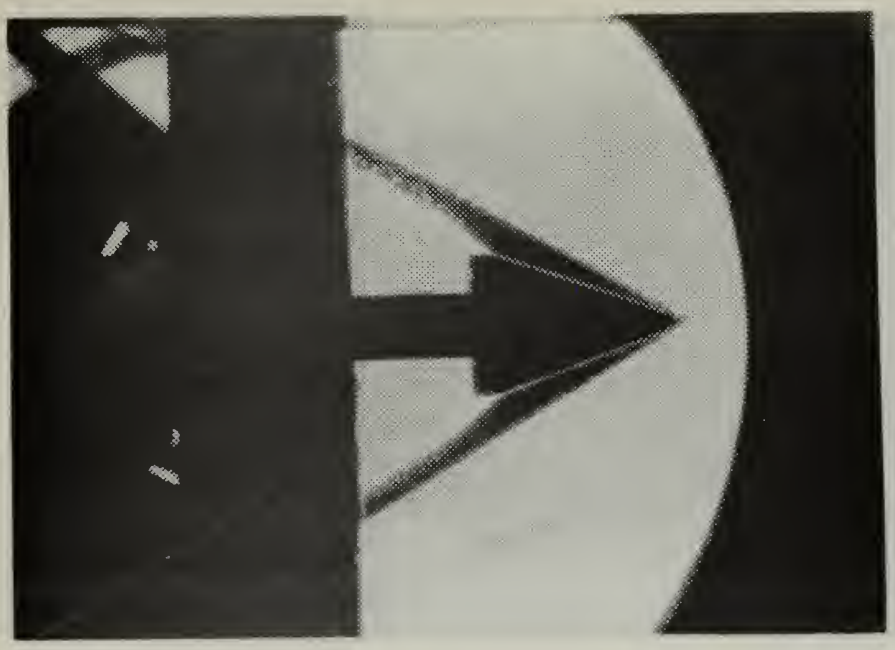

2 cycles per second

4 cycles per second

CONE GOING DOWN THRU ZERO AOA

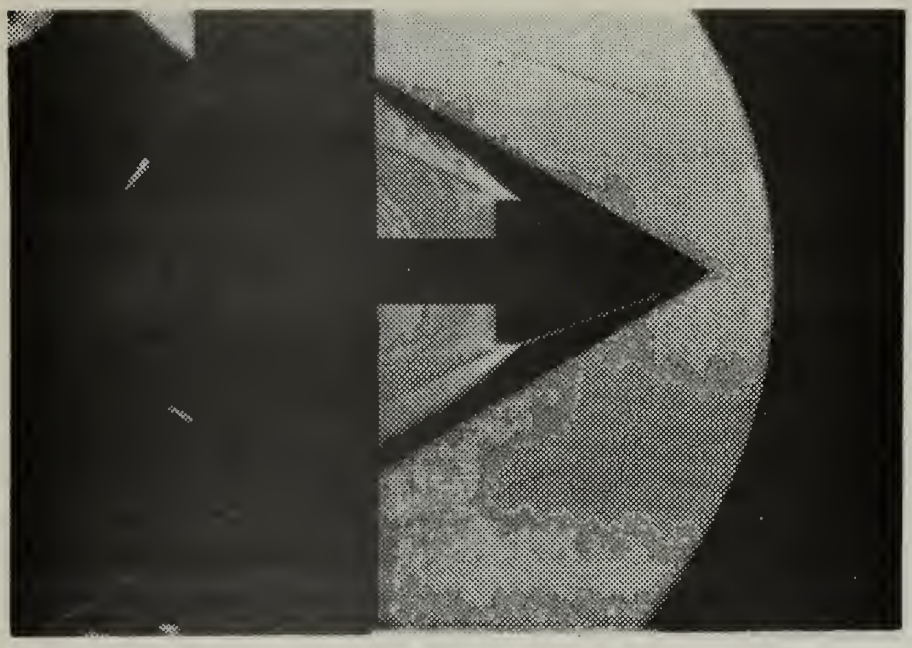

3 cycles per second

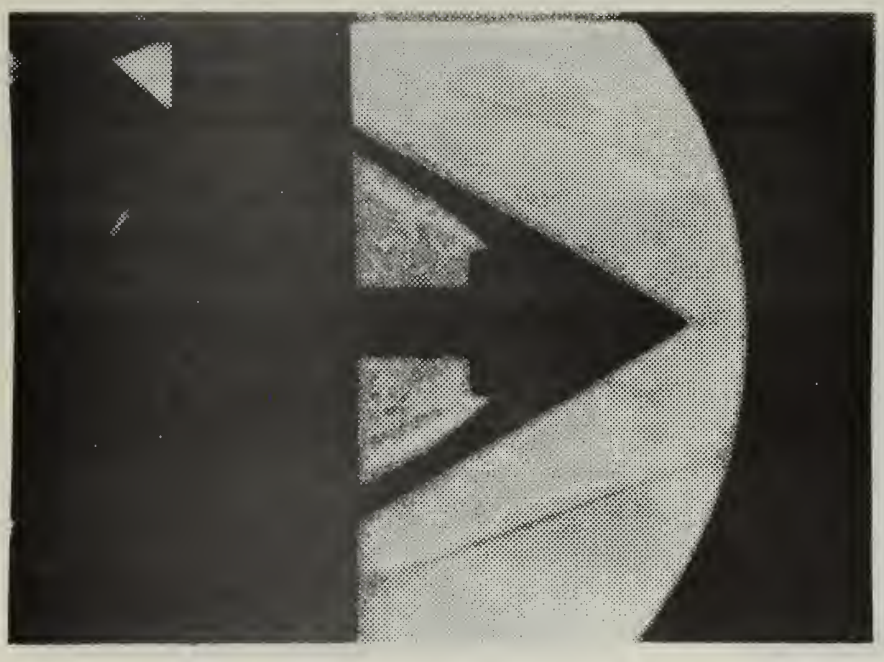

16 cycles per second

CONE GOING DOWN THRU ZERO AOA

2 cycles per second

4 cycles per second

WEDGE AT TOP OF CYCLE

8 cycles per second

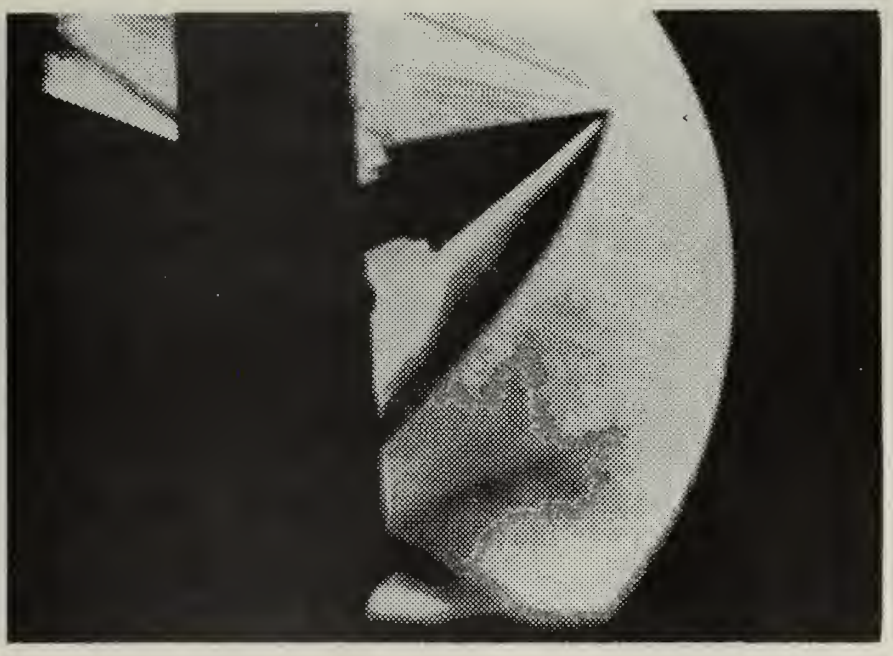

16 cycles per second

WEDGE AT TOP OF CYCLE

2 cycles per second

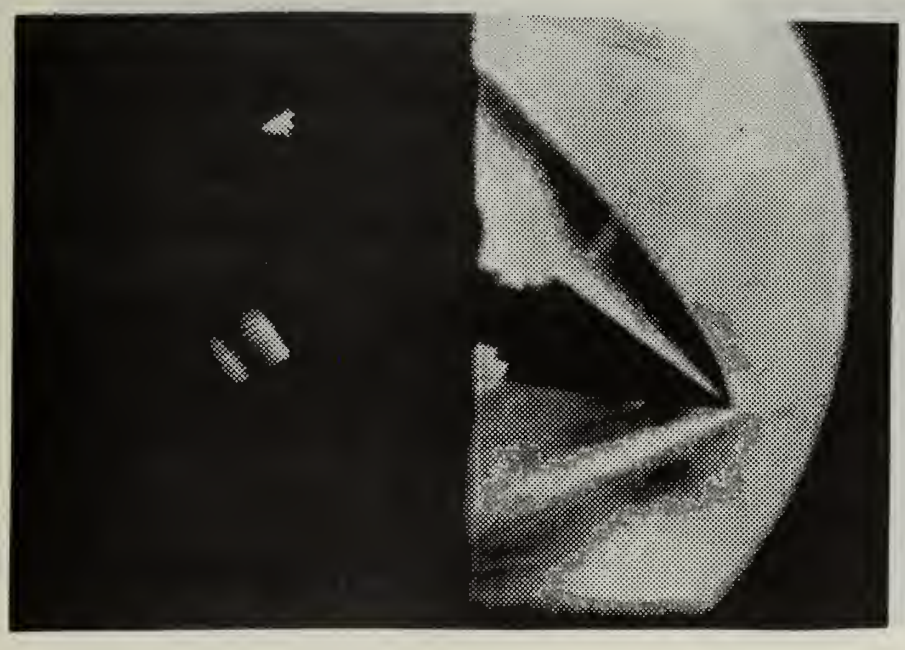

4 cycles per second

WEDGE AT BOTTOM OF CYCLE

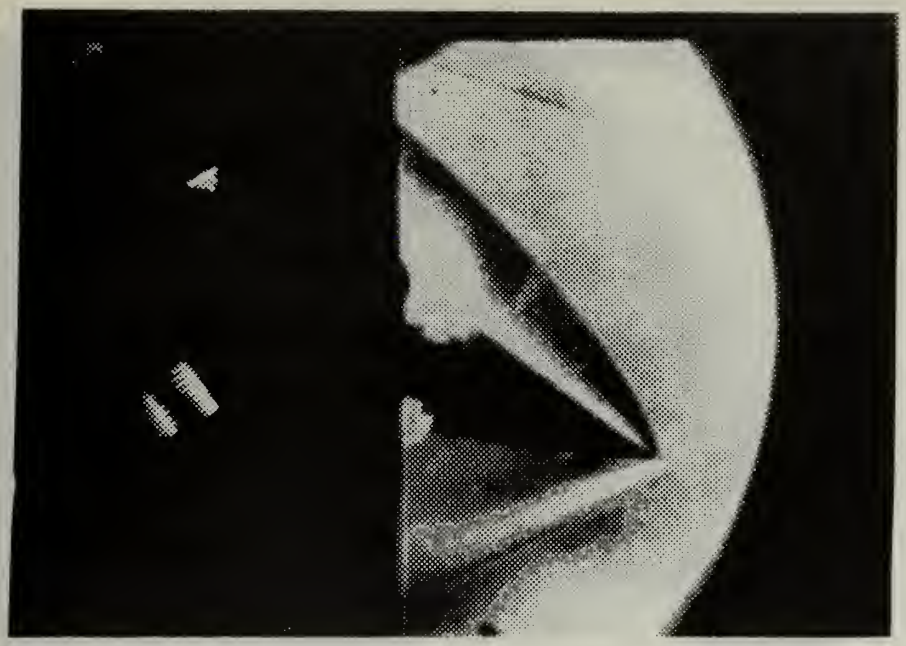

8 cycles per second

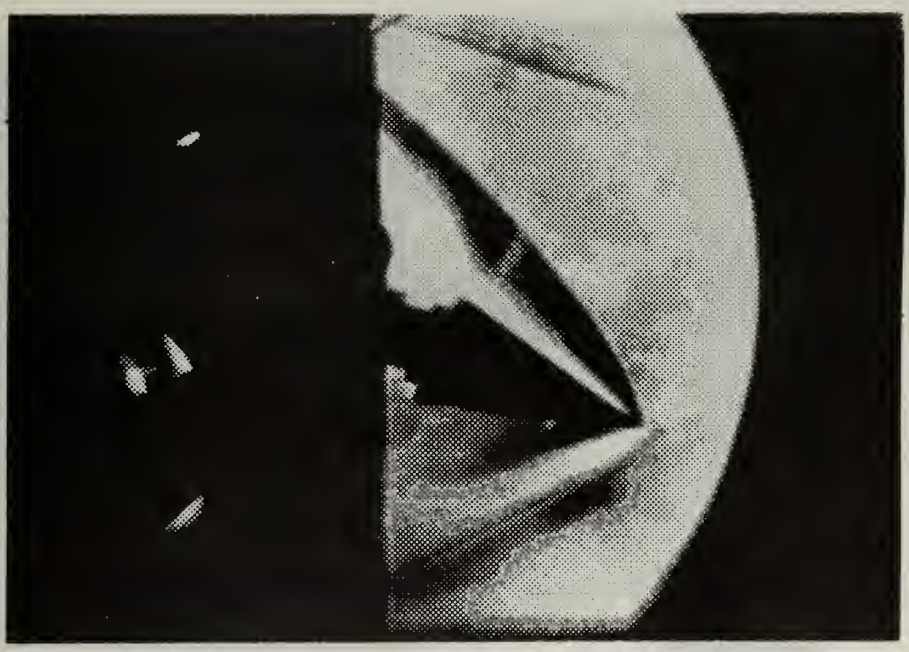

16 cycles per second

WEDGE AT BOTTOM OF CYCLE

2 cycles per second

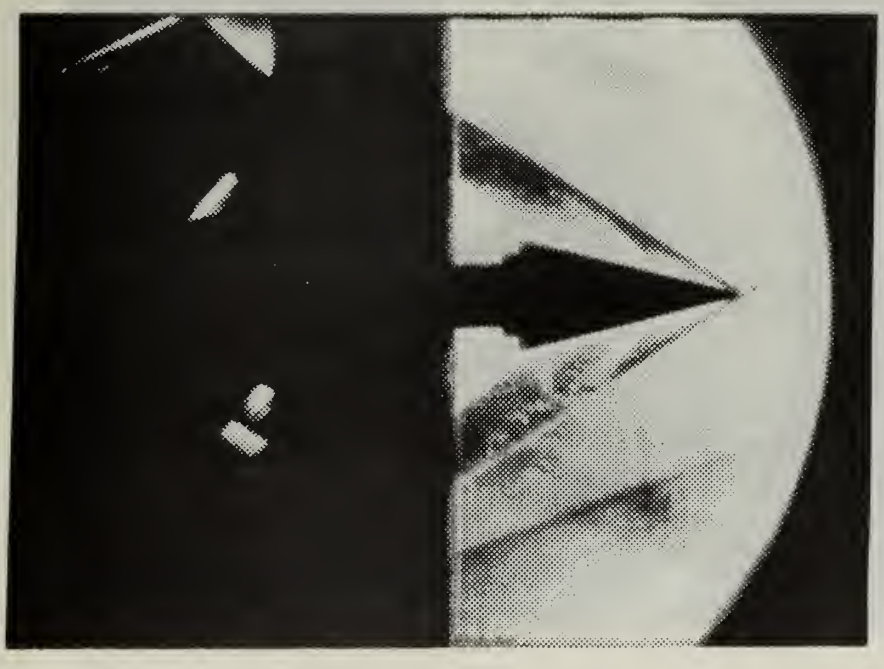

4 cycles per second

WEDGE GOING UP THRU ZERO AOA

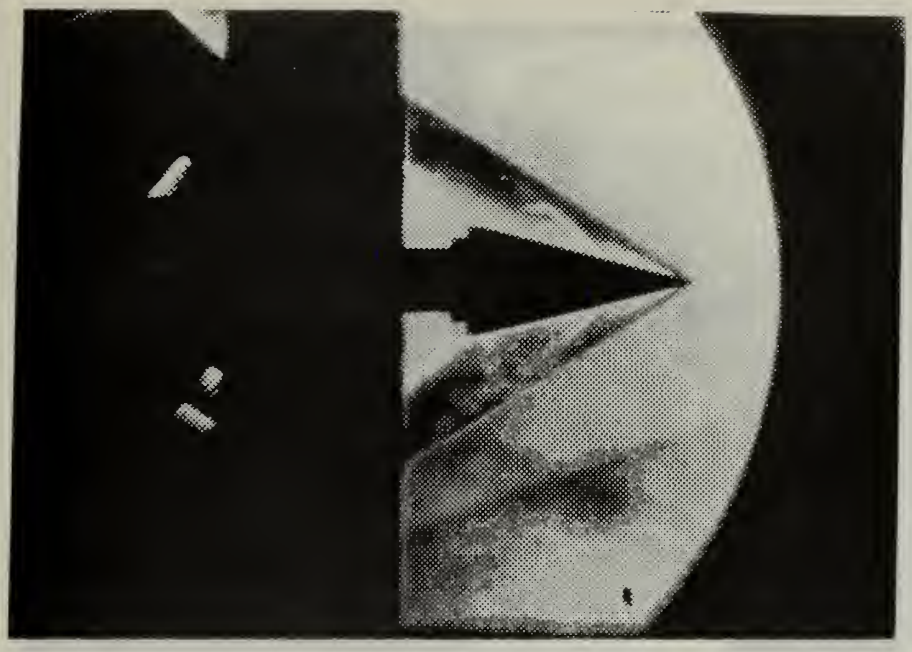

8 cycles per second

16 cycles per second

WEDGE GOING UP THRU ZERO AOA

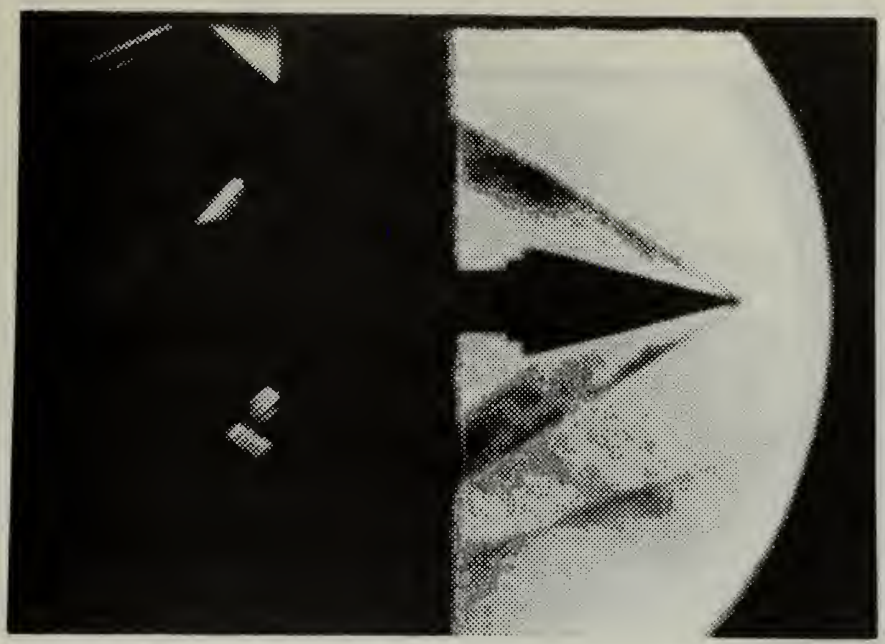

2 cycles per second

4 cycles per second

WEDGE GOING DOWN THRU ZERO AOA

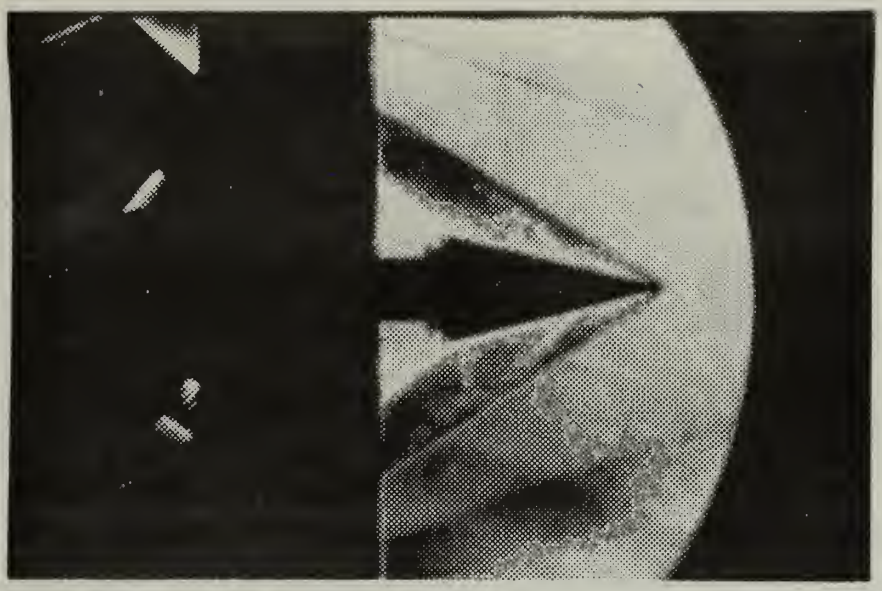

8 cycles per second

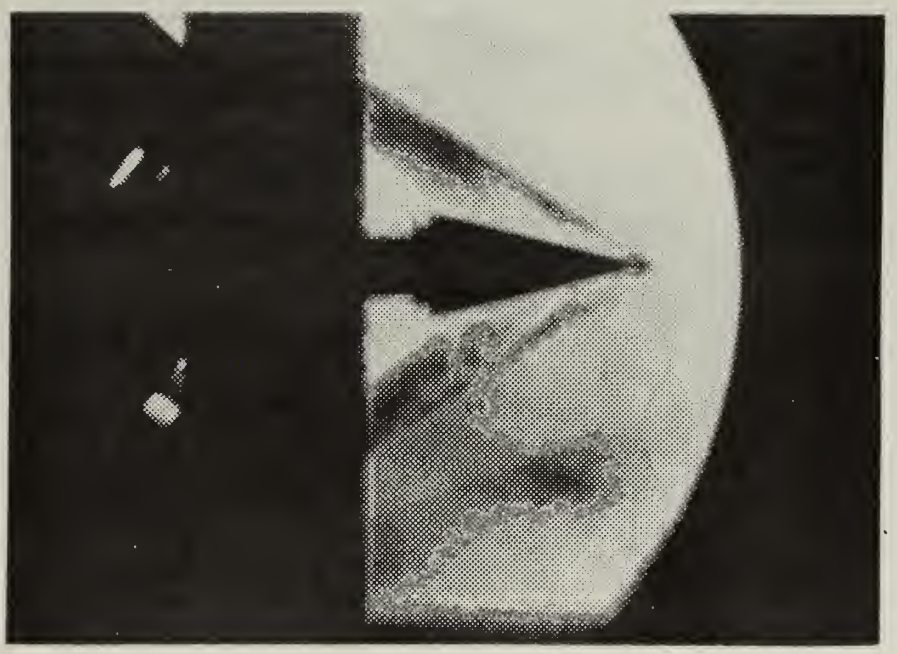

16 cycles per second

WEDGE GOING DOWN THRU ZERO AOA

LIST OF REFERENCES

1. Jones, D.J., Numerical Solutions of the Flow Field for Conical Bodies in a Supersonic Stream, National Research Council of Canada, Report LR-507, July 1968.

2. Statham Instruments Specification Number 12187 Revision A, September 1959.

3. Holman, J.P., Experimental Methods for Engineers, p. 155-156, McGraw-Hill, 1966.

4. Jones, D.J., Tables of Invicid Supersonic Flow About Circular Cones at Incidence γ=1.4, AGARDograph 137, AGARD, 1969.

5. National Advisory Committee for Aeronautics Report 1135, Equations, Tables, and Charts for Compressible Flow, by AMES Research Staff, U.S. Government Printing Office, 1953.

6. Gille, J.C., Pelegrin, M.J., and Decauline, P., Feedback Control Systems, p. 95-109, McGraw-Hill, 1959.

INITIAL DISTRIBUTION LIST

		No. Copies
1.	Defense Documentation Center Cameron Station Alexandria, Virginia 22314	2
2.	Library, Code 0212 Naval Postgraduate School Monterey, California 93940	2
3.	Dr. R. W. Bell Chairman, Department of Aeronautics Naval Postgraduate School Monterey, California 93940	1
4.	Professor G. J. Hokenson Department of Aeronautics Naval Postgraduate School Monterey, California 93940	3
5.	Professor Roy M. Carter Department of Paper and Wood Science North Carolina State University, Box 5988 Raleigh, North Carolina 27607	1
6.	Rodger B. Carter, Lt. USN 22753 Ordonez Drive Salinas, California 93901	1

Security Classification

DOCUMENT CONTROL DATA - R & D

(Security classification of title, body of abstract and indexing annotation must be entered when the overall report is classified)

ORIGINATING ACTIVITY (Corporate author)
Naval Postgraduate School
Monterey, California 93940

2a. REPORT SECURITY CLASSIFICATION
Unclassified

2b. GROUP

REPORT TITLE
Oscillating Bodies in Supersonic Flow

DESCRIPTIVE NOTES (Type of report and inclusive dates)
Master's Thesis

AUTHOR(S) (First name, middle initial, last name)
Rodger Besley Carter

REPORT DATE	7a. TOTAL NO. OF PAGES	7b. NO. OF REFS
December 1972	141	6

CONTRACT OR GRANT NO.	9a. ORIGINATOR'S REPORT NUMBER(S)
PROJECT NO.	
	9b. OTHER REPORT NO(S) (Any other numbers that may be assigned this report)

DISTRIBUTION STATEMENT

Approved for public release; distribution unlimited.

SUPPLEMENTARY NOTES	12. SPONSORING MILITARY ACTIVITY
	Naval Postgraduate School Monterey, California 93940

ABSTRACT

Three shapes — a cone, a wedge, and a flat plate — were oscillated at various frequencies up to 16 cycles per second in a Mach 2.8 flow to determine the extent of the validity of the quasi-steady flow assumption. Instantaneous static pressure measurements and schlieren high speed movies were made and analyzed.

It was found that at approximately 6 cycles per second the measured pressures started a linear deviation from quasi-steady flow. The absolute pressure being measured, the amplitude, and the transverse velocity of the static pressure port were additional variables. The schlieren photography did not show any measurable change in the inviscid shock structure from quasi-steady flow.

14 KEY WORDS	LINK A		LINK B		LINK C	
	ROLE	WT	ROLE	WT	ROLE	WT
oscillating bodies						
oscillating cone						
oscillating wedge						
oscillating flat plate						
unsteady supersonic flow						
unsteady pressure measurements						
oscillating pressure measurements						
quasi-steady supersonic flow						
quasi-steady assumption						
high speed schlieren photography						

141251

Thesis
C27376 Carter
c.1 Oscillating bodies
in supersonic flow.

Thesis
C27376 Carter
c.1 Oscillating bodies
in supersonic flow.

141251

thesC27376
Oscillating bodies in supersonic flow.
3 2768 002 09282 7
DUDLEY KNOX LIBRARY